Corrosion Behaviour of Fly Ash-Reinforced Aluminum-Magnesium Alloy A535 Composites

A Thesis Submitted to the College of Graduate Studies and Research

in Partial Fulfillment of the Requirement for the Degree of

Master of Science

in the Department of Mechanical Engineering

University of Saskatchewan, Saskatoon, Saskatchewan

Canada

By

Emenike Raymond Obi

PERMISSION TO USE

In presenting this thesis in partial fulfillment of the requirements for the Masters degree from the University of Saskatchewan, I agree that the Libraries of this University may make it freely available for inspection. I further agree that permission for copying of this thesis in any manner, in whole or in part, for scholarly purposes may be granted by the professor who supervised my thesis work, Professor I. N. A Oguocha, or, in his absence, by the Head of the Department or the Dean of the College in which my thesis work was done. It is understood that any copying or publication or use of this thesis or parts thereof for financial gain shall not be allowed without my written permission. It is also understood that due recognition shall be given to me and to the University of Saskatchewan in any scholarly use which may be made of any material in my thesis.

Requests for permission to copy or to make other use of material in this thesis in whole or part should be addressed to:

Head of the Department of Mechanical Engineering

57 Campus Drive

University of Saskatchewan

Saskatoon, Canada, S7N 5A9

ABSTRACT

The corrosion behaviour of cast Al-Mg alloy A535 and its composites containing 10 wt.% and 15 wt.% fly ash, and 10 wt.% hybrid reinforcement (5 wt.% fly ash + 5 wt.% SiC) was investigated using weight-loss and electrochemical corrosion tests, optical microscopy, Scanning Electron Microscopy (SEM) and Energy Dispersive X-ray Spectroscopy (EDS). The tests were conducted in fresh water collected from the South Saskatchewan River and 3.5 wt.% NaCl solution at room temperature. The pH of the salt solution varied from 3 to 9. For comparison, two other aluminum alloys, AA2618 and AA5083-H116, were tested in the same electrolytes.

The results of the weight-loss corrosion test showed that unreinforced A535 alloy had a lower corrosion rate in fresh water and seawater environments than the composites at all the tested pH values. The corrosion rate of the composites increased with increasing fly ash content. As expected, the corrosion rates of A535 alloy and the composites tested in fresh water were lower than those in salt solution.

The results of the potentiodynamic and cyclic polarization electrochemical tests showed that the corrosion potential (E_{corr}) and pitting potential (E_{pit}) of the alloy were more positive than those of the composites. The corrosion and pitting potentials of the composites became more negative (active) with increasing fly ash content. The composites showed more positive (noble) repassivation or protection potential (E_{rp}) than the matrix alloy, with the positivity increasing with fly ash content. Analysis of the

electrochemical noise data showed that pitting corrosion was the dominant mode of corrosion for the alloy in 3.5 wt.% NaCl solution. Optical microscopy and SEM revealed that Mg_2Si phase and Al-Mg intermetallics corroded preferentially to the matrix. The EDS data indicated that the protective oxide film formed on A535 contained Al_2O_3 and MgO.

ACKNOWLEDGEMENTS

I would like to express my appreciation to my supervisor, Professor I. N. A. Oguocha, for his guidance, support, and advice. My appreciation also goes to Professor R. W. Evitts for his guidance and advice, and for the provision of the electrochemical corrosion apparatus used in this study. I appreciate the support and encouragement I received from the members of my research committee, Professor R. W. Evitts and Professor Q. Yang. I wish to thank Dr. Jason Lo of CANMET MTL, Ottawa, Ontario for supplying the test materials and the staff of the Engineering Shop at the University of Saskatchewan for machining the test samples. I am grateful to Professor M. C. Chaturvedi (University of Manitoba) for use of his optical microscopy, SEM, and EDS facilities. I also wish to thank Mr. Robert Peace for advice and training on optical microscopy, and Mr. Douglas Fischer, for analyzing water samples from the South Saskatchewan River as well as allowing me to use his pH meters.

I am grateful to my family whose encouragement has been vital to the completion of my study. The support provided by my colleagues in the Materials Science Group is also highly appreciated.

Financial assistance from the Natural Sciences and Engineering Research Council (NSERC) to my supervisor, and Teaching Fellowship from the College of Graduate Studies and Research (CGSR) through the Department of Mechanical Engineering are highly appreciated.

TABLE OF CONTENTS

PERMISSION TO USE			i
ABSTRACT			ii
ACKNOWLEDGEMENTS			iv
TABLE OF CONTENTS			v
LIST OF TABLES			viii
LIST OF FIGURES			xii
ACRONYMS AND SYMBOLS			xviii
1.0	INTRODUCTION		1
	1.1	Background	1
	1.2	Aluminum A535 Alloy	4
	1.3	Motivation	4
	1.4	Objectives	5
	1.5	Methods of Evaluation	5
	1.6	Thesis Outline	6
2.0	LITERATURE REVIEW		7
	2.1	Types of corrosion	7
	2.2	Thermodynamics and Kinetics of Corrosion Reaction	8
		2.2.1 Thermodynamics of Corrosion	9
		2.2.2 Kinetics of Corrosion Reaction	11
	2.3	Corrosion Rate Measurement	14
		2.3.1 Immersion Test	14

2.3.2 Potentiodynamic Electrochemical Measurements 15
2.3.3 Cyclic Polarization Electrochemical Measurements 15
2.3.4 Electrochemical Noise Measurements 16
2.3.5 Optical Microscopy 18
2.3.6 Scanning Electron Microscopy 18
2.4 Fly Ash 18
2.5 Aluminum Alloys 19
2.6 Casting Aluminum Alloy A535 20
2.7 Corrosion of Aluminum 21
2.8 Aluminum Alloys and Metal Matrix Composites 24
2.8.1 Effect of Particulate Reinforcing Phase 24
2.8.2 Effect of Magnesium 27
3.0 MATERIALS AND EXPERIMENTAL PROCEDURE 30
3.1 Materials 30
3.2 Experimental Methods 33
3.2.1 Immersion Test 33
3.2.2 Electrochemical Corrosion Tests 37
3.3 Optical Microscopy 49
3.4 Scanning Electron Microscopy 50
3.5 Water Analysis 50
4.0 RESULTS AND DISCUSSION 52
4.1 General Corrosion Behaviour of A535, AA5083-H116 and AA2618 in Neutral 3.5 wt.% NaCl Solution

Maintained at pH 7 52

4.2 Effect of Fly Ash Addition on the Corrosion Behaviour of A535 in Neutral 3.5 wt. % NaCl Solution 74

4.3 Effect of pH on the Corrosion Behaviour of A535 and the Composites 84

4.3.1 Corrosion in 3.5 wt.% NaCl solution maintained at pH 4 84

4.3.2 Corrosion in 3.5 wt.% NaCl solution maintained at pH 9 92

4.3.3 Corrosion in 3.5 wt.% NaCl solution maintained at pH 3 100

4.5 Effect of Fly Ash Addition on the Corrosion Behaviour of A535 in South Saskatchewan River Water 106

5.0 CONCLUSIONS AND RECOMMENDATIONS 115

REFERENCES 119

APPENDICES 132

LIST OF TABLES

Table 2.1.	Canadian fly ash classification according to CSA A23.5	20
Table 3.1.	Chemical compositional limits of A535	31
Table 3.2.	Chemical composition of A535 obtained using EPMA	31
Table 3.3.	Chemical composition of fly ash obtained by XRF	31
Table 3.4.	Chemical composition of AA5083-H116	32
Table 3.5.	Chemical composition of AA2618	32
Table 3.6.	Number of samples used in the immersion test	35
Table 3.7.	Parameters used in the potentiodynamic electrochemical test	42
Table 3.8.	Number of samples used in the potentiodynamic corrosion test	42
Table 3.9.	Parameters used in cyclic polarization in fresh water	44
Table 3.10.	Parameters used in cyclic polarization in 3.5 wt.% NaCl solution pH 7	45
Table 3.11.	Parameters used in cyclic polarization in 3.5 wt.% NaCl solution pH 4	46
Table 3.12.	Parameters used in cyclic polarization in 3.5 wt.% NaCl solution pH 9	47
Table 3.13.	Parameters used in cyclic polarization in 3.5 wt.%NaCl solution pH 3	48
Table 3.14.	Parameters used in the electrochemical noise corrosion test	50
Table 4.1.	Corrosion potentials and current densities and Tafel constants of A535, AA5083-H116, and AA2618 immersed in neutral salt solution	55

Table 4.2.	Corrosion potential, current densities, and Tafel constants of A535 and the composites immersed in neutral salt solution	77
Table 4.3.	Pitting and repassivation potentials of A535 and the composites immersed in neutral salt solution	81
Table 4.4.	Corrosion potentials, current densities, and Tafel constants of A535 and the composites immersed in 3.5 wt.% salt solution maintained at pH 4	87
Table 4.5.	Pitting and repassivation potentials of A535 and the composites immersed in 3.5 wt.% salt solution maintained at pH 4	90
Table 4.6.	Corrosion potentials, current densities, and Tafel constants of A535 and the composites immersed in 3.5 wt.% salt solution maintained at pH 9	96
Table 4.7.	Pitting and repassivation potentials of A535 and the composites immersed in 3.5 wt.% salt solution maintained at pH 9	98
Table 4.8.	Corrosion potentials, current densities, and Tafel constants of A535 and the composites immersed in 3.5 wt.% salt solution maintained at pH 3	101
Table 4.9.	Pitting and repassivation potentials of A535 and the composites immersed in 3.5 wt.% salt solution maintained at pH 3	104

Table 4.10.	Effect of pH on the pitting potentials of A535 and its composites in 3.5 wt.% NaCl solution	104
Table 4.11.	Effect of pH on the pitting potentials of A535 and its composites in 3.5 wt.% NaCl solution	105
Table 4.12.	Anion composition of the South Saskatchewan River water	107
Table 4.13	Corrosion potentials, current densities, and Tafel constants of A535 and the MMCs immersed in river water	109
Table 4.14.	Pitting and repassivation potentials of A535 and the composites immersed in river water	111
Table A.1.	Average values for weight loss for A535 and composites immersed in 3.5 wt. % NaCl solution maintained at pH 4	132
Table A.2.	Average values for weight loss for A535 and composites immersed in 3.5 wt. % NaCl solution maintained at pH 7	133
Table A.3.	Average values for weight loss for A535 and composites immersed in 3.5 wt. % NaCl solution maintained at pH 9	133
Table A.4.	Average values for weight loss for A535 and composites immersed in water from South Saskatchewan River	134
Table B.1.	Dimensions of samples immersed in 3.5 wt.% NaCl solution Maintained at pH 4	135
Table B.2.	Dimensions of samples immersed in 3.5 wt.% NaCl solution Maintained at pH 7	135
Table B.3.	Dimensions of samples immersed in 3.5 wt.% NaCl solution Maintained at pH 9	136

Table B.4. Dimensions of samples immersed in water from South Saskatchewan River 136

Table C.1. Densities of A535 alloy and its composites 137

Table D.1. Average values for corrosion rates for A535 and composites immersed in 3.5 wt.% NaCl solution maintained at pH 4 138

Table D.2. Average values for corrosion rates for A535 and composites immersed in 3.5 wt.% NaCl solution maintained at pH 7 138

Table D.3. Average values for corrosion rates for A535 and composites immersed in 3.5 wt.% NaCl solution maintained at pH 9 139

Table D.4. Average values for corrosion rates for A535 and composites immersed in water from the South Saskatchewan River 139

LIST OF FIGURES

Figure 2.1.	Illustration of the Pourbaix diagram for aluminum	12
Figure 2.2.	Polarization behaviour of aluminum	14
Figure 3.1.	Weight-loss corrosion test apparatus	36
Figure 3.2.	The ECM8 electrochemical multiplexer system equipped with a PCI4 potentiostat	38
Figure 3.3.	Exploded view of the working electrode holder	38
Figure 3.4.	Working electrode, reference electrode (SCE) and graphite counter electrode used in the study	40
Figure 3.5.	A schematic diagram of the working electrode and holder assembly	40
Figure 3.6.	Corrosion cell and electrodes used in electrochemical Measurement	41
Figure 4.1.	Variation of normalized weight loss (weight loss / initial weight) with time for A535, AA5083-H116, and AA2618 exposed in neutral 3.5 wt.% NaCl solution	53
Figure 4.2.	Variation of corrosion rate with time for A535, AA5083-H116, and AA2618 exposed in neutral 3.5 wt.% NaCl solution	53
Figure 4.3.	Potentiodynamic polarization curves for A535, AA5083, and AA2618 aluminum alloys exposed in neutral 3.5 wt.% NaCl solution	55

Figure 4.4.	Cylic polarization curves for A535, AA5083, and AA2618 aluminum alloys exposed in neutral 3.5 wt.% NaCl solution	57
Figure 4.5.	Pitting potentials of A535, AA5083, and AA2618 aluminum alloys immersed in neutral 3.5 wt.% NaCl solution	57
Figure 4.6.	Corroded specimens of AA2618 immersed in neutral salt solution for 14 days	59
Figure 4.7.	Corroded specimen of AA5083-H116 immersed in neutral salt solution for 14 days	60
Figure 4.8.	Optical micrograph showing Al-Mg rich intermetallic phase in A535 sample before exposure to corrosion attack	62
Figure 4.9.	EDS spectrum of the Al-Mg rich phase in A535 alloy	62
Figure 4.10.	SEM micrograph showing Mg_2Si intermetallic phase in A535 sample before exposure to corrosion attack	63
Figure 4.11.	EDS spectrum of the Mg_2Si rich phase in A535 alloy	63
Figure 4.12.	Optical micrograph of the $AlTi_3$ phase	64
Figure 4.13.	EDS spectrum of the $AlTi_3$ phase	64
Figure 4.14.	Optical micrographs of A535 alloy (a) before and (b) and (c) after immersion in neutral 3.5 wt.% NaCl solution for 14 days	65
Figure 4.15.	SEM micrographs of A535 alloy immersed in neutral 3.5 wt.% NaCl solution for 14 days	65
Figure 4.16.	Optical micrograph showing defective film formed on the corroded specimen of A535 immersed in neutral salt water for 14 days	66

Figure 4.17. SEM micrograph showing the non-defective film formed on the corroded specimen of A535 immersed in neutral salt water for 14 days 66

Figure 4.18. EDS spectrum of the defective film on formed on A535 alloy immersed in neutral salt solution for 14 days 68

Figure 4.19. EDS spectrum of the non-defective film on formed on A535 alloy immersed in neutral salt solution for 14 days 68

Figure 4.20. Electrochemical potential transients for A535 during the first four hours of immersion in neutral salt solution 69

Figure 4.21. Variation of average potential with time for A535 during the first 4 hours of immersion in neutral salt solution 70

Figure 4.22. Electrochemical current transients for A535 during the first 4 hours of immersion in neutral salt solution 72

Figure 4.23. Variation of average current with time for A535 during the first 4 hours of immersion in neutral salt solution 73

Figure 4.24. Variation of weight loss with time for A535 and the composites immersed in neutral 3.5 wt.% NaCl solution 74

Figure 4.25. Variation of corrosion rate with time for A535 and the composites immersed in neutral 3.5 wt.% NaCl solution 75

Figure 4.26. Potentiodynamic polarization curves for A535 alloy and the composites immersed in neutral 3.5 wt.% NaCl solution 77

Figure 4.27. Cyclic potentiodynamic polarization curves for A535 and the composites immersed in neutral 3.5 wt.% NaCl solution 78

Figure 4.28. Effect of fly ash content on the pitting potential of A535 and the composites immersed in neutral 3.5 wt.% NaCl solution 78

Figure 4.29. Effect of fly ash content on the repassivation potentials of A535 and the composites immersed in neutral 3.5 wt% NaCl 79

Figure 4.30. Optical micrographs of A535/hybrid/10_p (a) before and (b) after immersion in neutral 3.5 wt.% NaCl solution for 14 days 82

Figure 4.31. Variation of weight loss with time for A535 and the composites immersed in 3.5 wt.% NaCl solution (pH = 4) 85

Figure 4.32. Variation of corrosion rate with time of A535 and the composites immersed in 3.5 wt.% NaCl solution (pH = 4) 85

Figure 4.33. Potentiodynamic polarization curves for A535 alloy and its Composites immersed in 3.5 wt.% NaCl solution (pH =9) 87

Figure 4.34. Cyclic potentiodynamic polarization curves for A535 and the composites immersed in 3.5 wt.% NaCl solution (pH = 4) 88

Figure 4.35. Effect of fly ash content on the pitting potential of A535 and the composites immersed in 3.5 wt.% NaCl solution (pH = 4) 88

Figure 4.36. Effect of fly ash content on the repassivation potentials of A535 and the composites immersed in 3.5 wt.% NaCl (pH = 4) 89

Figure 4.37. Optical micrographs of (a) A535 alloy and (b) A535/fly ash/10_p after 14 days of immersion in 3.5 wt.% NaCl solution (pH = 4) 91

Figure 4.38. Variation of weight loss with time for A535 and the composites immersed in 3.5 wt.% NaCl solution (pH = 9) 92

Figure 4.39. Variation of corrosion rate with time for A535 and the composites immersed in 3.5 wt.% NaCl solution (pH = 9) 93

Figure 4.40. Potentiodynamic polarization curves for A535 alloy and the composites immersed in 3.5 wt.% NaCl solution (pH =9) 95

Figure 4.41. Cyclic potentiodynamic polarization curves for A535 and the composites immersed in 3.5 wt.% NaCl solution (pH = 9) 96

Figure 4.42. Effect of fly ash content on the pitting potential of A535 and the composites immersed in 3.5 wt.% NaCl solution (pH = 9) 96

Figure 4.43. Effect of fly ash content on the repassivation potentials of A535 and the composites immersed in 3.5 wt.% NaCl solution (pH = 9) 98

Figure 4.44. Optical micrographs of A535 and A535/fly ash/10_p after immersion in 3.5 wt.% NaCl solution for 14 days (pH = 9) 99

Figure 4.45. Potentiodynamic polarization curves for A535 alloy and the composites immersed in 3.5 wt.% NaCl solution (pH =3) 101

Figure 4.46. Cyclic potentiodynamic polarization curves for A535 and the composites immersed in 3.5 wt.% NaCl solution (pH = 3) 102

Figure 4.47. Effect of fly ash content on the pitting potential of A535 and the composites immersed in 3.5 wt.% NaCl solution (pH = 3) 102

Figure 4.48. Effect of fly ash content on the repassivation potentials of A535 and the composites immersed in 3.5 wt.% NaCl solution (pH = 3) 103

Figure 4.49. Variation of weight loss with time for A535 and the composites immersed in river water 107

Figure 4.50. Variation of corrosion rate with time for A535 and the composites immersed in river water 108

Figure 4.51. Potentiodynamic polarization curves for A535 alloy and the composites exposed in river water 109

Figure 4.52. Cyclic polarization curves for A535 and the composites immersed in river water 111

Figure 4.53. Effect of fly ash content on the pitting potentials of A535 and the composites immersed in river water 112

Figure 4.54. Effect of fly ash content on the repassivation potentials of A535 and the composites immersed in river water 112

Figure 4.55. Optical micrographs of A535 alloy immersed in river water 114

Figure 4.56. Optical micrographs of A535/hybrid/10_p immersed in river water 114

Figure E.1. Cylic polarization curves for A535 and the MMCs exposed in Neutral 3.5 wt.% NaCl solution 140

ACRONYMS AND SYMBOLS

A	Surface area (cm^2)
A535	Aluminum alloy A535
A535/hybrid/10_p	A535 alloy + 5 wt.% fly ash + 5 wt.% SiC
A535/fly ash/10_p	A535 + 10 wt.% fly ash
A535/fly ash/15_p	A535 + 15 wt.% fly ash
CTE	Coefficient of thermal expansion (K^{-1})
D	Density (gcm^{-3})
DC	Direct current (A)
ECN	Electrochemical noise
EDS	Energy dispersive X-ray spectroscopy
EPMA	Electron probe microanalyzer
e	Non-standard half cell potential (V)
e^o	Standard half-cell potential (V)
E_p	Pititng potential (V)
E_{rp}	Repassivation potential (V)
E_{corr}	Corrosion potential (V)
E_{prot}	Protection potential (V)
i_{corr}	Corrosion current density (Acm^{-2})
i_{pass}	Passivation current density (Acm^{-2})
i_{crit}	Critical current density (Acm^{-2})
MMC	Metal matrix composites

OCP	Open circuit potential (V)
OM	Optical microscopy
SA	Surface area composites (cm^2)
SCE	Saturated calomel electrode
SEM	Scanning electron microscopy
t	Time
ΔG	Free energy change in the non-standard state (kJ/mol)
ΔG^o	Free energy change in the standard state (kJ/mol)
XFS	X-ray fluorescence spectrometry
W	Weight loss (mg)
WE	Working electrode

1.0 INTRODUCTION

1.1 Background

Corrosion is the degradation of a material by electrochemical or chemical reaction with its environment. Various forms of corrosion exist and they are classified as uniform or general, galvanic, pitting, microbial, hydrogen embrittlement and blistering, stress corrosion cracking, corrosion fatigue, erosion, cavitation, filiform and intergranular corrosion [1]. Corrosion causes many problems for humankind. It damages equipment, structures, and the environment in the vicinity of corroded structures. Its cost ranges between 3.1 to 4.5% of the Gross Domestic Product (GDP) in industrialized nations [2]. The annual cost of corrosion in the United States is approximately $300 billion dollars [3]. Canada spends 3.1% of her Gross Domestic Product (GDP), or CAN$32.8 billon, on corrosion prevention and control [2]. This amount, which quantifies only the direct cost of corrosion prevention and control, amounts to approximately two-thirds of the Canadian government annual expenditure on health and education, twice the amount spent on research and development, and thrice the expenditure on national defense [2]. It is estimated that 25% to 30% of annual cost of corrosion could be saved with optimum corrosion management strategies [2].

In the past three decades, particle-reinforced aluminum matrix composites (MMCs) have received great attention because of their increased wear resistance, reduced coefficient of thermal expansion (CTE), increased elastic modulus, and improved strength over conventional aluminum alloys [4, 5]. Typical industrial applications of particle reinforced aluminum composites include: (i) ship hulls and deckhouses [6], (ii) aircraft frames, engines, accessories, pressure vessels for liquid fuel and oxidizers [7, 8], (iii) automobile engine blocks, pistons, cylinder heads, intake manifolds, crankcases, carburetors, transmission housings, rocker arms, brake valves and caliphers [9]; (iv) bicycle frames [10], and (v) advanced guidance equipment, lightweight optical assemblies [11, 12].

Particulate aluminum composites have commonly been reinforced with ceramic particles such as silicon carbide [13-18], alumina [19-22], garnet [23, 24], graphite [25, 26], and mica [27]. However, the cost of manufacturing these composites is high and this limits their utilization in several engineering designs. Recently, aluminum alloy composites reinforced with fly ash, a waste by-product of coal combustion, has been engineered [28-39] as potential substitutes to conventional composites in several applications in order to widen the engineering application of particulate aluminum composites. Fly ash comprises mainly small spheres of oxides of silicon, aluminum, iron, magnesium and calcium. Its size ranges from 1 μm to 150μm while its density varies from 1.3 to 4.8 depending on the mineralogy [29, 32]. Currently, fly ash is disposed in landfills, ash dams and lagoons thereby causing environmental pollution and costing thermal power plants a huge amount of money annually [40]. Therefore, the addition of fly ash into

aluminum matrix to produce composites is a value-added initiative that lowers disposal costs, increases energy savings by reducing the quantity of aluminum produced, and creates a healthier environment.

The resistance of particle reinforced MMCs to environmental attack is a critical design criterion. Several studies have indicated that the corrosion resistance of particle-reinforced composites depends on the composition of the base alloy, reinforcing particles, and corrosive environment [13-18, 23-27, 37, 41-49]. Other factors include the fabrication routes for the composites, volume fraction of the reinforcing particles, and the temperature of the corrosive medium. Aylor *et al.* [42] reported that pitting corrosion attack on SiC_p/Al composites was observed predominantly at the SiC/Al interfaces. They noted that the pits on the SiC/Al composites were greater in number, smaller in size, and shallower in depth than those on the unreinforced aluminum alloys. Feng *et al.* [50] investigated the pitting corrosion behaviour of SiC_p/Al 2024 composites and attributed the intense corrosion of the composites to pit nucleation and propagation at the SiC/Al interface. Interfacial reactions between liquid aluminum and SiC generated intermetallic particles which formed microgalvanic couples with the matrix.

1.2 Aluminum A535 Alloy

Cast aluminum alloy A535 is a non-heat treatable Al-Mg alloy with a good combination of strength, lightweight, stiffness, ductility, machinability, castability, and good surface finish. It is used in marine and naval vessels, architectural applications, aircraft landing

gears, rocket launchers, and light-weight armored vehicles and in the manufacture of components of instruments and computing devices where dimensional stability is of paramount importance [51].

1.3 Motivation

Although many researchers [12-17, 22-26, 41-50] have studied the corrosion behaviour of aluminum alloys and conventional aluminum alloy-based composites, there is dearth of information on the corrosion of A535 alloy and the effect of fly ash addition or any ceramic reinforcement on its corrosion behaviour. The studies by Bienias *et al.* [37] and Remachandra *et al.* [38] reported an increase in pitting corrosion of aluminum-silicon alloys reinforced with fly ash. Bienias [37] reported that the addition of fly ash to an aluminum-silicon (4xxx) alloy in 3.5 wt.% NaCl solution increased the susceptibility of the alloy to pitting corrosion. Si crystals that precipitated from the reaction between SiO_2 and liquid aluminum formed microgalvanic couple with the matrix. Since the matrix was anodic to Si, it dissolved. The addition of fly ash to the base alloy also generated sites for particle-matrix decohesion such as pores and voids. Corrosion attack at these sites increased the severity of pitting corrosion of the composites.

The main goal of the present study was to investigate the corrosion behaviour of A535 alloy and the effect of fly ash addition on its corrosion resistance. In addition, the mechanisms by which the alloy and its composites corrode in different media were studied.

1.4 Objectives

The objective of this study was to understand the corrosion behaviour of cast aluminum alloy A535 and its composites reinforced with fly ash in 3.5 wt.% NaCl solution and water from the South Saskatchewan River at room temperature. The effect of pH on their corrosion behaviour and pitting mechanism was also investigated.

1.5 Methods of Evaluation

The test specimens were evaluated using immersion corrosion test to determine their weight loss in 3.5 wt.% NaCl solutions with different pH and freshwater from the South Saskatchewan River. The corrosion potential (E_{corr}), pitting potential (E_p), and repassivation potential (E_{rp}) of the test specimens were measured by potentiodynamic and cyclic polarisation electrochemical corrosion tests. Pitting corrosion of the test materials were studied by the Electrochemical noise (ECN) technique. The morphology of the corroded specimens was examined using Optical Microscopy (OM) and Scanning Electron Microscopy (SEM). The chemical compositions of the corrosion products were determined using Energy Dispersive X-ray Spectroscopy (EDS).

1.6 Thesis Outline

This thesis is divided into five chapters. Chapter 1 presents an overview of the research project and its main objectives. A survey of the pertinent literature is presented in Chapter 2. Chapter 3 discusses materials and experimental methods used. Chapter 4 presents and discusses the experimental results, while Chapter 5 summarizes the conclusions deduced from the work and suggests some recommendations for future work.

2.0 LITERATURE REVIEW

This chapter reviews the common types of corrosion, and the thermodynamics and kinetics of corrosion reactions. In addition, the nature, types, compositions, and properties of fly ash particles, and aluminum casting aluminum alloy A535 are presented. Finally, the effects of the reinforcement phase and Magnesium (Mg) content on the corrosion behaviour of aluminum-based metal matrix composites (Composites) are discussed.

2.1 Types of Corrosion

Corrosion is the damage of materials due to chemical and/or electrochemical interactions with their environment. Corrosion can be classified as dry and wet corrosion. Dry corrosion occurs with gases as the corrosive agent and in the absence of aqueous phases on the metal surface. Wet corrosion occurs when aqueous phases are present on the surface of the metal. Various forms of wet corrosion have therefore been identified and classified [51] such as uniform, bimetallic, pitting, crevice, erosion, intergranular, filliform, dealloying, stress corrosion cracking, corrosion fatigue, hydrogen blistering and embrittlement, and microbial corrosion.

Uniform Corrosion: Uniform or general corrosion is the corrosion attack that is evenly distributed on the surface of a metal.

Pitting Corrosion: Pitting corrosion is the perforation of a metal at isolated anodic sites on the metal surface.

Crevice Corrosion: Crevice corrosion is the corrosion damage resulting from uneven distribution of oxygen on the surface of a metal. Anodic sites develop at oxygen-deficient sites, particularly within crevices, while cathodic sites simultaneously occur at oxygen-rich areas. Crevice corrosion usually occurs at flanges, bolt holes, gaskets, washers etc.

Galvanic Corrosion: Galvanic corrosion is the corrosion attack on a active metal with a low electrode potential that is electrically connected to a noble metal with a high electrode potential.

Erosion Corrosion: Erosion corrosion is the erosion caused or accelerated by relative motion between the metal surface and its environment.

Intergranular Corrosion: Intergranular corrosion is the corrosion attack which is confined to the depletion or deterioration of the grain boundaries of a material.

2.2 Thermodynamics and Kinetics of Corrosion Reaction

Corrosion reactions are accompanied by energy changes between reactants and corrosion products. Energy changes that take place during corrosion reactions can be analyzed using the principles of thermodynamics. Similarly, the rate at which corrosion reactions proceed can be studied by employing the theories of reaction kinetics.

2.2.1 Thermodynamics of Corrosion

Thermodynamics of corrosion reaction provides information regarding the energy changes, direction of reaction, and equilibrium states between reactants and products. The Nenst equation is used to determine the free energy changes involved in the anodic and cathodic processes taking place during corrosion. It determines energy changes for reactions of the type

$$aA + mH^{+} + ne^{-} \rightarrow bB + dH_2O \tag{2.1}$$

using

$$\Delta G - \Delta G^{o} = RT \ln \frac{(B)^{b}(H_2O)^{d}}{(A)^{a}(H^{+})^{m}} \tag{2.2}$$

or

$$e = e^{o} - \frac{RT}{nF} \ln \frac{(B)^{b}(H_2O)^{d}}{(A)^{a}(H^{+})^{m}} \tag{2.3}$$

where A is a metal, B is a corrosion product, H is hydrogen, e^{-} is Faraday electron, F is the Faraday constant, a, b, d, m are coefficients in the reaction, and n is the number of electron exchanged and F is the Faraday constant. ΔG and ΔG^{o} are free energy changes in the non-standard and standard states, respectively, R is the gas constant and T is the absolute temperature. Standard states represent 1 molar solution at 1 atmosphere pressure. e and e^{o} are respectively non-standard and standard half-cell electrode potentials.

A generalized form of the oxidation reaction which occurs at the anode is

$$M \rightarrow M^{+} + e^{-} \tag{2.4}$$

where M represents a corroding metal. The principal cathodic reactions are the reduction of hydrogen ion, oxygen gas, and water. At low electrode potentials in an acid solution, the reduction of hydrogen ion is expressed as

$$2H^{+} + 2e^{-} \rightarrow H_2 \tag{2.5}$$

In neutral or alkaline solutions, hydrogen ion reduction is expressed as

$$2H_2O + 2e^{-} \rightarrow H_2 + 2OH^{-} \tag{2.6}$$

At high electrode potentials, oxygen reduction occurs. In an acid solution, oxygen reduction is represented in the form:

$$O_2 + 4H^{+} + 4e^{-} \rightarrow 2H_2O \tag{2.7}$$

Similarly, in a neutral or alkaline solution, an equivalent oxygen reduction equation can be expressed as

$$O_2 + 2H_2O + 4e^{-} \rightarrow 4OH^{-} \tag{2.8}$$

The thermodynamics of corrosion reaction can be represented graphically using the Pourbaix diagram, which classifies corrosion reactions into active, passive, and immune zones. The active or corrosion zones on the diagram designate areas where the energy changes drive corrosion reactions towards the formation of corrosion products. The passive zone is the zone where layers of initially formed corrosion products insulate the metal from further attack, or minimize further corrosion damage. A metal is immune when there is no thermodynamic drive to form corrosion products. The Pourbaix diagram for pure aluminum is presented in Figure 2.1. At potentials below the hydrogen reduction line, water is thermodynamically unstable and decomposes according to equation (2.6) to hydrogen. Similarly, it decomposes as given in equation (2.8) forming hydroxyl ions at potentials above the oxygen reduction line. The intermediate region represents the range of potentials where water is thermodynamically stable.

2.2.2 Kinetics of Corrosion Reaction

The rates of corrosion reactions cannot be determined by considering only the energy changes involved in the reaction. They are estimated using the mixed potential theory and polarisation behaviour of the metal. According to the mixed potential theory [51], the total anodic currents must equal the total cathodic currents. Thus, all the electrons generated by an oxidation reaction at the anode are consumed by a reduction reaction at the cathode. At the anode, corrosion leads to the ionization of the metal. The potential of the metal deviates from its equilibrium potential as the metal ionizes by a process

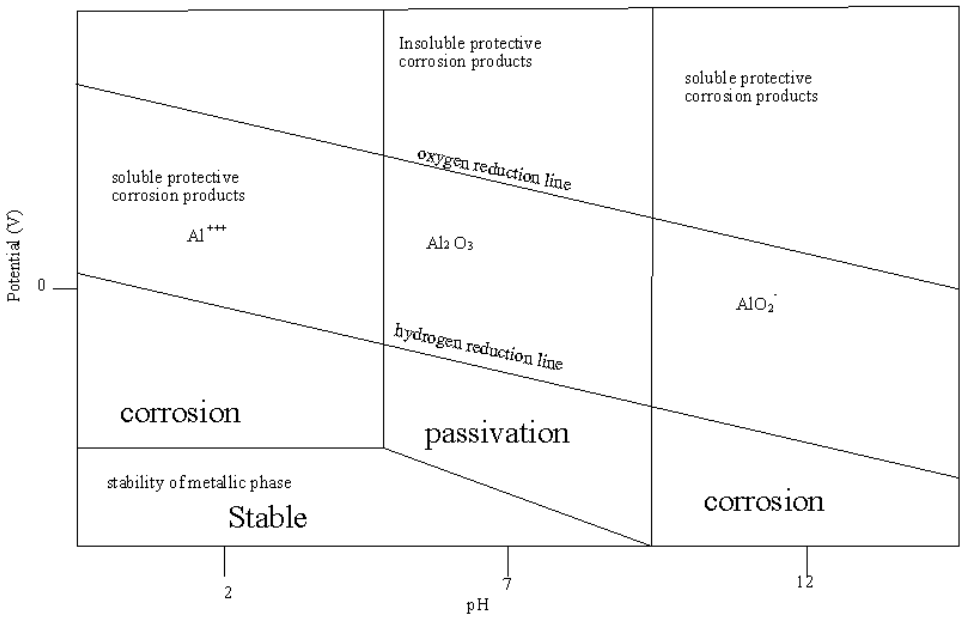

Figure 2.1. Illustration of the Pourbaix diagram for aluminium.

called polarization. The overpotential, η, is the difference between the potential of the metal surface at open circuit potential (OCP) (i.e., the potential on a freely corroding piece of material) and the corrosion potential, that is, $OCP - E_{corr}$. It provides the driving force for corrosion reactions.

Three types of polarization exist, namely: activation, concentration, and ohmic polarization. Activation polarization occurs when the overpotential of either the anodic or cathodic reaction is proportional to the logarithm of the current density. In other words, the current density increases by an order of magnitude for each unit increase in overpotential. The polarization which limits the cathodic current density by the amount of dissolved species transferable to the surface of the cathode for reductions is called concentration polarization. Ohmic polarization is the potential generated by resistance

to ionic current flow in the electrolyte or electronic current flow in the metallic circuit. Metals usually have high conductivity and low ohmic polarisation. However, polarization due to ohmic resistance of the electrolyte is usually significant. It reduces the potential available for corrosion reaction and decreases the corrosion current.

The anodic polarization behaviour of an active-passive metal such as aluminum (See Figure 2.2) shows an active region where an initial positive overpotential generates rapid increase in the anodic current density until a limiting critical current density called i_{crit} is attained. Beyond this potential, the metal passivates or develops a thin tenacious oxide film which significantly decreases the rate of corrosion until the passivation current density (i_{pass}) is reached. Further increase in potential to the pitting or breakdown potential (E_p) causes a rapid increase in the current density. Pitting potential marks the break down of the protective oxide film and the initiation of pits on the metal surface. The region of increasing current density above the pitting potential is called the transpassive region. Reversing the direction of the potential scan to more negative values generates a hysteresis loop with the current density curve intersecting the passive range at the protection potential (E_{prot}), or repassivation potential (E_{rp}) which measures the promptness with which the oxide film re-passivates At E_p, new pits initiate. Between E_p and E_{rp}, new pits do not form but existing pits continue to grow. Below E_{rp} existing pits passivate.

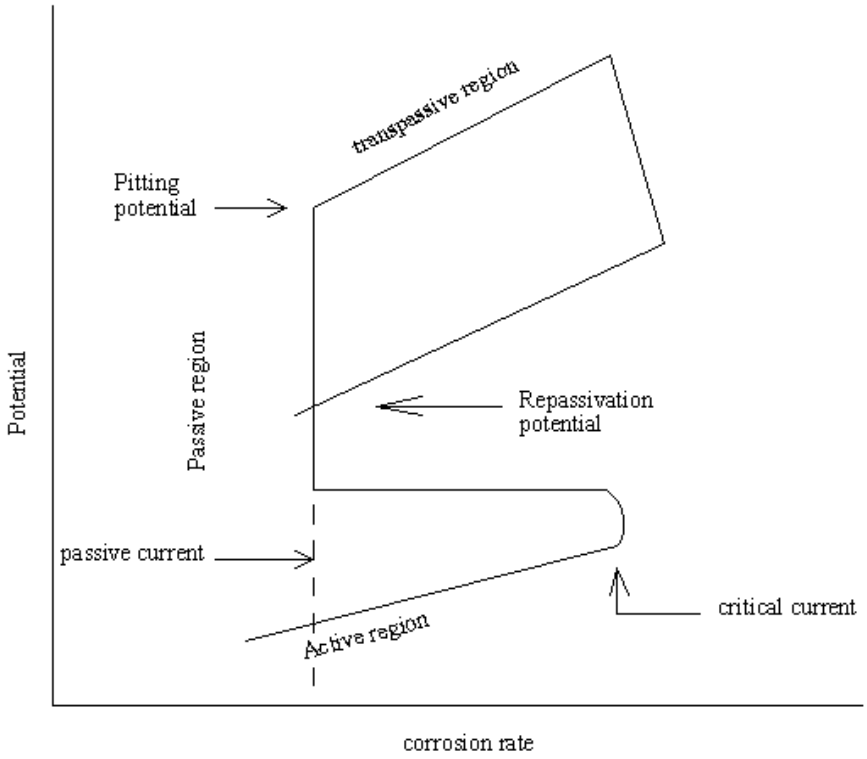

Figure 2.2. Polarization behaviour of pure aluminum.

2.3 Corrosion Rate Measurement

The level of corrosion attack can be evaluated by several methods including immersion test, electrochemical measurements, optical microscopy, scanning electron microscopy.

2.3.1 Immersion Test

Immersion test technique involves recording the weight loss of a sample immersed in a corrosive medium (ASTM G 1-90). Weight loss (in *mg*) may be converted to corrosion rate in mm per year using the expression [51]:

$$mm/yr = \frac{87.6W}{DAt} \tag{2.9}$$

where 87.6 is a constant, W is weight loss in mg, D is density in g/cm^3, A is surface area in cm^2, and t is time in hours.

The immersion test does not however provide information on other vital parameters such as corrosion potential, pitting, and repassivation potentials. This information is provided by the electrochemical techniques (ASTM G3-89), which include potentiodynamic, cyclic polarization, and electrochemical noise measurements.

2.3.2 Potentiodynamic Electrochemical Measurements

Potentiodynamic test monitors the changes in anodic and cathodic current over a given potential range. It provides information on the corrosion potential, the potential region for passivity, and cathodic and anodic current density curves [52].

2.3.3 Cyclic Polarization Electrochemical Measurements

Cyclic polarization electrochemical test monitors the changes in anodic and cathodic current densities as the potential is reversed from the anodic to the cathodic direction to form a hysteresis loop. It reveals the pitting and repassivation potentials, active, passive, and transpassive regions, and provides information on the passive and critical currents.

2.3.4 Electrochemical Noise Measurements

Electrochemical noise (ECN) measurements record fluctuations in corrosion current and open circuit potential on the corroding surface with respect to time. These changes correlate very well with localized corrosion attack [53]. Therefore, electrochemical noise data provide useful information on the corrosion behaviour of materials in different electrolytes and the dominant corrosion mechanisms at different stages in the corrosion process [53-55].

The current and potential data obtained by electrochemical noise measurement may be analyzed qualitatively, statistically, or as frequency domain transforms [53]. Qualitative analysis provides information on the intensity of corrosion activity (such as microgalvanic corrosion and/or breakdown of protective oxide film) which correlates with the severity of potential fluctuations per unit time. Fluctuations in open circuit potential can also be related to the prevalent corrosion mechanism. Furthermore, the direction of potential drift as exposure time increases also reveals any increase or decrease in corrosion activity [54]. Generally, an increase in open circuit potential correlates with passivation or repassivation activity, while a decrease reveals pit initiation and/or propagation [54]. Statistical analysis involves the examination of derived quantities such as the mean, standard deviation, variance, root mean square, etc. Frequency domain analysis utilizes power spectra density.

Corrosion current transients are directly related to localized corrosion on the corroding surface. Corrosion current increases during pit nucleation and propagation, but decreases during passivation or repassivation of metastable or stable pits [55]. Furthermore, the rate of change of current transients reveals the nature of the transition between pit formation and repassivation activities and vice versa [54, 55]. Similarly, when the average current or average potential values are plotted against time, the emerging curve shows the variation of the net corrosion activity resulting from the activities of pit dissolution and passivation with time. Pit formation occurs when the pit dissolution kinetics is greater than that of pit passivation. On the other hand, if the kinetics of pit passivation is greater than that of pit dissolution, pits repassivate [55].

Cheng *et al.* [54] studied the corrosion behaviour of AA2024, AA7075, and pure aluminum using electrochemical noise potential measurements. They observed that the potential amplitude of AA2024, which has a high density of intermetallic phases containing Cu, was much greater than those of AA7075 and pure Al. In addition, the potentials of AA2024 and AA7075 decreased with time indicating that the intensity of corrosion decreased with immersion time. In the same investigation, the potential electrochemical noise data of pure aluminum was different from those of AA2024 and AA7075. The corrosion of pure aluminum specimens was attributed to a breakdown of the surface oxide film, while AA2024 and AA7075 corroded by microgalvanic action initiated by the potential differences between the intermetallic phases and the matrix.

2.3.5 Optical Microscopy

Optical microscopy is used to examine the microstructure and morphology of samples before and after exposure to a corrosive medium in order to evaluate the severity of corrosion attack. Properly polished specimens examined using optical microscopes may show presence of intermetallic phases which are involved in corrosion.

2.3.6 Scanning Electron Microscopy (SEM)

Scanning electron microscopy is used to examine the microstructure and morphology of samples at a much greater resolution than optical microscopy. SEM provides detailed information on the severity of corrosion and the presence of intermetallic phases in the specimen. SEM equipped with Energy Dispersive X-ray Spectrometry (EDS) is used to study the chemical constituents of protective oxide films, intermetallic phases, and corrosion products.

2.4 Fly Ash

Fly ash is a light-weight by-product of coal combustion in thermal power plants. Its morphology reveals predominantly spherical glassy particles, while its density ranges between 1.3 g/cm^3 to 4.8 g/cm^3 [29, 32]. Its main components are the oxides of silicon, aluminum, iron, and calcium and small amounts of the oxides of other common elements such as magnesium and titanium are also present depending on the type and

mineralogy of the coal [29, 30]. The phases present in fly ash particles have been identified by x-ray diffraction, as quartz, mullite, lime, spinel, hematite, and ferrite [35].

Fly ash may be classified using either the ASTM classification or the Canadian specification. ASTM C 618 has classified fly ash into 2 groups, namely, classes C and F. Class C is generated from the combustion of lignite and has a lime content of 15-30 wt.%. Class F, which is low in lime (<7 wt.%), is obtained from the combustion of anthracite, bituminous or sub-bituminous coal [30]. Fly ash may also be grouped as dry bottom ash, wet bottom ash, and economizer ash. The Canadian Standard Association (CSA A23.5) has divided fly ash based on its calcium content into classes F, CI, or CH. Table 2.1 shows the calcium oxide content of the different types of fly ash used on the CSA A23.5 standards.

2.5 Aluminum Alloys

Aluminum alloys are classified based on manufacturing process into two groups, namely: cast and wrought aluminum alloys. Wrought alloys are designed to undergo bulk mechanical deformation processes such as extrusion, rolling, and forging to form aluminum products. Cast alloys, on the other hand, form aluminum products by solidifying in moulds. Cast and wrought aluminum can be sub-classified into two groups, namely, heat treatable and non-heat treatable aluminum alloys. Heat treatable alloys rely on heat treatment processes such as solutionizing, quenching, and precipitation or age-hardening to alter their mechanical, microstructural, and chemical

Table 2.1. Canadian fly ash classification according to CSA A23.5.

Type	Wt.% CaO
F	< 8
CI	8-20
CH	> 20

properties. The properties of non-heat treatable alloys, on the other hand, can not be altered by heat treatment process. Therefore, they depend on strain-hardening to alter their properties.

The wrought and cast aluminum alloy compositions are classified according to their major alloying element. For the cast compositions, a 4-digit system is used. The 1xx.x series represents the unalloyed composition. Copper is the major alloying element for the 2xx.x series alloys. 3xx.x designates alloys in which manganese is the principal alloying element. 4xx.x series alloys are mainly alloyed with silicon, while the 5xx.x series contain a relatively high proportion of magnesium. 6xx.x series are alloyed principally with magnesium and silicon. Zinc is the main alloying element in the 7xx.x series alloys, while the 8xx.x series is mainly alloyed with tin.

2.6 Casting Aluminum Alloy A535

Casting aluminium alloy A535 is a non-heat treatable Al-Mg alloy with an excellent combination of strength, machinability, castibility, ductility, shock resistance, and

fatigue strength [51, 56, 57]. In spite of its admirable mechanical properties, there is still a dearth of information on aluminum alloy A535. The only studies which exist in the open literature are the studies conducted in References [33-36] and [56, 57]. Gikunoo [33-36] investigated the mechanical properties of A535 and its composites reinforced with fly ash, while Fasoyinu *et al.* [56-57] studied the mechanical properties, metallography, and gravity permanent mold casting of Al-Mg A535.

2.7 Corrosion of Aluminum

Aluminum resists corrosion attack in neutral, mildly acidic, and alkaline solutions by forming a thin, tenacious, protective oxide film. Electrochemical, chemical, and environmental changes such as polarization, changes in pH, and the solubility of corrosion products affect the stability of this oxide film.

As aluminum is a very active metal, it oxidizes to Al^{3+} in acid solutions with pH below 3. In alkaline solutions with pH above 9, it is reduced to aluminate ions (AlO_2^-). In solutions with pH between 4 and 9, aluminum instantaneously covers its surface with an oxide film and resists corrosion attack, that is, aluminum passivates [52]. A schematic representation of the zones of corrosion, immunity, and passivity of aluminum in water at 25^{o}C is shown in Figure 2.1. Pourbaix [58] stated that "in practice, the corrosion behaviour of aluminum is determined essentially by the behaviour of the oxide film with which it is almost always covered in the corroding media. Cases of bad resistance to

corrosion are often connected with a change in this oxide film, notably in its degree of hydration and porosity".

Aluminum oxide (Al_2O_3) exists in various forms such as α-alumina or corundum (in the rhombohedral system), β-alumina (with hexagonal crystals), γ-alumina (with cubic crystals), and δ-alumina (with rhombohedral crystals) [58]. On the other hand, aluminum hydroxide, $Al(OH)_3$, exists as a gel which is amphoteric in nature. That is, it can react as an acid or a base. Aluminum hydroxide gel is not stable but crystallizes progressively to form different hydrated products as follows [58]: firstly, to monohybrate γ-$Al_2O_3.H_2O$ or bohmite (with rhombohedral crystals); secondly, to trihydrate $Al_2O_3.\ 3H_2O$ or bayerite (in the monoclinic system); and then, to a trihydrate hydroxide called hydrargillite (in the monoclinic system). Furthermore, Pourbaix [58] stated that "the various hydrates formed during the ageing are characterized by an increasing stability and an accompanying variation in all their properties, in particular their solubility in acids, bases, and pure water".

The formation of a protective oxide film on the surface of aluminum is a complex process. Wood [59] reported that the barrier film formed on anodic surfaces is not a layer of pure oxide. It contains imperfections including impurities such as water and solution anions, pores, flaws, and cracks. He defined "pores" as capillaries and cavities visible under high resolution microscopes. Flaws may be defined as thin regions or holes present in the protective film at sites containing second phase particles and gas bubbles. The stability of the oxide film depends on the presence, configuration, density,

and distribution of micro and macro defects such as vacancies and voids, inclusions, second phase particles, crystal structure of the oxide film, and composition, potential, and temperature of the electrolyte [60].

Szklarska-Smialowska [61] reported that localized corrosion of aluminum in halogen-containing electrolyte can occur in the absence of pores, flaws and cracks in the barrier protective film. She reported that Al_2O_3 had a grain boundary thickness of 8.5 nm while the diameters of chloride ion and water molecule were 0.36 and 0.31 nm, respectively [61]. Therefore, it is conceivable that the chloride ions can instantaneously arrive at the metal-passive film interface in a chloride-containing electrolyte. The presence, magnitude, and distribution of defects in the oxide film provide access for the chloride ions to reach the aluminum metal. The transportation of the chloride ions to the metal-passive film interface also depends on chloride ion concentration, temperature, potential, and defect size in the oxide film [61]. Szklarska-Smialowska reported that the penetration of the barrier film by chloride ions and their arrival at the metal-passive film interface are not the rate-determining step in pitting corrosion of aluminum alloys. She stated that the rate-determining step is the formation and maintenance of appropriate solution acidity in the pre-existing defects at the metal-passive film interface. The acidity of the solution within the pits permits the dissolution of aluminum and, consequently, the propagation of pits.

Szklarska-Smialowska [61] reported that repassivation of metastable pits occurs when metal dissolution and hydrolysis do not furnish the critical quantity of hydrogen ions to

sustain low pH for pit propagation. Furthermore, repassivation also occurs when the oxide films formed by aluminum and other alloying elements within the pits are insoluble or partially soluble in the acidic pit environment. Insoluble or partially soluble oxides increase the pitting potential of the aluminum alloy or cause metastable pits to passivate. Passivation of metastable pits drives the repassivation potential of the alloy to more noble potentials.

2.8 Aluminum Alloys and Metal Matrix Composites

Metal matrix composites are materials which consist of a ductile metallic matrix and one or more embedded reinforcing phases. The reinforcing phases may be particles, continuous fiber, whiskers, and laminates. Particulate reinforcing phases such as SiC [13-18], Al_2O_3 [19-22], and garnet [23, 24] are the most commonly used particulates.

2.8.1 Effect of Particulate Reinforcing Phase

The chemical composition, size and distribution of the particles, and the processing route of composites influence their corrosion behaviour [37, 42, 62, 63]. Conflicting observations have been made in the open literature regarding the contribution of SiC particles to the corrosion of the composites. Candan *et al.* [64] reported that the addition of SiC particles to Al-4 wt.% Mg improved the corrosion resistance of the composites over that of the base alloy in 3.5 wt.% NaCl solution. They postulated that the Mg_2Si phase generated from a two-step reaction between liquid Al and SiC hindered the

passage of electrons thus improving the corrosion resistance of the composites. On the other hand, Kiourtsidis *et al.* [62] noted that although SiC was not directly responsible for the enhanced pitting corrosion of aluminum AA2024 Composites in 3.5 wt.% NaCl solution, intermetallic phases surrounding the particles initiated pitting attack of the material. They attributed the pits adjacent to the interdendritic zone to galvanic couples between the cathodic Al_2Cu and anodic α-phases. Furthermore, in the dendrite cores, depletion of Cu created local anodes which coupled galvanically with the α-phase. Similarly, Aylor *et al.* [42] reported that the presence of SiC in AA6061 matrix did not increase the susceptibility of the composites to pitting attack in marine environment. Pits however occurred at the SiC/Al interface. Prado *et al.* [47], Feng et al [50], Griffiths *et al.* [45] also reported that the SiC particles and Al matrix did not form any galvanic couple.

Graphite particles, unlike SiC_p, formed galvanic couple with aluminum matrix. In a galvanic couple between aluminum and graphite, aluminum,which has a more active potential, preferentially corrodes. Saxena *et al.* [25] attributed the inferior seawater corrosion resistance of a 4xx.x cast aluminum alloy (LM-13 alloy), containing 3 wt.% graphite particles, to galvanic corrosion between the cathodic graphite particles and active aluminum matrix. However, the 4xx.x cast aluminum-graphite composites displayed excellent corrosion resistance in SAE-40 engine oil at 150^{o}C. Saxena *et al.* [26] made similar observation while studying AA6061 Composites containing 7 wt.% graphite particles in SAE 30 lubricating oil.

Seah *et al.* [23] reported that the use of inert, ceramic garnet particles, composed mainly of alumino-silicates of calcium (with a chemical formula $Ca_2Al_2(SiO_4)_3$), as a reinforcement in cast aluminum (4xx.x) containing 10-12 wt.% Si improved the corrosion resistance of the composites over that of the base alloy. The superior corrosion resistance of the composites in 1M HCl solution at room temperature was attributed to the restriction of pit growth by the inert garnet. In 3.5 wt.% NaCl solution, Nath *et al.* [27] observed that Al-Mg and Al-Cu composites exhibited superior corrosion resistance than their composites reinforced with mica particles. The inferior corrosion resistance of the mica reinforced composites was attributed to the distortion of the passive protective films and provision of pit nucleation sites by the mica particles.

Bienias *et al.* [37] reported that the addition of fly ash increased the corrosion rate of an Al-Si (4xxx) alloy in 3.5 wt.% NaCl solution at pH 7. They attributed the decrease in corrosion resistance of the composite to increased galvanic corrosion between the Si liberated in the reaction between silica in fly ash particles and liquid aluminum. Furthermore, the deterioration of the corrosion resistance of the composites was also attributed to the porosities created in the matrix by the introduction of fly ash particles [37]. These porosities distorted the protective oxide layer; thus increasing the accessibility of Cl^- ions to the aluminum metal. Similarly, Ramachandra *et al.* [38] observed that the corrosion resistance of an Al-7.2 wt.% Si reinforced with 5 wt.%, 10 wt.%, 12 wt.%, and 15 wt.% fly ash decreased as their fly ash contents increased.

2.8.2 Effect of Mg

The strength of commercially pure aluminum is enhanced by the addition of alloying elements. While alloying elements increase its strength, hardness, and Young's modulus, they can adversely affect its corrosion resistance. Many authors have studied the effect of alloying elements on the corrosion resistance of aluminum. Bhattamishra [65] observed that the segregation of Si particles and Mg_2Si at the grain boundaries were responsible for the intergranular corrosion of two Al-Mg-Si (6xxx) alloys in chloride and acid media. In another study, Baer *et al.* [66] investigated the influence of Mg on the corrosion of Al. The corrosion potential and film formation on pure Al, Al implanted with Mg, a 7 wt.% Mg-Al alloy, and Al_3Mg_2 phase were studied in 3.5 wt.% NaCl solution. Al, Al implanted with Mg, and the 7 wt.% alloy displayed similar open circuit potentials, with the potential of the Al_3Mg_2 phase being significantly different from rest. The authors concluded that hydrogen molecules generated at the Al_3Mg_2 particles in alloys with high magnesium content was responsible for the increased susceptibility to stress corrosion cracking. Bovard [67] also attributed the increase in the susceptibility of AA5083 to stress corrosion cracking and intergranular corrosion with increased sensitization time to the precipitation of the β-phase (Mg_2Al_3) on the grain boundaries.

The work of Flores *et al.* [68] on Al-Mg binary alloys, AA5083 (with 4.52 wt.% Mg) and AA5754 (with 2.82 wt.% Mg) in HNO_3 revealed that AA5754 alloy with low Mg content was more resistant to intergranular corrosion (IGC) attack at room temperature

than AA5083. However, susceptibility to IGC increased with increase in temperature. As the temperature increased, the amount of Al_3Mg_2 precipitates at the grain boundaries also increased. Intergranular corrosion attack was observed in AA5083 with 4.52 wt.% Mg content at room temperature since the fabrication process had induced the precipitation of the Al_3Mg_2 phase in the alloy. The authors concluded that the presence of higher proportion of Mg in the alloy increased the susceptibility of the tested Al-Mg alloys to IGC attack.

Intermetallics containing Mg have contributed to localized corrosion attack of Al-Zn-Mg alloys. Al-Zn-Mg alloys with 2.5 wt.% Mg and variable Zn content suffered pitting corrosion in the vicinity of $MgZn_2$ precipitates in 3.5 wt.% NaCl solution at pH 7 [69]. The severity of pitting attack increased as the amount of $MgZn_2$ precipitates in the samples increased. The presence of $Al_4Mg_8Si_7Cu_2$ (Q-phase) and Mg_2Si precipitates in Al-Mg-Si alloys with low Cu (0.0005 wt.%) and high Cu (0.12 wt.%) content exposed to air in industrial and marine environments was the cause of intergranular corrosion [70]. The susceptibility to IGC increased with increase in Cu content of the samples. Sameljuk *et al.* [71] reported that the dissolution of Zn-Mg and Zr-Sc precipitates in 0.3 and 3 wt.% NaCl solutions created sites for the initiation of pitting corrosion in an Al-Zn-Mg alloy containing of 5 wt.% Zn, 3 wt.% Mg, and 0.7 wt.% Zr. Furthermore, Leyun *et al.* [72], who studied seawater corrosion attack on a 5xxx series Al-Mg alloy containing 6 wt.% Mg, observed severe IGC at grain boundaries containing $(MnFe)Al_6$.

The addition of Mg to a binary age-hardenable Al-Li alloy system improved its corrosion resistance [73]. In the Al-Li binary system, the metastable Al_3Li or δ' phase is responsible for strengthening the binary alloy. However, it transformed to the more insidious AlLi or δ phase which deposited along the grain boundaries and increased susceptibility to SCC and IGC. In the same investigation, the overaged Al-Li-Mg alloys formed Al_2MgLi which retarded the transformation of δ' to δ and, consequently, improved the corrosion resistance of the alloy.

Flores *et al.* [68] found that the oxide film formed on Al-Mg binary alloys is significantly different from that formed on pure aluminum. The density and distribution of Mg atoms in the oxide layer was a function of temperature and Mg concentration. The incorporation of Mg into the aluminum protective film did not significantly affect its corrosion resistance. However, high Mg content predisposed the alloys to IGC attack at low sensitization temperatures because of grain boundary precipitation of Al_3Mg_2 phase. Baer *et al.* [66] reported that the presence of Mg in Al did not significantly change the thickness of the oxide film in 3.5 wt.% NaCl solution at open circuit potential. However, there were significant differences in Mg/Al ratios between films formed in 3.5 wt.% NaCl solution and those formed in air.

3. MATERIALS AND EXPERIMENTAL PROCEDURE

This chapter discusses the materials and experimental methods used as well as the problems and challenges encountered in this study.

3.1 Materials

The materials investigated in this work were cast aluminium alloy A535 and its composites reinforced with 10 wt.% fly ash (A535/fly ash/10_p) and 15 wt.% fly ash (A535/fly ash/15_p) as well as a hybrid composite comprising 5 wt.% fly ash and 5 wt.% SiC (A535/hybrid/10_p). The composites were fabricated using the stir casting technique. Table 3.1 shows the chemical composition of A535 as specified in ASTM B108, while Tables 3.2 and 3.3 show the chemical composition of A535 alloy and the reinforcing fly ash, respectively, as reported in Reference 35. The chemical composition of A535 was determined by Gikunoo and Oguocha [35] using Electron Probe Microanalyzer (EPMA), while fly ash was analyzed by X-ray Fluorescence Spectrometry (XFS).

Samples of aluminium alloys AA5083-H116 and AA2618 were received from Alcan Aluminium Limited, Kingston, Ontario, and Duralcan Aluminium, San Diego, California, USA, respectively. Their corrosion behaviour was compared with that of A535. AA5083-H116 is a wrought non-heat treatable Al-Mg alloy, while AA2618 is an

Table 3.1. Chemical compositional limits of A535.

Element	Mg	Cu	Si	Mn	Fe	Ti	Others	Al
Weight %	6.2-7.5	0.05	0.15	0.10-0.25	0.15	0.10-0.25	0.15	Bal

Table 3.2. Chemical composition of A535 obtained using EPMA [35].

Element	Mg	Cu	Si	Fe	Ti	Al
Weight %	6.17	0.01	0.01	0.02	0.04	Bal

Table 3.3. Chemical composition of fly ash obtained by XFS [35].

Compound	SiO_2	Al_2O_3	Fe_2O_3	MgO	CaO	TiO_2	K_2O	Na_2O	SO_3
Weight %	44.8	22.2	24.0	0.9	1.8	0.8	2.4	0.9	1.4

Balance = oxides of other trace elements

age hardenable Al-Cu-Mg alloy. The chemical compositions of these alloys are presented in Tables 3.4 and 3.5, respectively.

Test samples of A535 and its composites were tested in the as-cast condition. The samples were machined into rectangular specimens with dimensions of 1cm by 1cm by 0.5 cm, giving a total surface area of 4 cm^2. The porosities contained in the composites hampered machining the specimens accurately to the designed specifications. A535/fly ash/15_p has the highest level of porosity [36] and the smallest external surface area after

Table 3.4. Chemical composition of AA5083-H116.

Element	Cu	Fe	Mg	Mn	Si	Ti	V	Cr	Al
Wt.%	0.03	0.275	4.942	0.538	0.04	0.004	.012	0.091	Bal

Table 3.5. Chemical composition of AA2618.

Element	Si	Fe	Cu	Mg	Ni	Ti	Al
Wt.%	0.18	1.19	2.34	1.59	1.05	.007	Bal

machining. The actual surface areas of the specimens of the composites were estimated from a scaled (graph) paper on which the surface area of every specimen was mapped prior to each experiment. The actual surface areas of the composites estimated using graph paper were comparable to the surface areas calculated using percentage porosities obtained by Gikunoo [36] (See Appendix B). He reported that the percentage porosity of the specimens increased with fly ash content from 0% in A535 alloy to 9.52% A535/fly ash/15_p. A535/hybrid/10_p and A535/fly ash/10_p had porosity contents of 3.2% and 5.04%, respectively. The actual surface area of the composites was then estimated by subtracting the area occupied by porosity from the designed surface area (SA) using the expression

$$SA = 2[(lxw) + (wxh) + (lxh)] - \%\, porosity\{[2(lxw) + (wxh) + (lxh)]\} \quad (3.1)$$

where *l*, *w*, and *h* represents the length, width, and height of the specimen, respectively, and % porosity represents the porosity content of the composites expressed in percentage. Samples of AA5083-H116 were tested in the as-received (as-rolled) condition. AA2618 samples were solutionized at $530 \pm 5\,^{o}C$ in a furnace for 2 hours and quenched in laboratory water and allowed to age naturally.

3.2 Experimental Methods

3.2.1 Immersion Corrosion Test

Standard immersion corrosion test was used to investigate the weight loss and corrosion rates of each material in the specified electrolytes. Test specimens of each material were polished using several grades of emery paper ranging from 240 to 600 grit, rinsed in distilled water and methanol, and dried. They were then weighed using an electronic weighing balance (Shimadzu Corporation, Model AUW120D). The sample weights were measured in grams to 5 decimal places. After weighing, the specimens were immersed in 3.5 wt.% NaCl solution of different pH or in fresh water collected from the South Saskatchewan River. The salt used was produced by the Canadian Salt Company Limited, Pointe-Claire, Quebec, Canada. The constituents of the salt were NaCl and yellow prussiate of soda (anti-cracking agent). The pH values used for the salt solution were 4, 7 and 9. These pH values were selected to simulate mildly acidic, neutral, and alkaline conditions in which structural applications made of A535 and its composites

may be exposed. The pH of the fresh water was determined to be 8.2. All tests were carried out at room temperature and exposed to atmospheric air.

Table 3.6 shows the number of specimens of each material used in the immersion test, while Figure 3.1 shows the immersion test apparatus. The specimens were immersed in the electrolytes using plastic crocodile clips hung by plastic threads. The possibility of crevice corrosion of the samples was reduced as the contact areas between the crocodile clips and sample surfaces were negligible. The plastic threads were attached to a wooden support as shown in Figure. 3.1. The solution-to-specimen surface area ratio was about 312.5 ml cm^{-2}. After each immersion test, the samples were extracted from the electrolyte and cleaned in 70 wt.% HNO_3 (specific gravity = 1.4134) for 1 to 5 minutes as specified by ASTM G1 (2003). The corrosion products on the surface of the specimens were then removed by rubbing gently against a soft wet nylon sponge drenched in water. The specimens were then ultrasonically cleaned in methanol. To ensure that any water which might have seeped into the compositess pores during immersion was removed, the specimens were placed in an air furnace maintained at 100 ^{o}C for 3 hours. They were subsequently cooled to room temperature and re-weighed. The exposure times used were 1, 3, 5, 7, 10, and 14 days (giving a cumulative total exposure time of 40 days for each specimen). The cleaning procedure was observed after each exposure. To account for metal loss resulting from cleaning of the specimens, the weight loss of uncorroded control specimens was obtained using the same cleaning procedure. The weight loss for the

Table 3.6. Number of samples used in the immersion corrosion test.

pH	Number of samples			
	A535	A535/hybrid/10p	A535/fly ash/10p	A535/fly ash/15p
7	2	2	2	2
4	2	2	2	2
9	2	2	2	2
8.2 (South Saskatchewan River water)	2	2	2	2

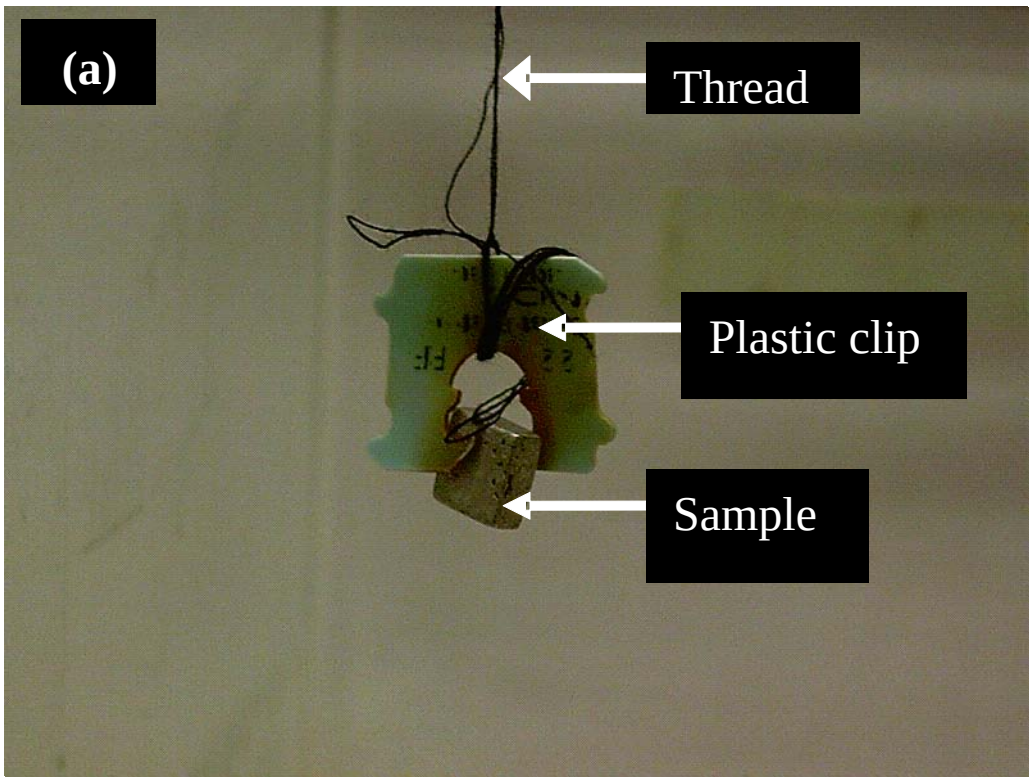

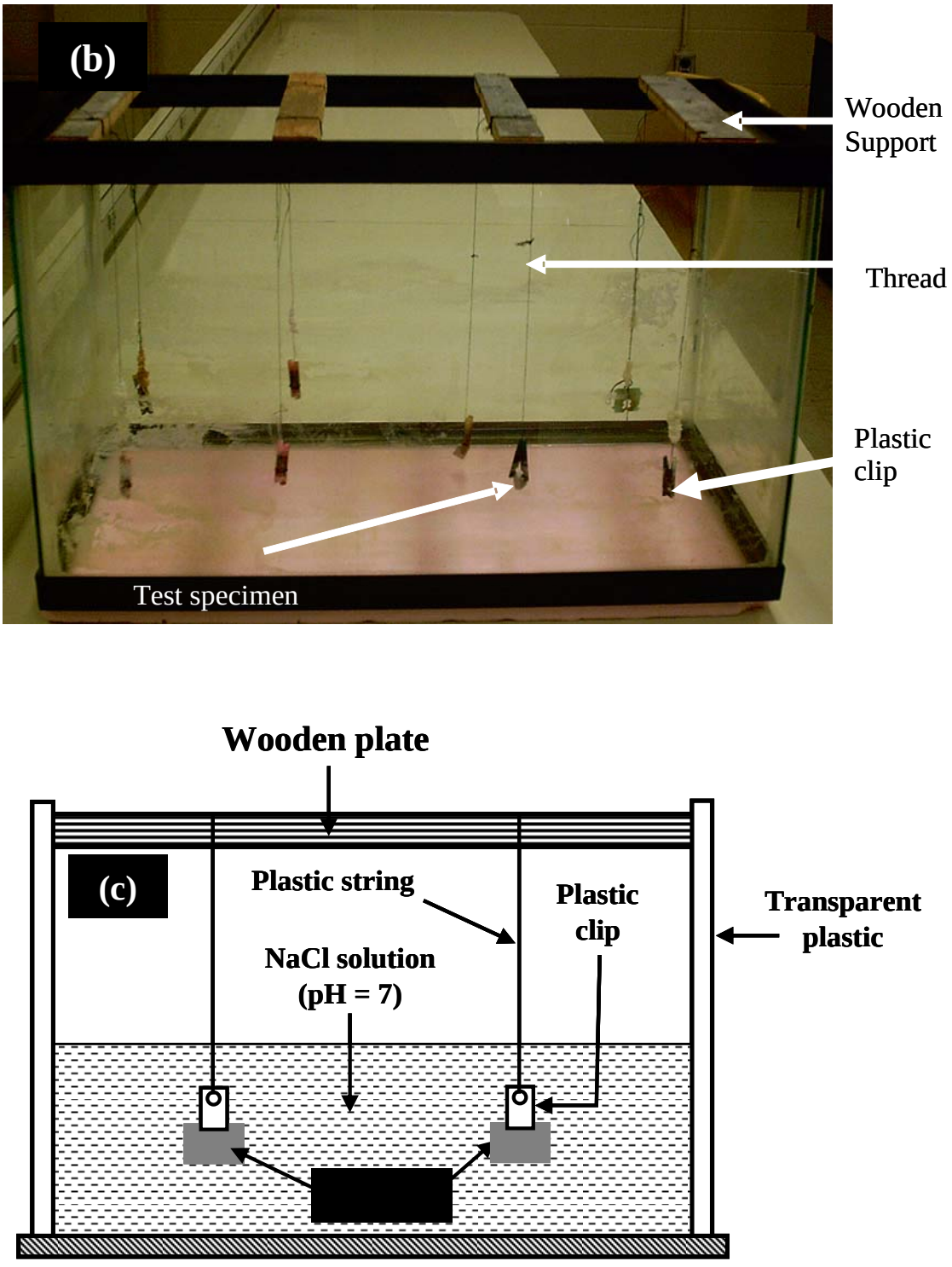

Figure 3.1. Weight-loss corrosion test apparatus: (a) specimen suspended by plastic clip and thread (b) immersion corrosion cell (c) a schematic of the immersion corrosion cell.

control specimens was used to correct for metal loss of the alloy and composites resulting from the cleaning procedure (ASTM G1: 7.1.1). Weight loss data were obtained by subtracting weights obtained after each exposure to the electrolyte from the initial weights before the exposure (See Appendix A). The corrosion rate of each specimen in mm/year was determined using the expression [51]:

$$mm/yr = \frac{87.6W}{DAt} \tag{3.2}$$

where W is weight loss in mg, D is density in g/cm^3, A is surface area in cm^2, and t is time in hours. A sample corrosion rate calculation is shown in Appendix C.

3.2.2 Electrochemical Corrosion Measurements

Three electrochemical measurements were carried out, namely: potentiodynamic, cyclic polarization, and electrochemical noise (ECN) measurements. All electrochemical corrosion tests were conducted using a Gamry ECM8 electrochemical multiplexer system equipped with a PCI4 potentiostat (see Figure 3.2). The samples were machined to the same dimensions as those used for immersion test, with a total surface area of 4 cm^2. A 6.35 mm (0.25 inch) diameter hole was drilled through each specimen to accommodate the working electrode (WE) holder (see Figure 3.3). The surface area of the alloy was obtained by subtracting the surface area of the hole in the specimen from the rectangular surface area of 4 cm^2. As in the case of immersion test, the actual

Figure 3.2. The ECM8 electrochemical multiplexer system equipped with a PCI4 potentiostat.

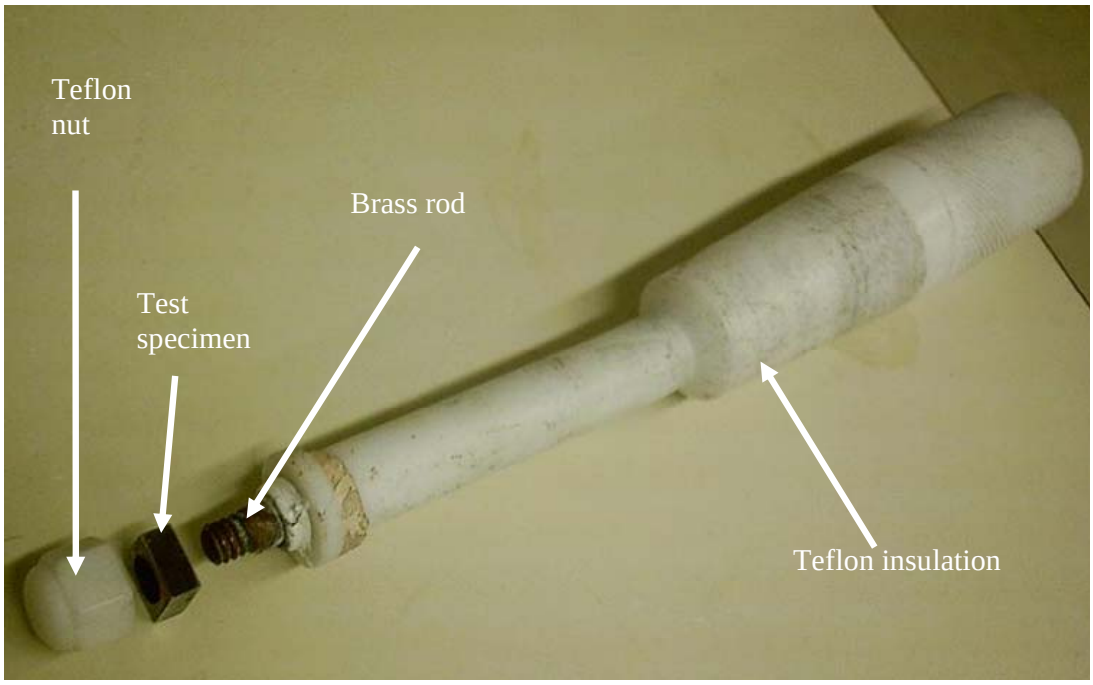

Figure 3.3. Exploded view of the working electrode holder.

surface areas of the compositess were adjusted to account for porosities. The WE holder was a brass rod, the mid-section of which was covered by teflon in such a way that both ends of the brass rod were exposed to allow other connectors to be attached to it. The test samples were ground using 240 to 600-grit emery papers, rinsed in distilled water and methanol to remove any surface contaminants, and dried. The clean sample was then mounted on the WE holder. The holder was connected to the multiplexer at one end using crocodile clip while the other end held the working electrode (the sample to be studied) between two teflon washers snugly held in position by a teflon nut as shown in Figure 3.4. The WE holder was designed to ensure that the test sample made adequate electrical contact with the brass rod. The corrosion current generated by the sample was therefore effectively conducted to the multiplexer through the brass rod. A saturated calomel electrode (SCE) was used as the reference electrode. The counter electrode was a graphite rod measuring 6.1 mm (0.24 inch) diameter and 30 cm (12 inches) in length (see Figure 3.4). Figure 3.5 presents a schematic diagram of the electrode and holder assembly, while Figure 3.6 shows an enlarged picture of the corrosion cell.

1. Potentiodynamic Measurements

Potentiodynamic measurements were used to examine the behaviour of anodic and cathodic currents passing through each material when the potential was varied over a given potential range. The information obtained from this test included corrosion potential (E_{corr}) and cathodic and anodic current density curves. The direct current (DC)

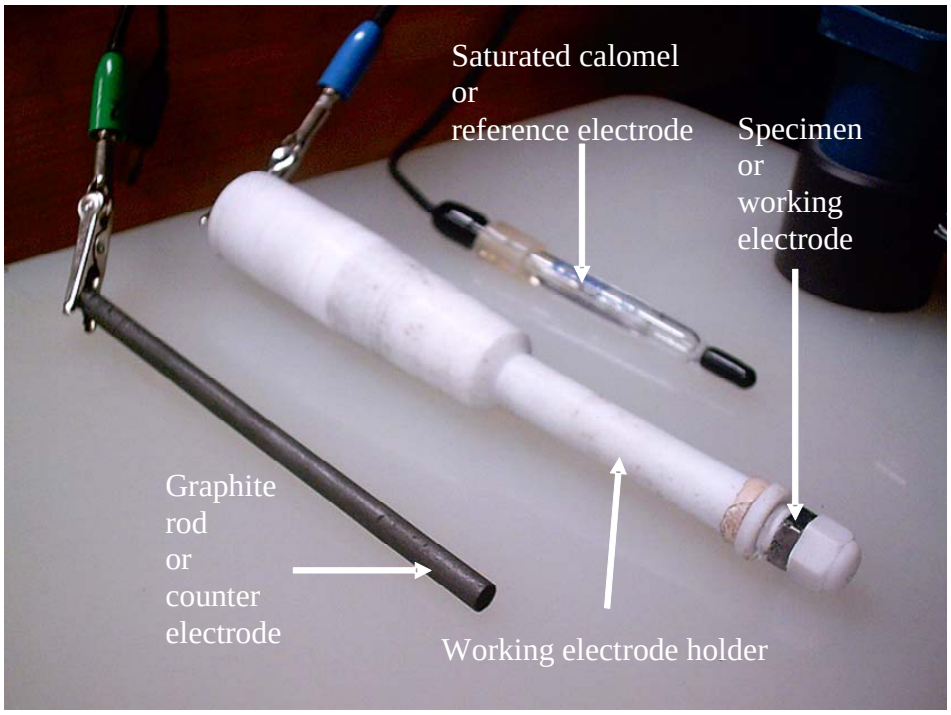

Figure 3.4. Working electrode, reference electrode (SCE) and graphite counter electrode used in the study.

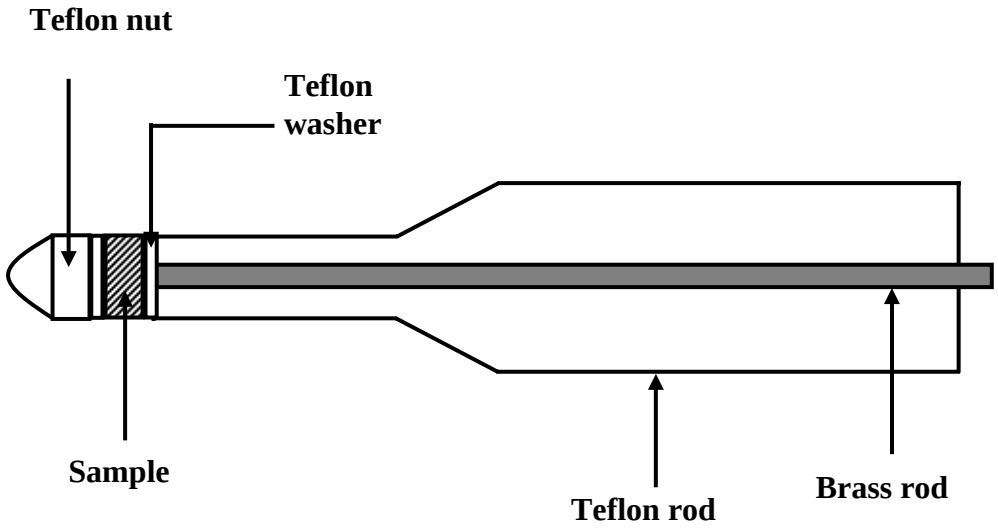

Figure 3.5. A schematic diagram of the working electrode and holder assembly.

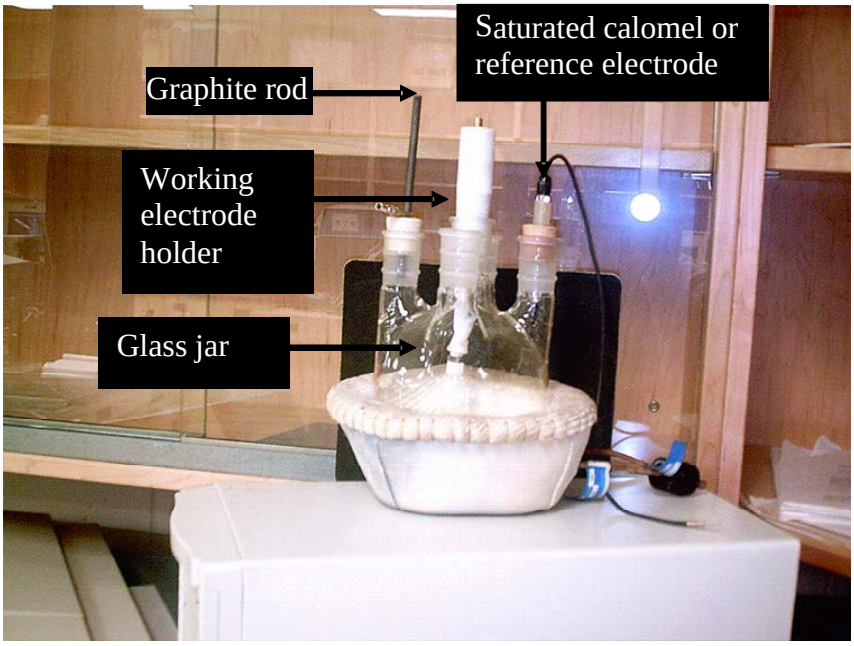

Figure 3.6. Corrosion cell and electrodes used in electrochemical measurements

corrosion module was used for the potentiodynamic measurements. Before each potentiodynamic scan, the electrochemical cell was stabilizied for 30 minutes to reduce fluctuation in the open circuit potential (OCP) before the potential was ramped from an initial voltage of -0.8 V with respect to OCP to 0.2 V with respect to OCP at a scan rate of 1 mV/s. To arrive at a scan rate of 1 mV/s, different scan rates were tried until good and repeatable results were obtained. The potential range spanned from -1.1 V to +1.6 V. At least two scans were acquired for each specimen to ensure representative results and reproducibility (See Appendix E). The parameters used for the potentiodynamic measurements are presented in Table 3.7. Table 3.8 provides information on the number of specimens used for the potentiodynamic corrosion measurements.

Table 3.7. Parameters used in the potentiodynamic electrochemical test.

Parameter	All Materials
Initial voltage (V) wrt OCP	-0.8
Final voltage (V) wrt OCP	0.2
Scan rate (mV/s)	1
Sample period	5

Table 3.8. Number of samples used in the potentiodyanmic corrosion test.

pH	Number of samples			
	A535	A535/hybrid/10_p	A535/fly ash/10_p	A535/fly ash/15_p
7	2	2	2	2
4	2	2	2	2
9	2	2	2	2
8.2 (South Saskatchewan River water)	2	2	2	2

2 Cyclic Polarization Measurements

Cyclic polarization measurements were used to investigate the pitting resistance of the test materials. The DC corrosion module was used for the cyclic polarization measurements. In each scan, the potential of the specimen was swept towards the

anodic direction and then reversed towards the cathodic direction at a scan rate of 1 mV/s after a limiting value of current (apex current) and/or potential (apex voltage) had been reached. The apex current density was adjusted for each sample and each solution pH from 2 mA/cm^2 in the neutral salt water solution to 7 mA/cm^2 in acidified solution maintained at pH 3 in order to obtain a proper cyclic polarization plot. Similarly, the apex voltage was adjusted from 1 V in the neutral salt water solution to 5 V in the fresh water electrolyte. The scan started at -0.8 V with respect to the OCP and ended at -0.7 V with respect to the OCP after generating the cyclic loop. The potential range spanned from -1.1 V to -1.3 V. The resultant potential versus current density plot provided information on the corrosion potential (E_{corr}), pitting potential (E_p), repassivation potential (E_{rp}), and the hystersis loop (area between pitting and repassivation potentials). Parameters used for cyclic polarization measurements are presented in Tables 3.9 - 3.14. In the tables, the term “sample period” determined the spacing between data points.

Table 3.9. Parameters used for cyclic polarization measurement in fresh water.

Parameters	A535	A535/hybrid/10_p	A535/fly ash/10_p	A535/fly ash/15_p
OCP (V_{SCE})	-0.25	-0.22	-0.26	-0.33
Initial voltage (V_{SCE})	-0.80	-0.80	-0.80	-0.80
Final voltage (V_{SCE})	-0.70	-0.70	-0.70	-0.70
Apex voltage (V_{SCE})	5.00	5.00	1.50	1.50
Apex current (mA/cm^2)	2.00	2.00	2.00	2.00
Forward scan rate (mV/s)	1.00	1.00	1.00	1.00
Reverse scan rate (mV/s)	1.00	1.00	1.00	1.00
Sample period (*s*)	5.00	5.00	5.00	5.00

All voltages are with respect to OCP.

Table 3.10. Parameters used for cyclic polarization measurement in neutral 3.5 wt.% NaCl solution.

Parameters*	A535	A535/hybrid/10_p	A535/fly ash/10_p	A535/fly ash/15_p
OCP (V_{SCE})	-0.27	-0.33	-0.29	-0.33
Initial voltage (V_{SCE})	-0.80	-0.80	-0.80	-0.80
Final voltage (V_{SCE})	-0.70	-0.70	-0.70	-0.70
Apex voltage (V_{SCE})	1.00	1.00	1.00	1.20
Apex current (mA/cm^2)	2.00	2.00	2.00	2.00
Forward scan rate (mV/s)	1.00	1.00	1.00	1.00
Reverse scan rate (mV/s)	1.00	1.00	1.00	1.00
Sample period (s)	5.00	5.00	5.00	5.00

*All voltages are with respect to OCP.

Table 3.11. Parameters used for cyclic polarization measurement in 3.5 wt.% NaCl solution maintained at pH 4.

Parameters*	A535	A535/hybrid/10_p	A535/fly ash/10_p	A535/fly ash/15_p
OCP (V_{SCE})	-0.25	-0.32	-0.41	-0.56
Initial voltage (V_{SCE})	-0.80	-0.80	-0.80	-0.80
Final voltage (V_{SCE})	-0.70	-0.70	-0.70	-0.70
Apex voltage (V_{SCE})	1.20	1.20	1.20	1.20
Apex current (mA/cm^2)	2.00	2.00	2.00	2.00
Forward scan rate (mV/s)	1.00	1.00	1.00	1.00
Reverse scanrate (mV/s)	1.00	1.00	1.00	1.00
Sample period (*s*)	5.00	5.00	5.00	5.00

*All voltages are with respect to OCP.

Table 3.12. Parameters used for cyclic polarization measurement 3.5 wt.% NaCl solution maintained at pH 9.

Parameters	A535	A535/hybrid/10_p	A535/fly ash/10_p	A535/fly ash/15_p
OCP (V_{SCE})	-0.39	-0.40	-0.42	-0.42
Initial voltage (V_{SCE})	-0.80	-0.80	-0.80	-0.80
Final voltage (V_{SCE})	-0.70	-0.70	-0.70	-0.70
Apex voltage (V_{SCE})	1.20	1.20	1.20	1.20
Apex current (mA/cm^2)	3.00	3.00	2.00	2.00
Forward scan rate (mV/s)	1.00	1.00	1.00	1.00
Reverse scanrate (mV/s)	1.00	1.00	1.00	1.00
Sample period (*s*)	5.00	5.00	5.00	5.00

*All voltages are with respect to OCP.

Table 3.13. Parameters used for cyclic polarization measurement in 3.5 wt.% NaCl solution maintained at pH 3.

Parameters	A535	A535/hybrid/10_p	A535/fly ash/10_p	A535/fly ash/15_p
OCP (V_{SCE})	-0.38	-0.46	-0.42	-0.40
Initial voltage (V_{SCE})	-0.80	-0.80	-0.80	-0.80
Final voltage (V_{SCE})	-0.70	-0.70	-0.70	-0.70
Apex voltage (V_{SCE})	1.20	1.20	1.20	1.20
Apex current (mA/cm^2)	7.00	7.00	7.00	7.00
Forward scan rate (mV/s)	1.00	1.00	1.00	1.00
Reverse scan rate (mV/s)	1.00	1.00	1.00	1.00
Sample period (*s*)	5.00	5.00	5.00	5.00

*All voltages are with respect to OCP.

3 Electrochemical Noise Measurement

The electrochemical noise measurement was used to investigate the stability of the aluminium oxide films formed on the specimens in a given electrolyte and the initiation and propagation of pits in the specimens. The electrochemical noise module and the potentiostatic mode electrochemical noise were used for the measurements. All samples were tested at the open circuit potential for a period of 4 hours immediately after they

were exposed to the 3.5 wt.% NaCl solution maintained at pH 7, 4, 3, 9 and in South Saskatchewan River water. The current and potential transients were recorded.

Qualitative analysis of the fluctuations in the open circuit potential provided information on the intensity of the corrosion activity (such as micro-galvanic corrosion and/or breakdown of protective oxide film). Fluctuations in open circuit potential provided information on the dominant corrosion mechanism. The average current and average potential values were determined by calculating the arithmetic mean of the transient current and potential data obtained during each 25 minutes of exposure. The plot of average current or average potential against time provided information on the net corrosion activity involving pitting and passivation. The electrochemical noise parameters used in this study are presented in Table 3.14.

3.3 Optical Microscopy

Optical microscopy was used to provide information about the microstructure of A535 alloy and the composites before and after exposure in 3.5 wt.% NaCl solution maintained at pH 7, 4, 3, 9, and in South Saskatchewan River water. The samples for optical microscopy were encased in an epoxy mold and polished using 240-600 grit emery papers and diamond paste (1 μm) to high smoothness, rinsed in distilled water and methanol, and dried. All specimens were imaged before and after immersion in the electrolytes for 14 days. A Nikon Optiphot^{TM} upright microscope equipped with Paxcam 3^{TM} CCD camera interfaced with Pax-it^{TM} image analysis software and a Zeiss Axiovert

Table 3.14. Parameters used for the electrochemical noise measurement in 3.5 wt.% NaCl solutions maintained at pH 7, 4, 3, 9, and in South Saskatchewan River water.

Parameter	All Materials
Block time (s)	4
Sample period (s)	0.05
Repeat time (min)	0.25
Total time (hour)	4

25 inverted microscope powered by Clemex Vision (version 3.0.037) data acquisition and analysis software were used in this study.

3.4 Scanning Electron Microscopy

The specimens examined using the optical microscope were re-examined using a Scanning Electron Microscope (SEM) in order to determine the morphology of the corroded specimens. All specimens were imaged using a JEOL JSM 5900LV SEM equipped with an Oxford INCA Energy Dispersive X-ray Spectrometer (EDS).

3.5 Water Analysis

The chemical composition of the fresh water collected from the South Saskatchewan River was determined in the Environmental Engineering Laboratory, Civil Engineering Department, University of Saskatchewan. The test was conducted to determine the

presence and quantity of corrosive agents such as chloride and sulphate ions in the fresh water.

4.0 RESULTS AND DISCUSSION

Chapter 4 presents a discussion of the results of experiments carried out in this study. The results of the general corrosion behaviour of A535 alloy is first presented and compared with that of two aluminum alloys, AA5083-H116 and AA2618. The corrosion behaviour of these alloys is fairly reported in the open literature. The results of the effect of fly ash on the corrosion behaviour of A535 are then presented.

4.1 General Corrosion Behaviour of A535, AA5083-H116 and AA2618 in Neutral 3.5 Wt.% NaCl Solution

The variation of normalized weight loss with exposure time for A535, AA5083-H116 and AA2618 is presented in Figure 4.1. It can be seen that A535 and AA2618 lost the least and greatest weight, respectively, during the exposure period. The weight lost by A535 and AA5083-H116 increased gradually as the immersion time increased. The weight lost by AA2618 was gradual until the third day of immersion after which its weight loss increased sharply for the rest of the exposure period. The variation of the corrosion rate of the alloys with immersion time is presented in Figure 4.2. It can be seen that the highest corrosion rate for each alloy occurred during the first day of immersion. It is also evident that A535 alloy has the lowest corrosion rate. Although

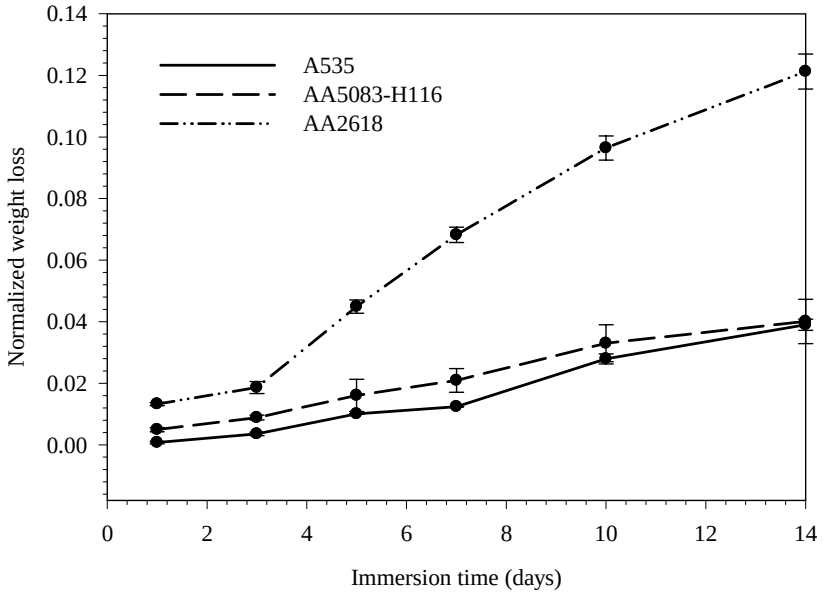

Figure 4.1. Variation of normalized weight loss (i.e. weight loss / initial weight) with time for A535, AA5083-H116, and AA2618 immersed in neutral 3.5 wt.% NaCl solution. Error bars are based on standard deviation.

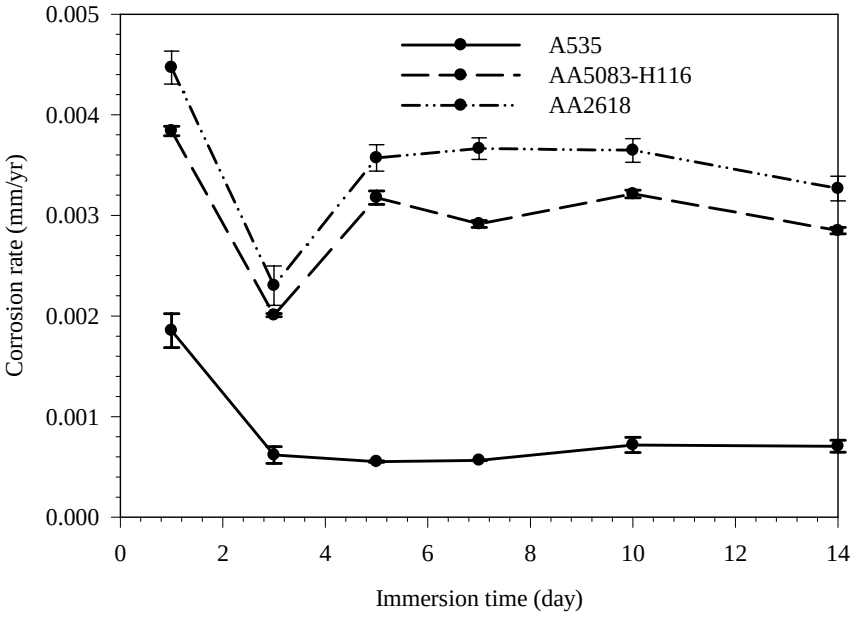

Figure 4.2. Variation of corrosion rate with time for A535, AA5083-H116, and AA2618 immersed in neutral 3.5 wt.% NaCl solution. Errors bars are based on standard deviation.

the corrosion rates of AA5083-H116 and AA2618 decreased rapidly during the first three days of exposure to the electrolyte, they did not remain unchanged as the exposure time increased as in the case of A535. Rather, they increased between the third and fifth day to a certain level and remained practically constant as the exposure time further increased. The differences in the weight loss and corrosion rates of the alloys can be attributed to differing alloy chemistry. There is a substantial difference in Mg content between A535 (6.17 wt.% Mg) and AA5083-H116 (4.942 wt.% Mg). AA2618 has 2.34 wt.% Cu compared to 0.05 wt.% and 0.03 wt.% for A535 and AA5083-H116, respectively.

Figure 4.3 presents the potentiodynamic curves obtained for A535, AA5083-H116, and AA2618. It can be seen that all curves showed similar trends. Table 4.1 summarizes the corrosion potentials, current densities, and Tafel constants of the three alloys. The corrosion potentials are in agreement with the potentials of -546 mV_{SCE}, -704 mV_{SCE}, and -683 mV_{SCE} reported by Turnbull [74] for aluminum alloys AA2024, AA5456, and AA6061, respectively, exposed to 0.1 M NaCl solutions. Similarly, the E_{corr} obtained for AA2014-T6 exposed to NaCl maintained at pH 6 was reported to be -600 mV [75].

Figure 4.3 shows that A535 alloy has more positive corrosion potential (E_{corr}) than A5083-H116 and AA2618, while AA2618 has the most active corrosion potential. Thus, A535 has superior corrosion resistance to the other two alloys. Davis [51] reported that copper–containing aluminum alloys are less resistant to corrosion than other aluminum alloys, while Saraswathi *et al*. [75] reported that the presence of Al_2Cu

Table 4.1. Corrosion potentials, current densities, and Tafel constants of A535, AA5083-H116, and AA2618 immersed in neutral salt solution.

Material	Corrosion potential (mV)	Corrosion current density i_{corr} (μ Acm^{-2})	Tafel constants (mV)
A535 alloy	-415 ± 4.2	0.865 ± 0.01	$\beta_a = 31 \pm 0.15$
			$\beta_c = 36 \pm 0.18$
AA5083-H116	-517 ± 5.8	1.00 ± 0.01	$\beta_a = 36 \pm 0.23$
			$\beta_c = 38 \pm 0.32$
AA2618	-576 ± 4.5	2.34 ± 0.03	$\beta_a = 268 \pm 0.17$
			$\beta_c = 103 \pm 0.33$

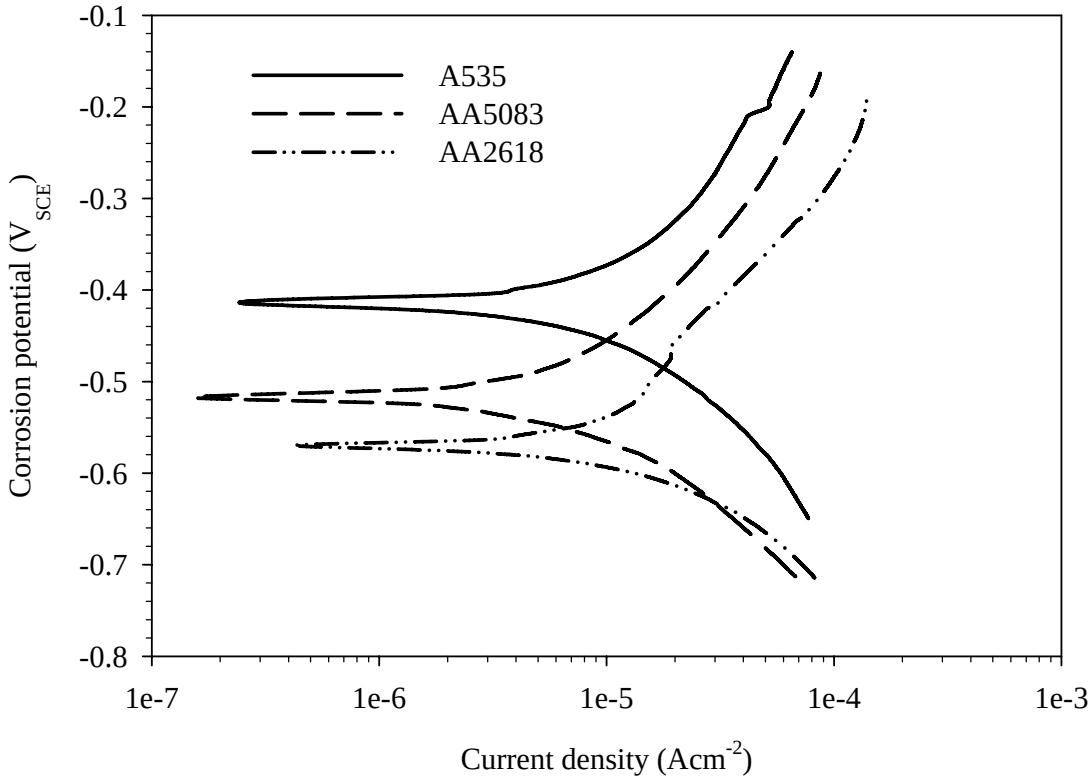

Figure 4.3. Potentiodynamic polarization curves for A535, AA5083, and AA2618 aluminum alloys exposed in neutral 3.5 wt.% NaCl solution.

(or θ phase) in AA2014 alloy contributed to the pitting corrosion attack on the alloy. Birbilis [76] reported that the corrosion potentials (E_{corr}) of Al_2Cu phase and the solid solution of Al-4% Cu alloy (i.e. α phase) in 0.6 M NaCl solution were -695 mV_{SCE} and -642 mV_{SCE}, respectively. The E_{corr} of the θ and α phases are more noble than that of Al, which is -849 mV_{SCE}. Similarly, Buchheit [77] reported that the E_{corr} of Al_2Cu phase in 0.5 M NaCl solution exposed to the atmosphere was -700 mV_{SCE}. The inferior corrosion resistance of Cu-containing Al alloys can be attributed to the dissolution of anodic α-Al phase in the presence of the noble Cu-rich second-phase particles.

Furthermore, the corrosion of the anodic portions of the θ and α phases liberate Cu ions which eventually replates on the matrix. The E_{corr} of Cu exposed to 0.6 M NaCl solution is -220 mV_{SCE} [76]. Cu is therefore cathodic to Al. Al preferentially corroded in the presence of Cu cathodes resulting in decreased corrosion resistance. Similarly, Ambat *et al.* [78], who reported on the influence of alloying elements on the corrosion behaviour of aluminum alloys, attributed the high corrosion rate exhibited by AA2014-T6 in NaCl solutions to its high Cu content.

The results of cyclic polarization measurements are plotted for the three alloys in Figure 4.4. It can be seen that all the curves are similar, which suggests that the polarization behaviour of these alloys is similar. The pitting potentials for the tested materials presented in Figure 4.5 indicate that A535 has the most positive pitting potential, while AA2618 had the most active pitting potential. 2xxx Al alloys have known Cu-containing second-phases such as the θ and S phases. Buchheit *et al.* [79] reported that

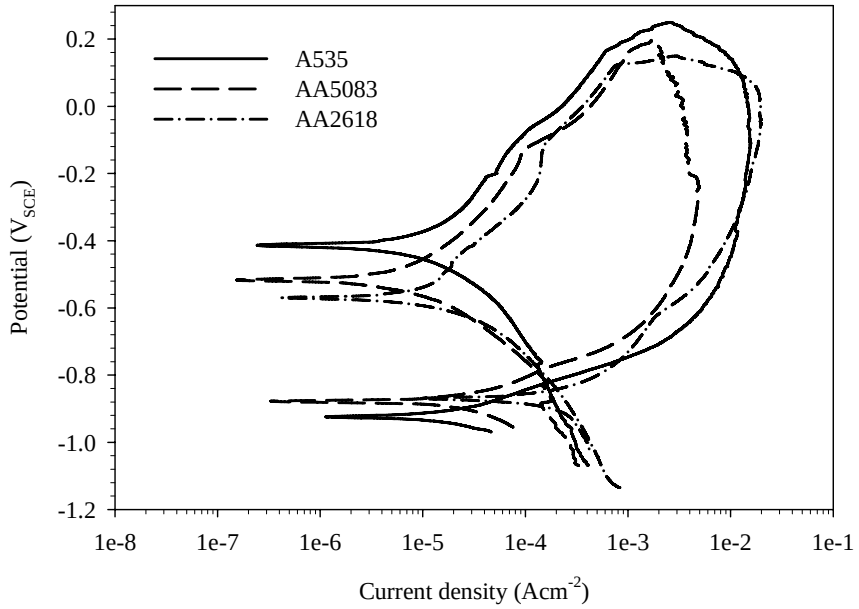

Figure 4.4. Cylic polarization curves for A535, AA5083-H116, and AA2618 aluminum alloys immersed in neutral 3.5 wt.% NaCl solution.

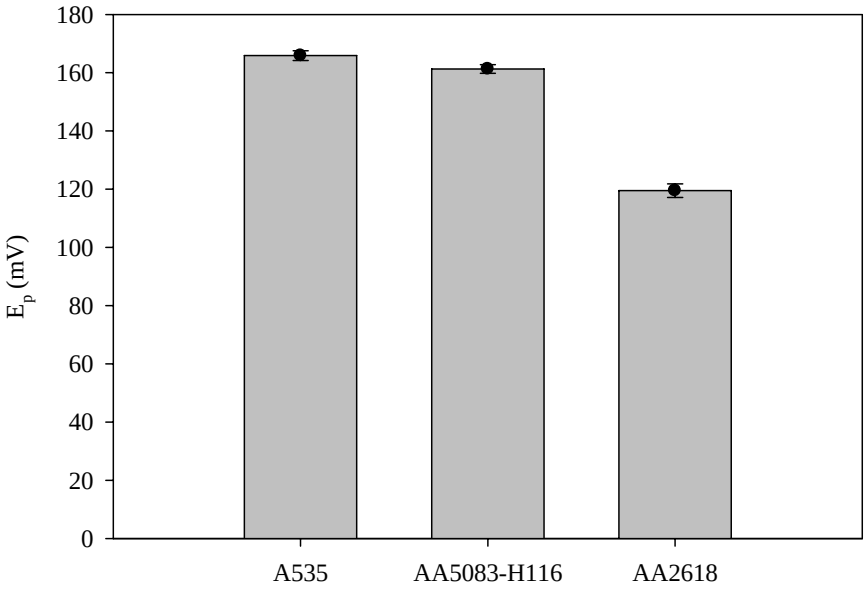

Figure 4.5. Pitting potentials for A535, AA5083, and AA2618 aluminum alloys immersed in neutral 3.5 wt.% NaCl solution. Error bars are based on standard deviation.

the open circuit potential (OCP) of the S-phase ranged from -0.920 to -0.930 V_{SCE} in 0.5 M NaCl solution. The E_{corr} of θ and S phases are anodic to that of Cu [76]. It was reported by Davis [51] that Cu-rich second-phase particles present in 2xxx series aluminum alloys corrode with Cu as the cathode. He further stated that Cu liberated from the corrosion of these second-phase particles replate on the anodic Al matrix and cause further corrosion damage.

Flores *et al.* [68] reported the presence of Al_3Mg_2 or β phase in grain boundaries of AA5083 alloy which disposed the alloy to intergranular corrosion attack. The E_{corr} of Al_3Mg_2 in 0.6M NaCl solution and in a solution containing 53g/liter NaCl and 3 g/liter H_2O_2 are -1161 mV_{SCE} [76] and -1150 mV_{SCE} [77], respectively. Therefore, the E_{corr} of Al_3Mg_2 is anodic to that of Al, with an E_{corr} of -849 mV_{SCE} in 0.6 M NaCl solution. The corrosion attack on AA5083-H116 can be attributed to the dissolution of anodic phases such as Al_3Mg_2 phase in the presence of the α-Al matrix.

Figure 4.6 is an optical micrograph of a corroded specimen of aluminum alloy AA2618. It can be seen that the pits are distributed evenly on the surface of the specimen. The optical micrograph of a corroded specimen of AA5083-H116 is shown in Figure 4.7. Figure 4.7(a) shows that some portions of the specimen were covered by a defective protective film, while Figure 4.7(b) shows that cracks formed on regions of the protective film of the corroded specimen of AA5083-H116 immersed in neutral salt solution.

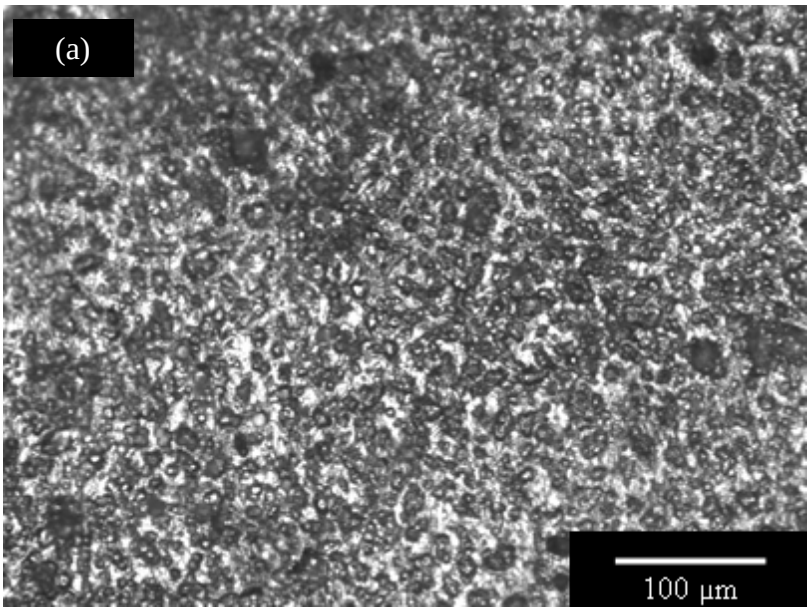

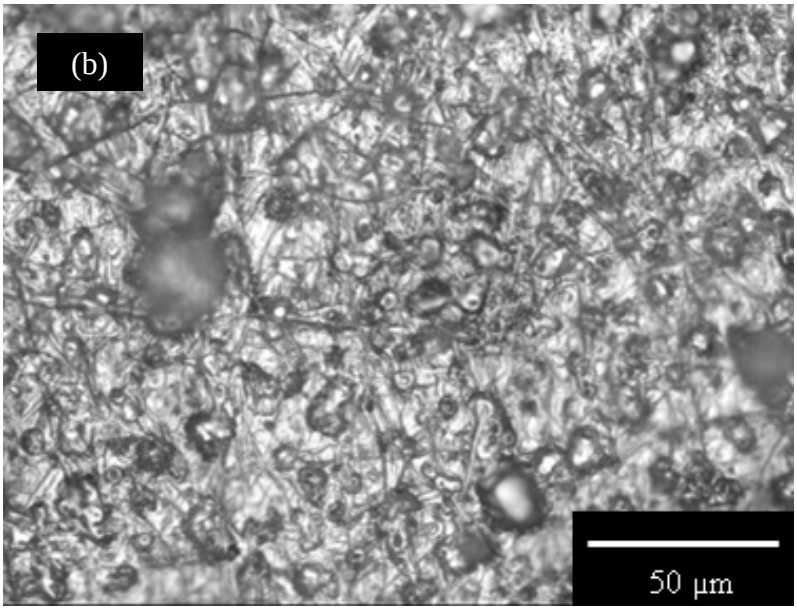

Figure 4.6. Corroded specimens of AA2618 exposed in neutral salt solution for 14 days.

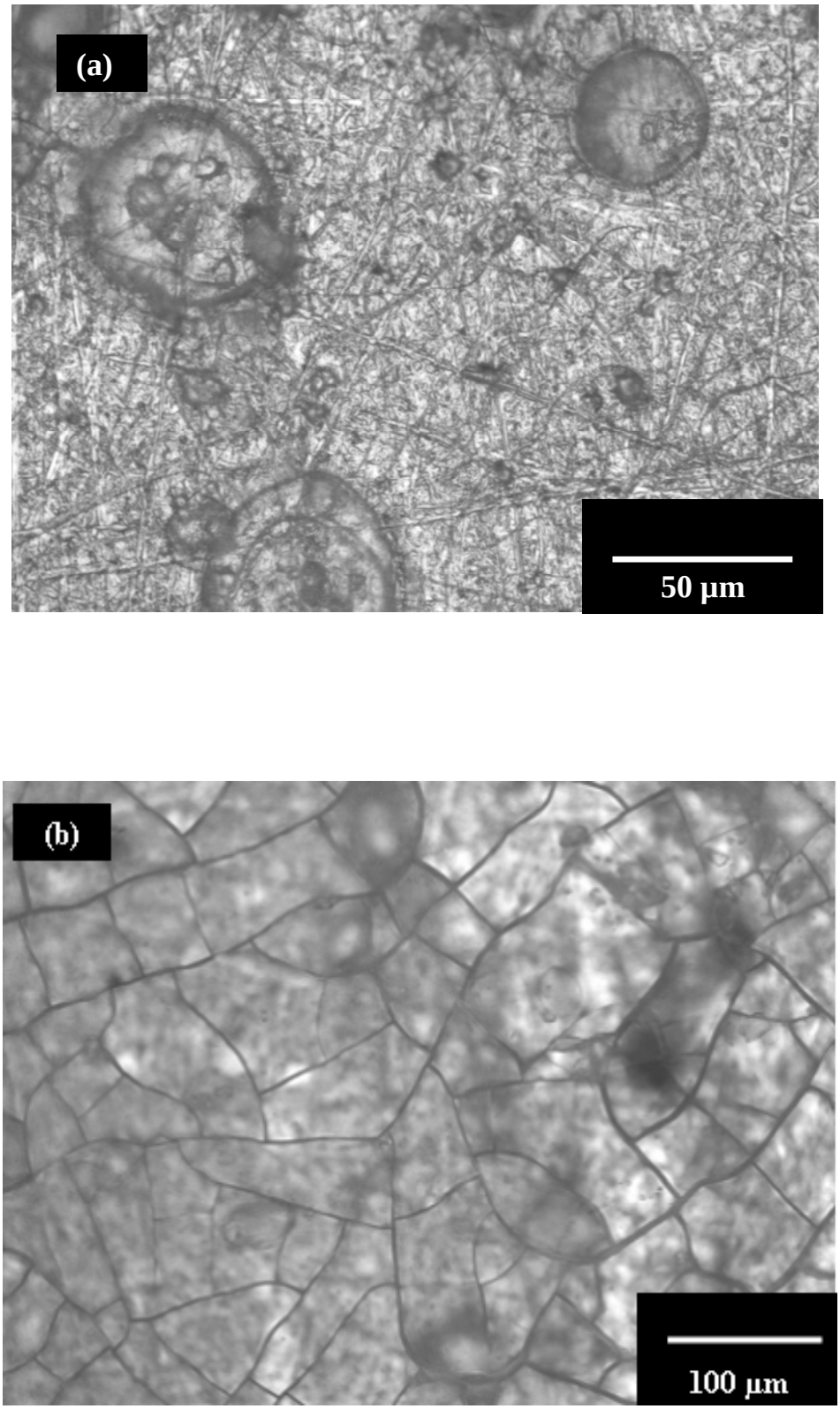

Figure 4.7. Corroded specimen of AA5083-H116 exposed in neutral salt solution for 14 days.

Microstructural examination showed that the three main intermetallic phases which can influence the corrosion behaviour of A535 alloy [36] are Al-Mg-rich, Mg_2Si, and $AlTi_3$ phases. Figure 4.8 is an optical micrograph of the Al-Mg-rich phase, while Figure 4.9 is the corresponding EDS spectrum. Figure 4.10 shows the SEM image of the Mg_2Si phase, while Figure 4.11 shows the corresponding EDS spectrum. The optical micrograph of the $AlTi_3$ phase is shown in Figure 4.12, while Figure 4.13 is the corresponding EDS spectrum.

Figure 4.14 shows the optical micrograph of A535 alloy after immersion in neutral 3.5 wt.% NaCl solution for 14 days. A comparison of Figures 4.8 and 4.14 shows that the sample immersed in salt solution for 14 days contains pits at sites previously occupied by the Al-Mg-rich and Mg_2Si phases, thus indicating that these phases are anodic to the matrix alloy [76, 77]. Figure 4.15 shows an SEM micrograph of corroded specimen of A535 alloy immersed in neutral salt solution for 14 days. It can be seen that Mg_2Si corroded preferentially to the matrix leaving deep pits in the matrix. In addition, the matrix alloy contains other numerous shallow pits.

SEM examination of the protective oxide film formed on corroded specimens of A535 alloy showed that defective and non-defective films formed on the surfaces after 14 days of immersion in neutral salt solution. Figures 4.16 and 4.17 show SEM micrographs of the defective and non-defective films formed on the surface of the alloy exposed for 14 days, respectively. It is believed that the defective film was formed on regions of the alloy that were populated by intermetallic phases anodic to the base alloy. It is possible

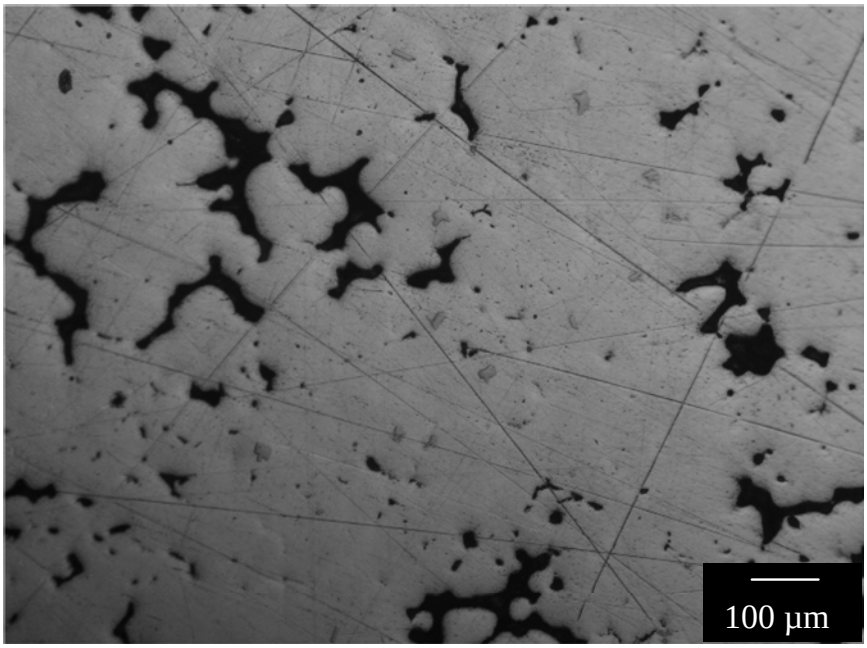

Figure 4.8. Optical micrograph showing Al-Mg-rich phase in A535 sample before immersion in 3.5 wt.% NaCl solution.

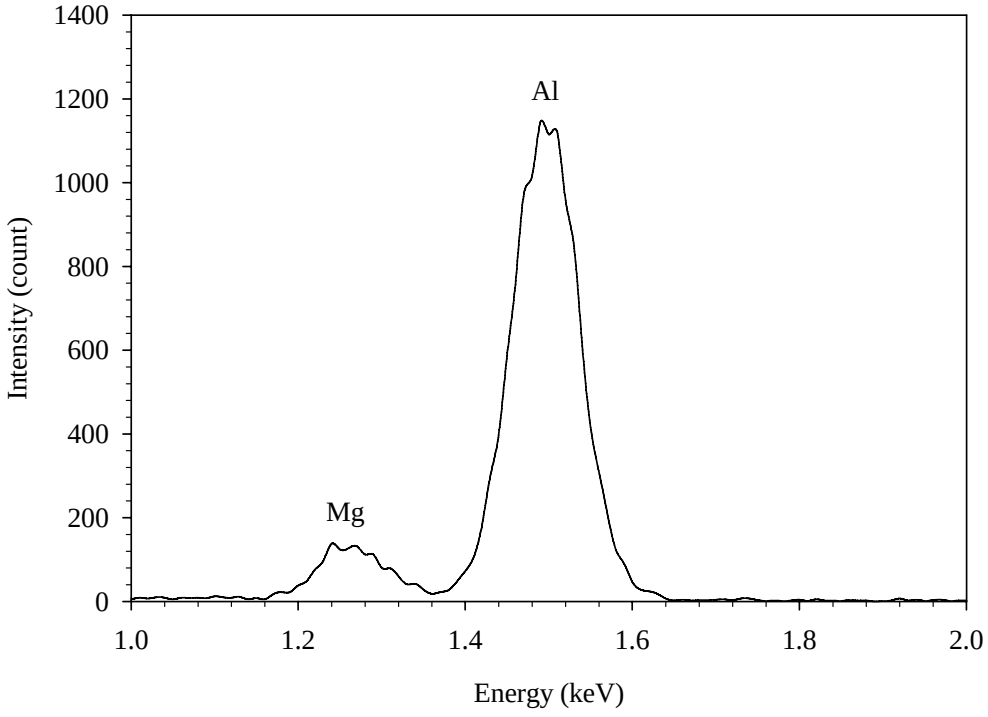

Figure 4.9. EDS spectrum of a typical Al-Mg-rich phase.

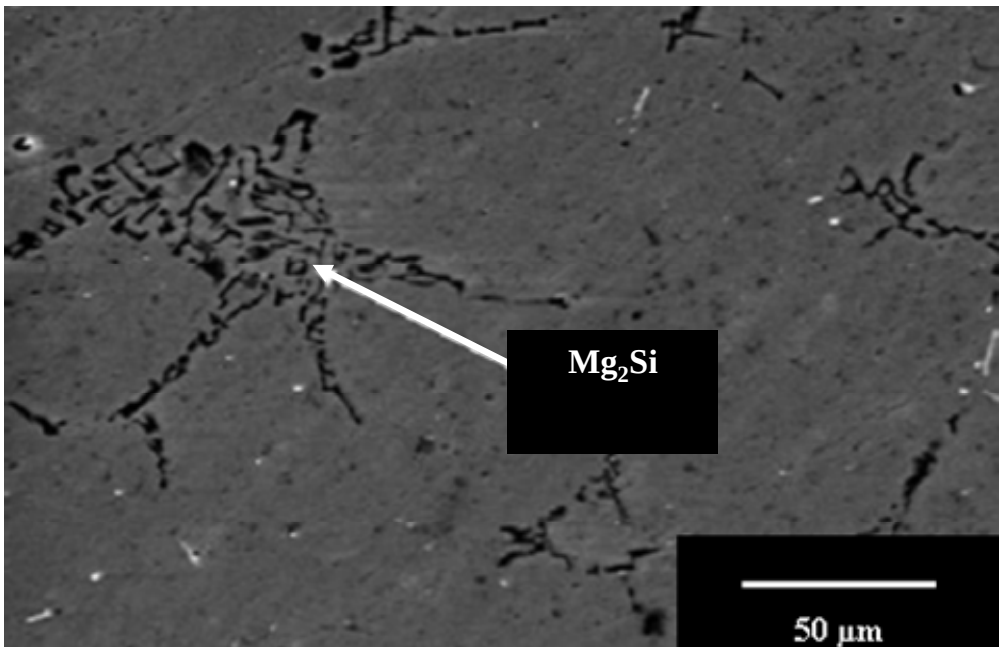

Figure 4.10. SEM micrograph showing Mg_2Si in A535 sample before immersion in salt solution.

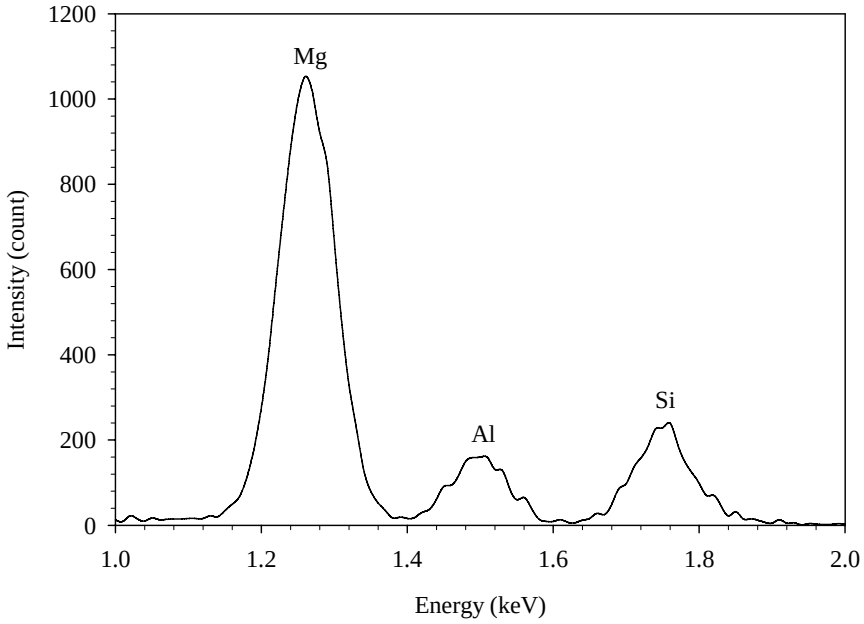

Figure 4.11. EDS spectrum of the Mg_2Si phase.

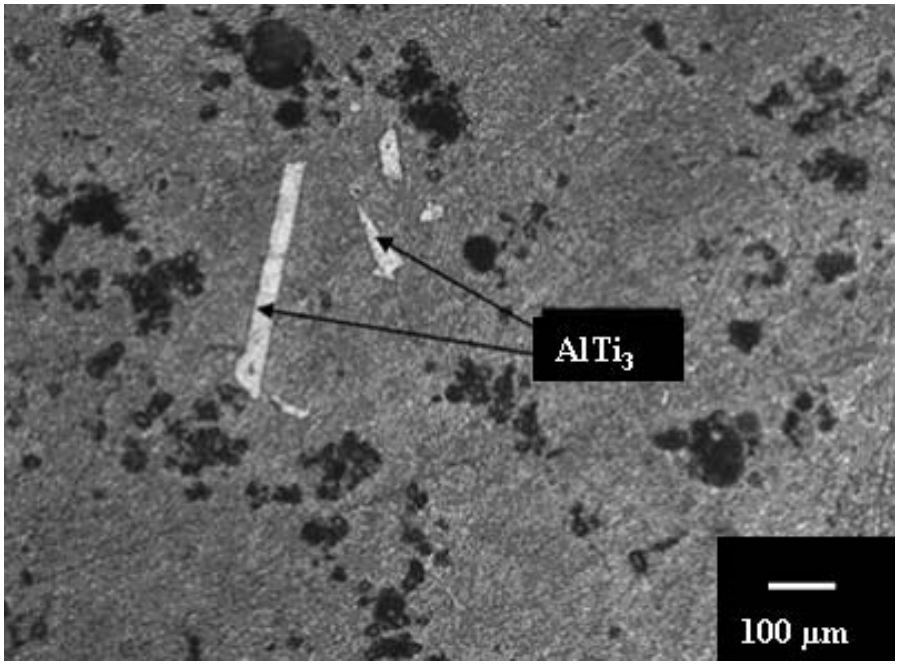

Figure 4.12. Optical micrograph of the $AlTi_3$ phase.

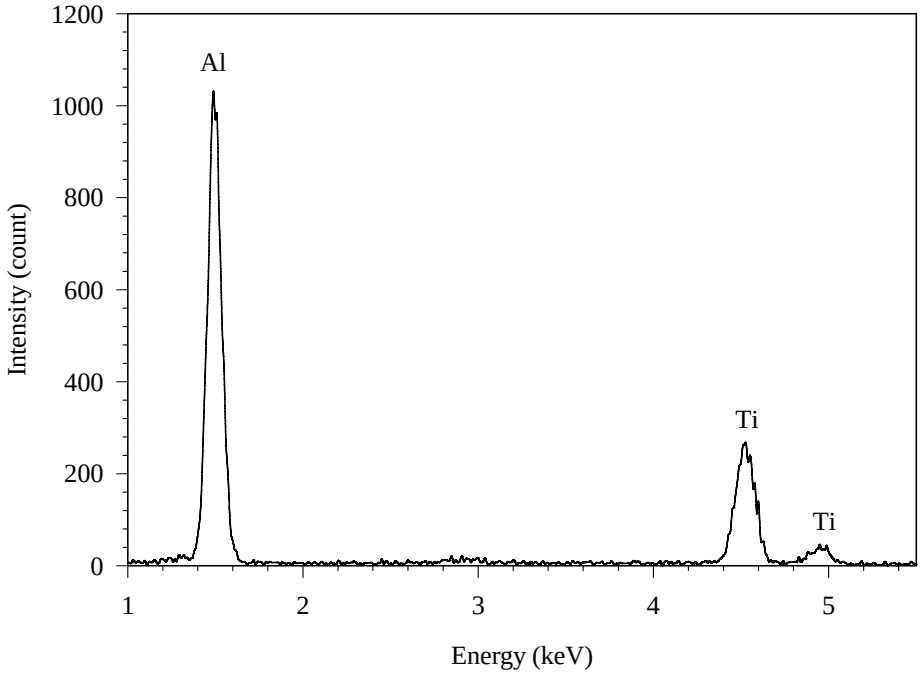

Figure 4.13. EDS spectrum of the $AlTi_3$ phase in A535 alloy.

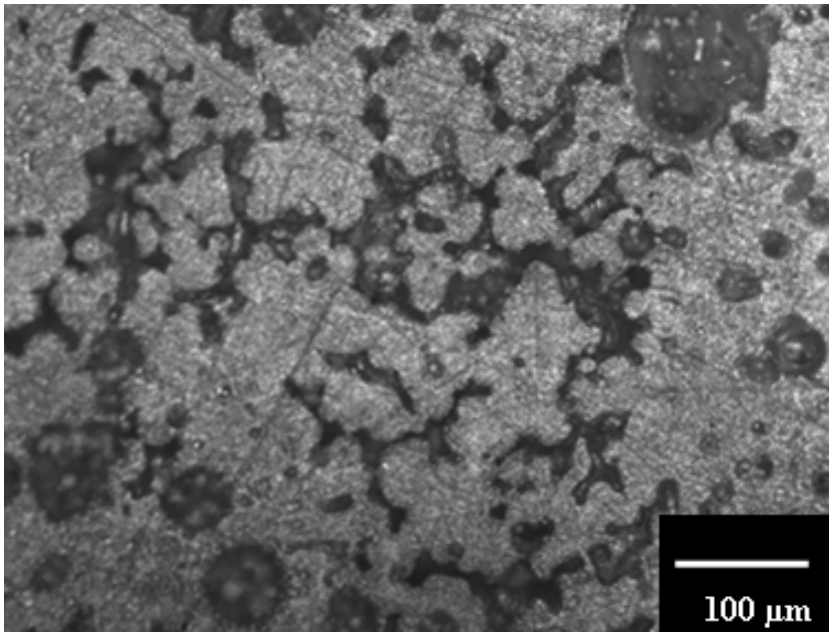

Figure 4.14. Optical micrograph showing the corroded surface of A535 specimen immersed in neutral salt solution for 14 days.

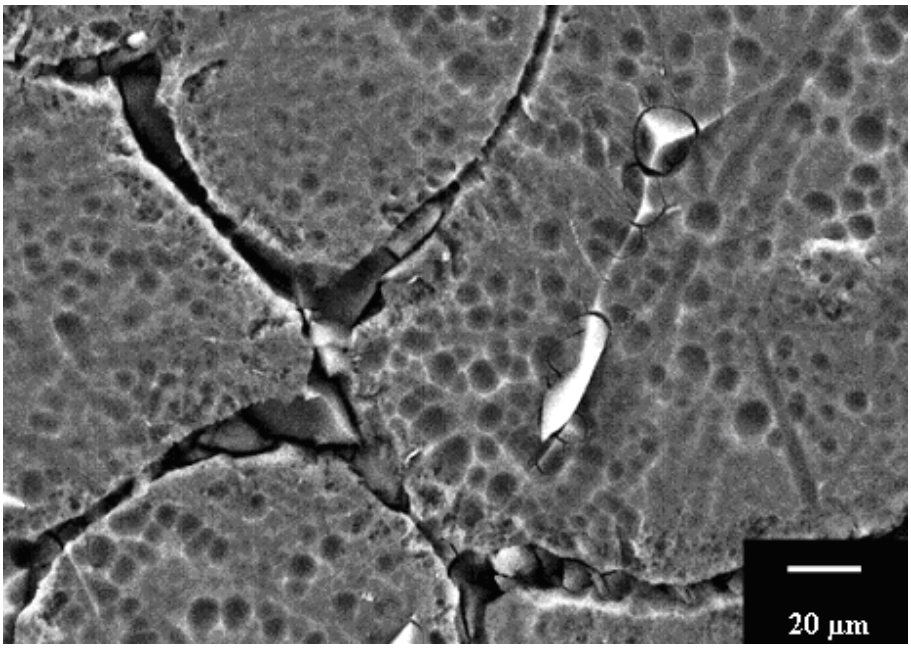

Figure 4.15. SEM micrograph of A535 alloy immersed in neutral 3.5 wt.% NaCl solution for 14 days.

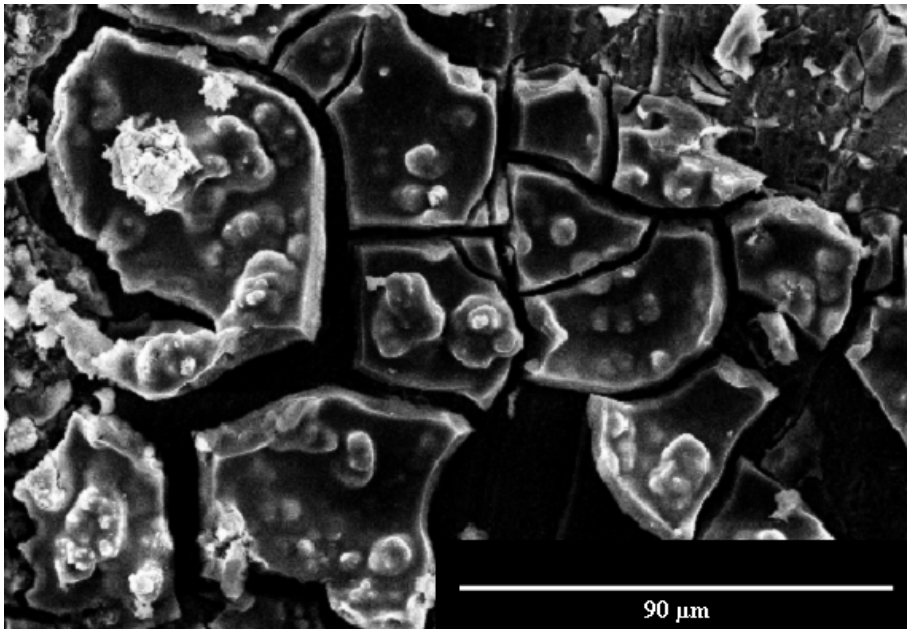

Figure 4.16. SEM micrograph showing defective film formed on the corroded specimen of A535 immersed in neutral salt solution for 14 days.

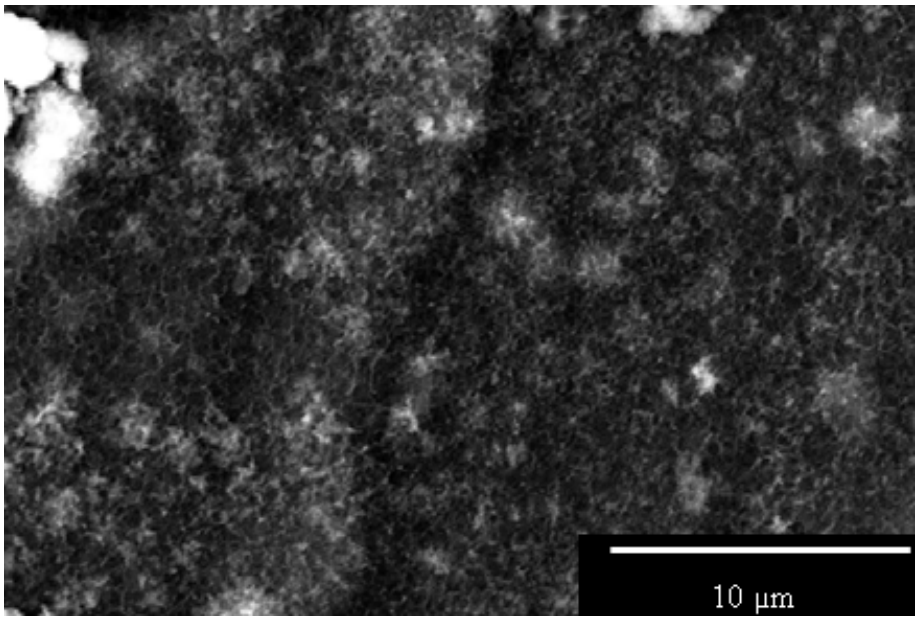

Figure 4.17. SEM micrograph showing the non-defective film formed on the corroded specimen of A535 immersed in neutral salt solution for 14 days.

that the corrosion activity emanating from the intermetallic phases damaged the protective oxide films. It is also postulated that the non-defective film protected the matrix where minimum corrosion activity occurred. Figure 4.18 is an EDS spectrum of a typiccal defective film formed on the corroded A535 specimen. It indicates that the film is composed of Al_2O_3 and MgO. The presence of Na and Cl is not suprising as the specimens were immersed in a salt solution. Figure 4.19 is an EDS spectrum acquired from a typical non-defective protective film. Al, Mg, and O, are also present in this film, while Na and Cl are absent. The intensity of oxygen (O) peak in the defective film is more than the corresponding peak in the non-defective film. This difference in the intensities of oxygen peaks suggests that the defective film may be composed of more Al_2O_3 and MgO than the non-defective film.

Figure 4.20 shows the electrochemical potential noise data acquired for A535 in the first 4 hours of immersion in neutral salt solution at room temperature. The potential transients show that during this period corrosion attack occurred in the material [54, 80-82]. The corrosion attack is attributable to the microgalvanic corrosion between the anodic Mg_2Si and Al-Mg-rich phase and the cathodic matrix [76, 77]. Birbilis and Buchheit [76, 77] reported that the corrosion potential (E_{corr}) of α-Al matrix (-849 mV_{SCE}) is cathodic to the E_{corr} of Mg_2Si and Al-Mg-rich compounds. In 0.6 M NaCl solution, the E_{corr} of Mg_2Si, Mg_2Al_3, Mg(AlCu), and Al_2CuMg are -1536 mV_{SCE}, -1162 mV_{SCE}, -936 mV_{SCE}, -1061 mV_{SCE}, respectively [76]. Similarly, Buchheit [77] reported that the E_{corr} of Mg_2Al_3, Mg_5Al_8, and Al_2CuMg are -1150 mV_{SCE}, -1050 mV_{SCE}, and-910 mV_{SCE}, respectively.

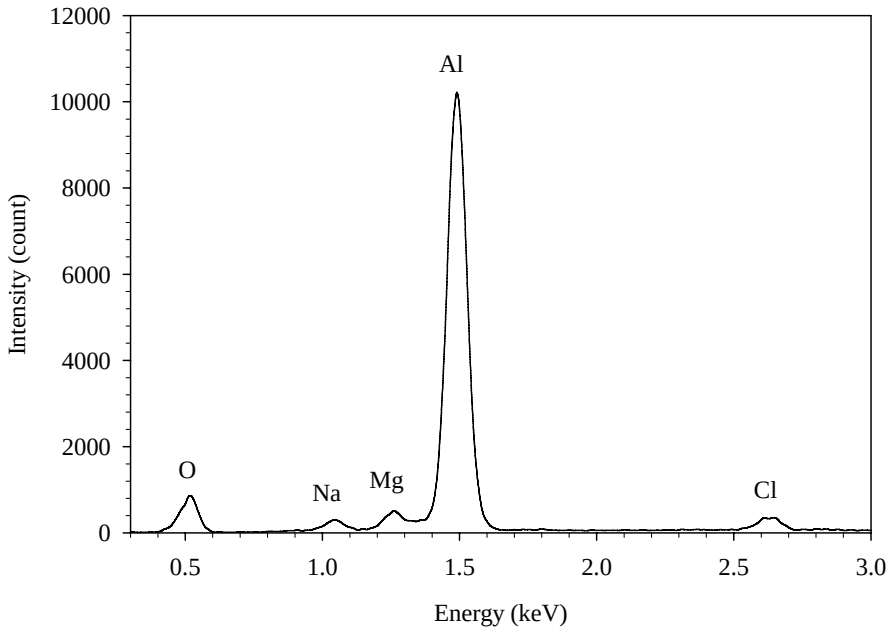

Figure 4.18. EDS spectrum of the defective film on formed on A535 alloy immersed in neutral salt solution for 14 days.

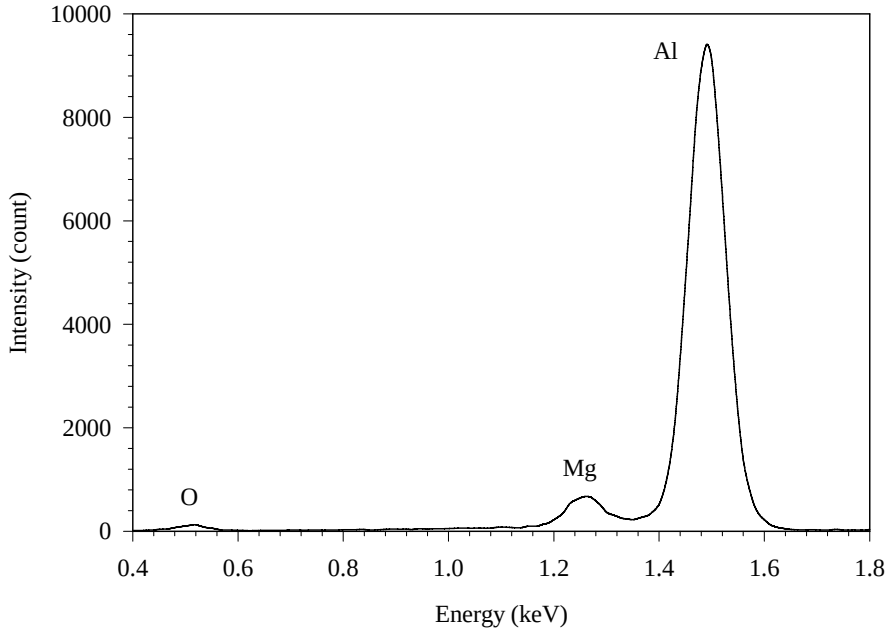

Figure 4.19. EDS spectrum of the non-defective film on formed on A535 alloy immersed in neutral salt solution for 14 days.

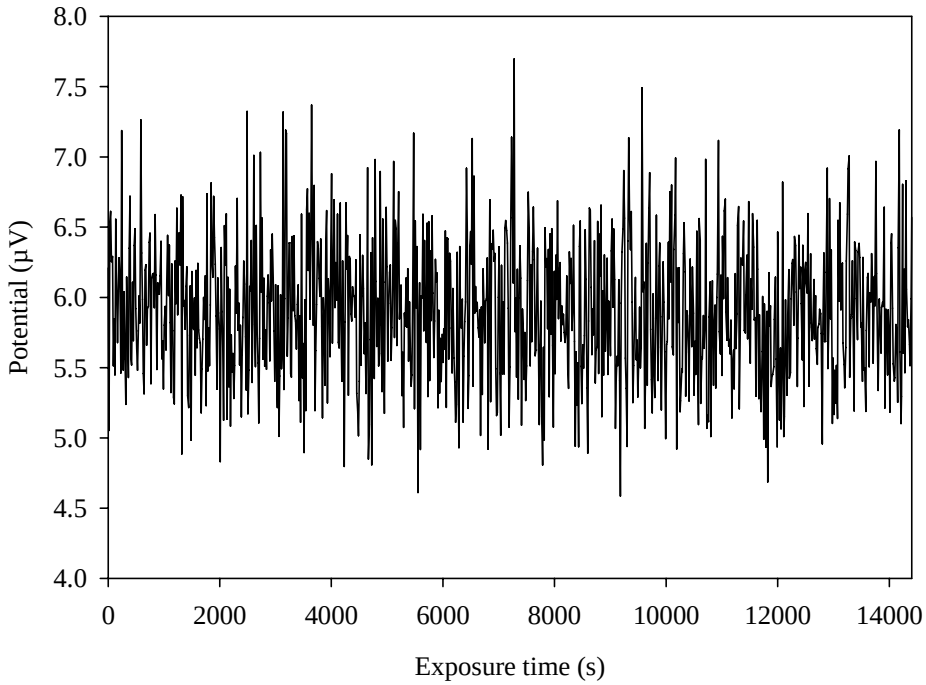

Figure 4.20. Electrochemical potential transients for A535 in the first 4 hours of exposure in neutral salt solution.

Figure 4.21 shows the average electrochemical noise (ECN) potential data derived from Figure 4.20. Average electrochemical noise current and potential have been reported as electrochemical variables which provide insights into the mechanism of corrosion processes [81, 82]. Kelly *et al.* [81] studied the corrosion behaviour of 410 stainless steel in phosphate buffer with added chloride and peroxide using electrochemical measurements. Their corrosion cell comprised a saturated calomel reference electrode, three working electrodes, and a platinum mesh auxiliary electrode. One of the working electrodes (which the authors called reference electrode) was used to measure the potential between it and the other two working electrodes, while the saturated calomel electrode was used to measure the E_{corr}. The authors monitored the changes in potential and average potential with time before and after the addition of 0.5 M NaCl and

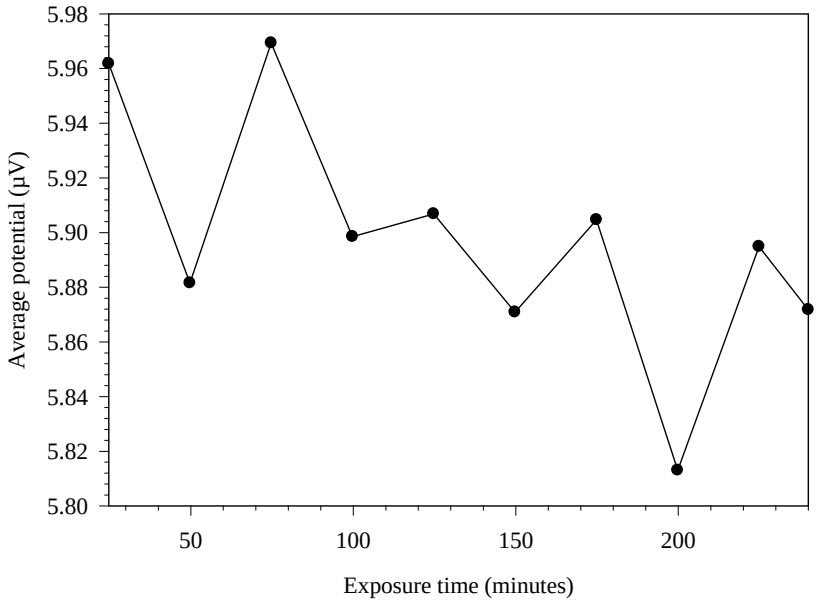

Figure 4.21. Variation of average ECN potential with time for A535 in the first 4 hours of immersion in neutral salt solution.

0.01 M H_2O_2 solutions. Kelly *et al.* [81] reported that the addition of NaCl and H_2O_2 solutions to the buffer caused a decrease in potential, which indicated pit initiation on the working electrode. The average potential fluctuated between -22 and -29 mV_{SCE}. The authors explained that the fluctuation in average potential might have been caused by pit formation on the working electrode. Similarly, the increase in average corrosion current with the addition of chloride ions and peroxide solution indicated pitting initiation and propagation in the working electrode [81].

Mansfeld *et al.* [82] studied the corrosion behaviour of iron exposed to chloride media by analyzing average corrosion potential and average corrosion current with time. In the medium which was exposed to the atmosphere, the average corrosion potential decreased with time as rust formed on the surface of the specimen. Jones [52] reported

that iron forms a stable, resistant film in strong oxidizing media such as concentrated nitric acid. In less oxidizing conditions, iron rusts by forming a diffusion barrier-type film. The decrease in average corrosion potential with time in Reference [82] may be attributed to the formation of rust in the chloride medium exposed to the atmosphere. Mansfeld *et al.* [82] reported that the average corrosion current fluctuated with positive and negative peaks in the same medium where significant corrosion occurred.

In Figure 4.21, the average ECN potential became more negative in the first 50 minutes of immersion, which suggests that pits formation was the dominant corrosion activity [81]. Between 50 and 75 minutes of exposure, the average ECN potential became more noble which indicates a decrease in corrosion activity [81]. Subsequently, it decreased until after 200 minutes. This corrosion behaviour suggests that the net corrosion activity resulted from pit propagation and repassivation [81]. The pitting process was dominant between 75 and 200 minutes after immersion.

Figure 4.22 shows the ECN current transients obtained during the first 4 hours of immersion in 3.5 wt.% NaCl solution maintained at pH 7. It can be seen that the ECN current transients were very high immediately after immersion, which indicates that localized corrosion attack occurred [55]. The amplitude of the corrosion current transient decreased rapidly which indicated that the transient pits or metastable pits which were initiated did not grow but repassivated [55]. The fluctuations in the current transient however deviated from the base line as exposure time increased. This deviation is an indication that pit formation increased with exposure time [55].

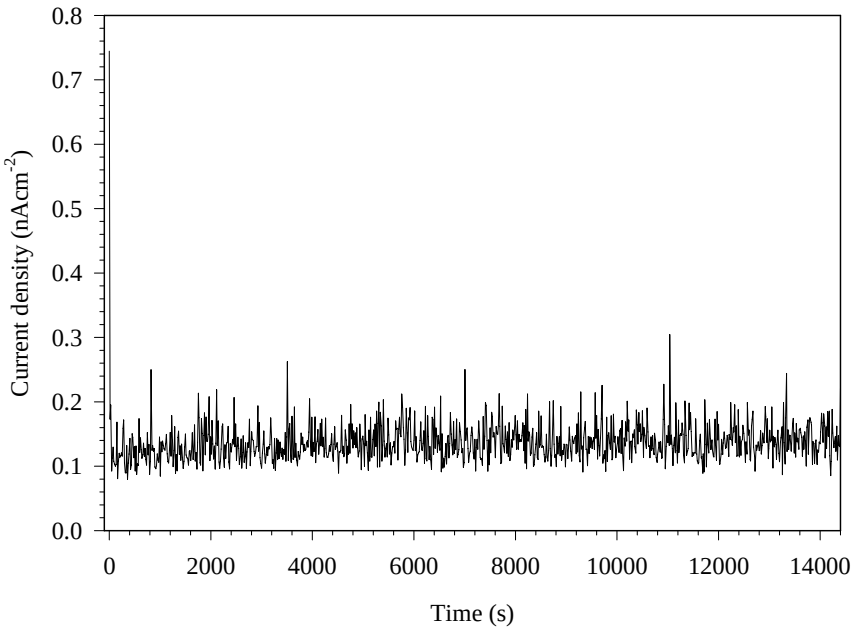

Figure 4.22. Electrochemical noise current density for A535 in the first 4 hours of exposure in neutral salt solution.

Figure 4.23 shows the average current data derived from Figure 4.22. It can be seen that, generally, it increased with exposure time. The trend indicates that pits initiated and deepened as exposure time increased [81].

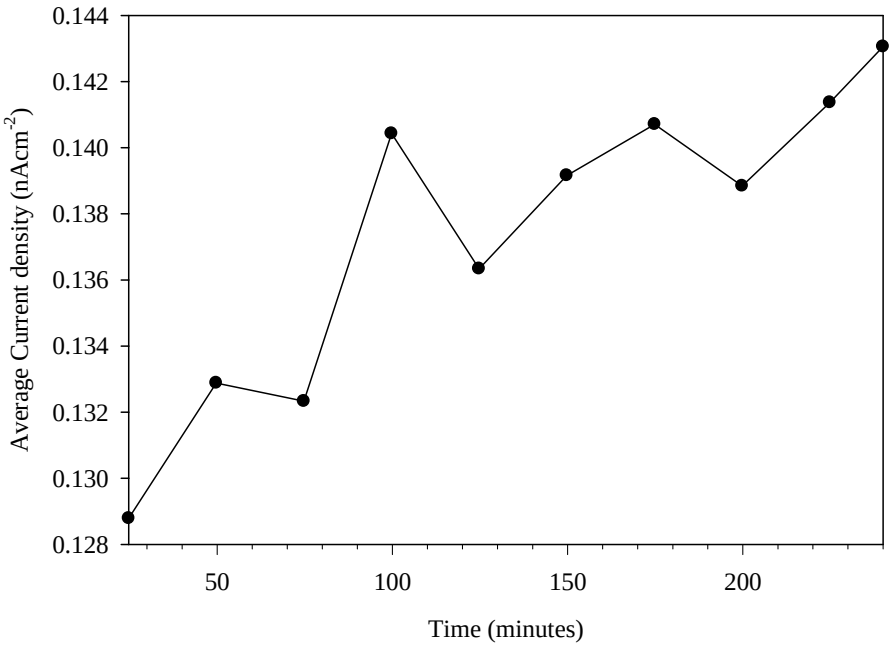

Figure 4.23. Variation of average ECN current density for A535 in the first 4 hours of immersion in neutral salt solution.

4.2 Effect of Fly Ash Addition on the Corrosion Behaviour of A535 in Neutral 3.5 Wt.% NaCl Solution

Figure 4.24 shows the variation of weight loss with time for A535 and its composites in neutral 3.5 wt.% salt solution. The weight loss of the materials increased as their fly ash content increased, with the unreinforced A535 and A535/fly ash/15_p losing the least and greatest weight, respectively. Figure 4.25 shows the variation of corrosion rate of A535 and the MMCs with immersion time in neutral salt solution. It can be seen that the matrix alloy (A535) and its composites showed similar corrosion behaviour. The corrosion rates of all the tested materials decreased rapidly during the first three days of exposure to the electrolyte but, with further exposure time, the decrease was very gradual. Passivation of the matrix alloy is believed to be responsible for the monotonic decrease in corrosion rate with increasing exposure time observed in these materials. It is also seen that A535/fly ash/15_p showed the highest rate of corrosion, followed by A535/fly ash/10_p, A535/hybrid/10_p, and A535. It was also observed that the corrosion of the composites was accompanied by the loosening of fly ash particles. It is believed that the corrosion of the fly ash-matrix interface caused the loosening of fly ash particles which were finally dislodged from the specimens during post-immersion cleaning process.

Bienias *et al.* [37] and Ramachandra *et al.* [38] have reported that fly ash particles acted as pit initiation sites in fly ash/Al-Si alloy composites and that there was a buildup of corroded fly ash particle debris in corrosion pits. The loss of such particles during post-

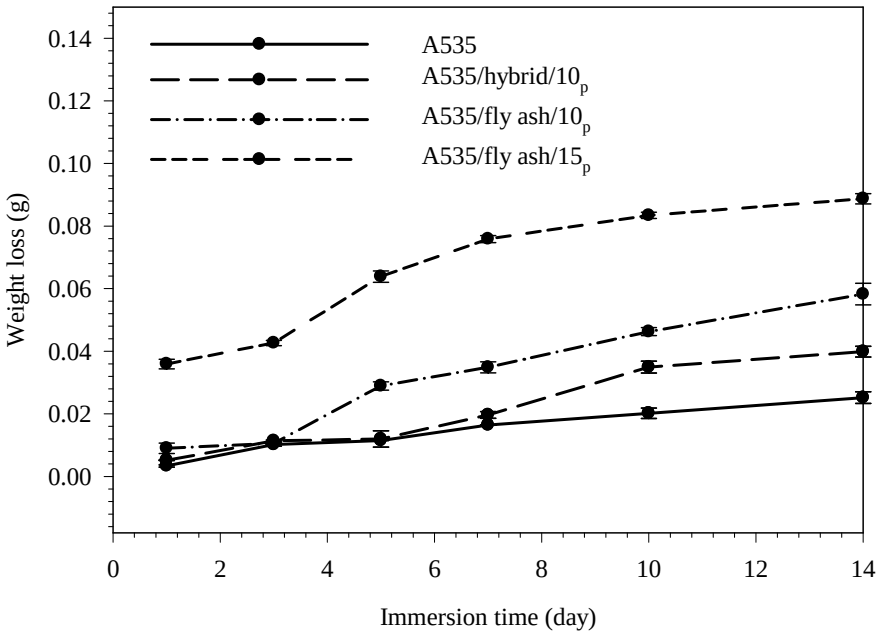

Figure 4.24. Variation of weight loss with time for A535 and the MMCs immersed in neutral 3.5 wt.% NaCl solution. Error bars are based on standard deviation.

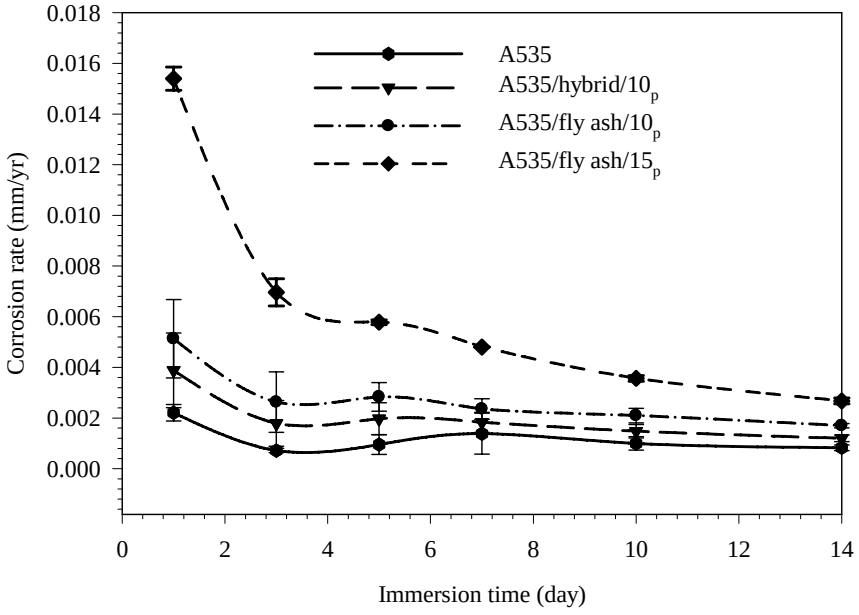

Figure 4.25. Variation of corrosion rates with time for A535 and the composites immersed in neutral 3.5 wt.% NaCl solution. Error bars are based on standard deviation.

immersion cleaning contributed to the high weight loss recorded for the composites in the present study. Figure 4.26 shows the effect of fly ash addition on the corrosion potential (E_{corr}) of A535 alloy. Table 4.2 shows the corrosion potentials, corrosion current densities (i_{corr}), and Tafel constants for the unreinforced alloy and the composites. It can be seen from Figure 4.26 that all the curves are similar, which indicates that the polarization behaviour of unreinforced A535 alloy and its composites is similar. The corrosion potential (E_{corr}) of the unreinforced alloy is more noble than that of the MMCs, which increases with increasing fly ash content. Similar observation was made by Bienias *et al.* [37]. They reported that that the corrosion and pitting potentials of fly ash/Al-Si alloy composites became more negative as their fly ash content increased.

Figure 4.27 shows the cyclic potentiodynamic polarization curves obtained for A535 alloy and the MMCs immersed in neutral 3.5 wt.% NaCl solution. It can be seen that the curves are similar, which indicates that the polarization behaviour of the MMCs are similar to that of the alloy. Thus, the addition of fly ash did not alter the corrosion polarization of the alloy. Figures 4.28 and 4.29 show respectively the variation of critical pitting potential (E_p) and repassivation potential (E_{rp}) with increasing fly ash content. Figure 4.28 shows that the E_p of the tested materials became more negative with the addition of fly ash. It has been reported by Gikunoo *et al.* [35] that Mg_2Si and Al-Mg-rich compounds, which are anodic to matrix [76, 77], increased with increase in fly ash content. Therefore, pitting corrosion resistance of the composites decreased with fly ash content.

Table 4.2. Corrosion potentials, current densities, and Tafel constants of A535 and the MMCs immersed in neutral salt solution.

Material	Corrosion potential (mV)	Corrosion current density i_{corr} (μ Acm^{-2})	Tafel constants (mV)
A535 alloy	-415 ± 4.2	0.865 ± 0.01	$\beta_a = 31 \pm 0.15$
			$\beta_c = 36 \pm 0.18$
A535/hybrid/10$_p$	-423 ± 4.6	1.83 ± 0.01	$\beta_a = 46 \pm 0.23$
			$\beta_c = 38 \pm 0.32$
A535/fly ash/10$_p$	-443 ± 7.2	2.5 ± 0.04	$\beta_a = 52 \pm 0.17$
			$\beta_c = 40 \pm 0.33$
A535/fly ash/15$_p$	-507 ± 6.1	2.74 ± 0.04	$\beta_a = 67 \pm 0.17$
			$\beta_c = 48 \pm 0.33$

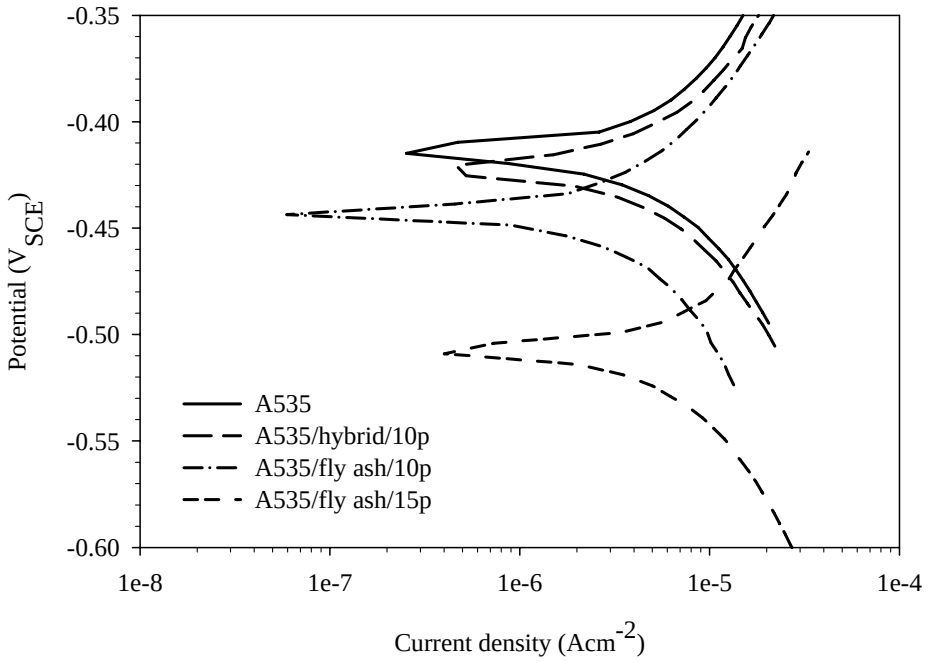

Figure 4.26. Potentiodynamic polarization curves for A535 alloy and the MMCs immersed in neutral 3.5 wt.% NaCl solution.

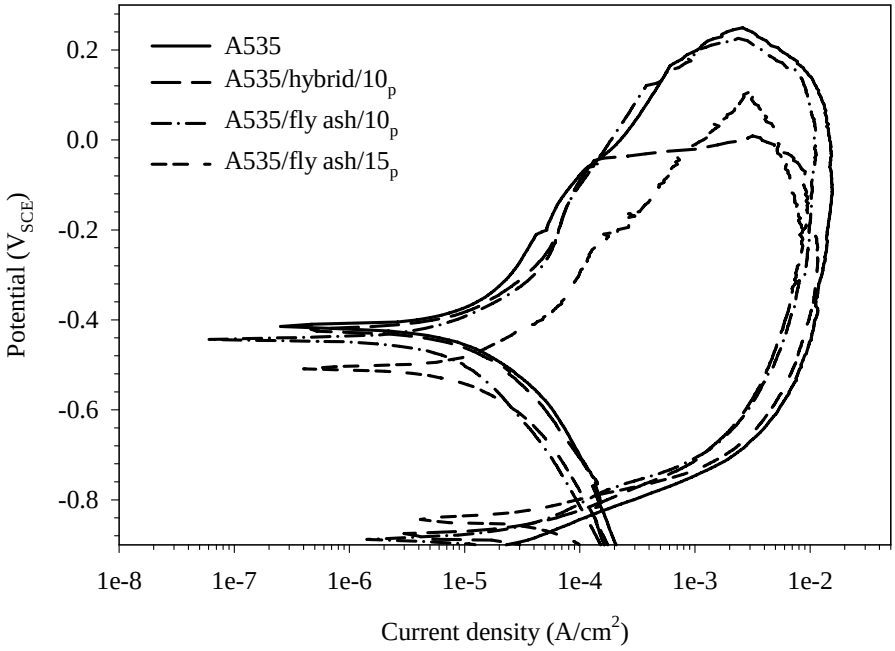

Figure 4.27. Cyclic potentiodynamic polarization curves for A535 and the MMCs immersed in neutral 3.5 wt.% NaCl solution.

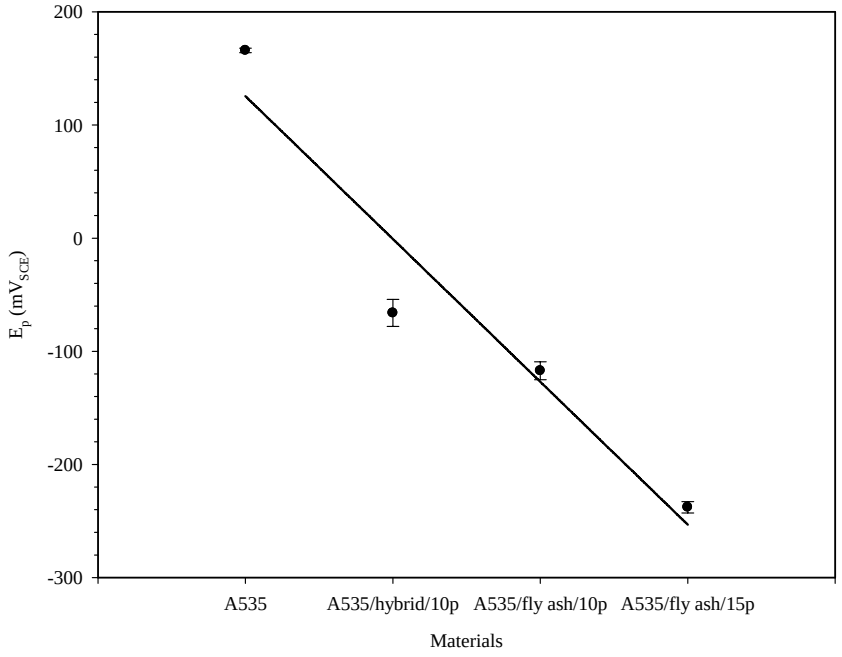

Figure 4.28. Effect of fly ash content on the pitting potential of A535 and the MMCs immersed in neutral 3.5 wt.% NaCl solution. Error bars based on standard deviation.

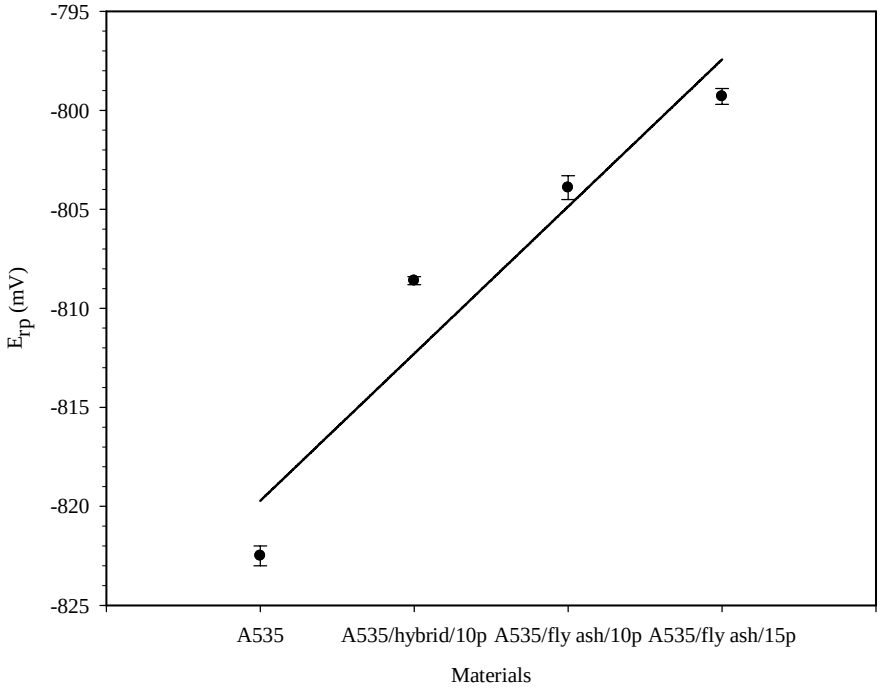

Figure 4.29. Effect of fly ash content on the repassivation potential of A535 and the MMCs immersed in neutral 3.5 wt.% NaCl solution. Error bars are based on standard deviation.

Figure 4.29 shows that E_{rp} increases (in the noble direction) with increasing fly ash content. Since E_{rp} measures the ability of a material to repassivate, the present results show that pit propagation in the composites is retarded more than in the matrix alloy. The superior repassivation potential exhibited by the MMCs containing fly ash is attributable to the reduction in the pit dissolution kinetics by the oxides of metals generated by introduction of fly ash particles into the matrix. Similar observations were made by Szklarska-Smialowska [60, 61] who studied the effect of alloying elements on the pit dissolution kinetics of aluminum alloys. The author reported that the oxides of metals within a pit which are insoluble or partially soluble in the acidic solution within

the pit cause metastable pits to passivate. Table 4.3 shows the pitting and repassivation potentials of A535 and the MMCs.

The cyclic polarization behaviour of particulate Al MMCs is influenced by several factors such as porosity, high dislocation densities at the matrix-reinforcement interfaces, the presence of intermetallic compounds and reaction products, and the electrical conductivity of the reinforcing phases [37, 46]. It was reported in Reference [35] that the amount of dimagnesium silicide (Mg_2Si) and spinel (Al_2MgO_4) in fly ash/A535 composites increased with increasing fly ash content. Mg_2Si is produced in the matrix alloy through a solid-state reaction between Si and Mg.

$$2Mg + Si \leftrightarrow Mg_2Si \tag{4.1}$$

In the MMCs, the SiO_2 phase present in fly ash particles or covering the surface of SiC particles in A535/hybrid/10_p composite is reduced by molten magnesium through a two-step reaction leading to the formation of the Mg_2Si phase:

$$2Mg + SiO_2 \leftrightarrow 2MgO + Si \tag{4.2}$$

$$2Mg + Si \leftrightarrow Mg_2Si \tag{4.3}$$

The spinel phase is formed in the MMCs through a reaction between elemental magnesium of the matrix alloy and fly ash constituents, particularly alumina (Al_2O_3) and SiO_2, following either of the chemical reactions:

$$3Mg + 4Al_2O_3 \leftrightarrow 2Al + 3MgAl_2O_4 \tag{4.4}$$

$$2SiO_2 + 2Al + Mg \leftrightarrow MgAl_2O_4 + 2Si \tag{4.5}$$

Table 4.3. Pitting and repassivation potentials of A535 and the composites immersed in 3.5 wt.% neutral salt solution.

Material	Pitting potential (mV)	Repassivatin potential (mV)
A535 alloy	116 ± 2	-822.5 ± 0.5
A535/hybrid/10_p	-66.3 ± 12	-808.6 ± 0.2
A535/fly ash/10_p	-117.2 ± 8	-803.9 ± 0.6
A535/fly ash/15_p	-237.8 ± 5	-799.3 ± 0.4

The presence of the intermetallic phases and porosities in the MMCs serve as potential preferential sites for localized corrosion [37]. It was reported by Birbilis [76] and Buchheit [77] that Mg_2Si does not show any breakdown potential and is capable of corroding freely above its E_{corr}, which was measured to be -1536 mV (SCE) in 0.6M NaCl [76] and -1530 to -680 mV (SCE) in 3 wt.% NaCl [77] as compared to -849 mV_{SCE} for pure aluminum in 0.6M NaCl [74] and -760 to -810 mV (SCE) for Al-Mg binary alloy in 53 g/l NaCl+3 g/l H_2O_2 solution [77]. Since aluminum is noble to Mg_2Si, the microgalvanic couple formed between them in A535 alloy and its composites would selectively corrode Mg_2Si away. Therefore, the deep pits observed in the A535 alloy are attributed to the dissolution of the Mg_2Si and the Al-Mg rich phases.

Figure 4.30 shows the microstructure of as-cast A535/hybrid/10_p composite before and after immersion in the salt solution. Apart from fly ash, pores and SiC particles, the matrix contained secondary phases including Mg_2Si, Al-Mg-rich, and $AlTi_3$

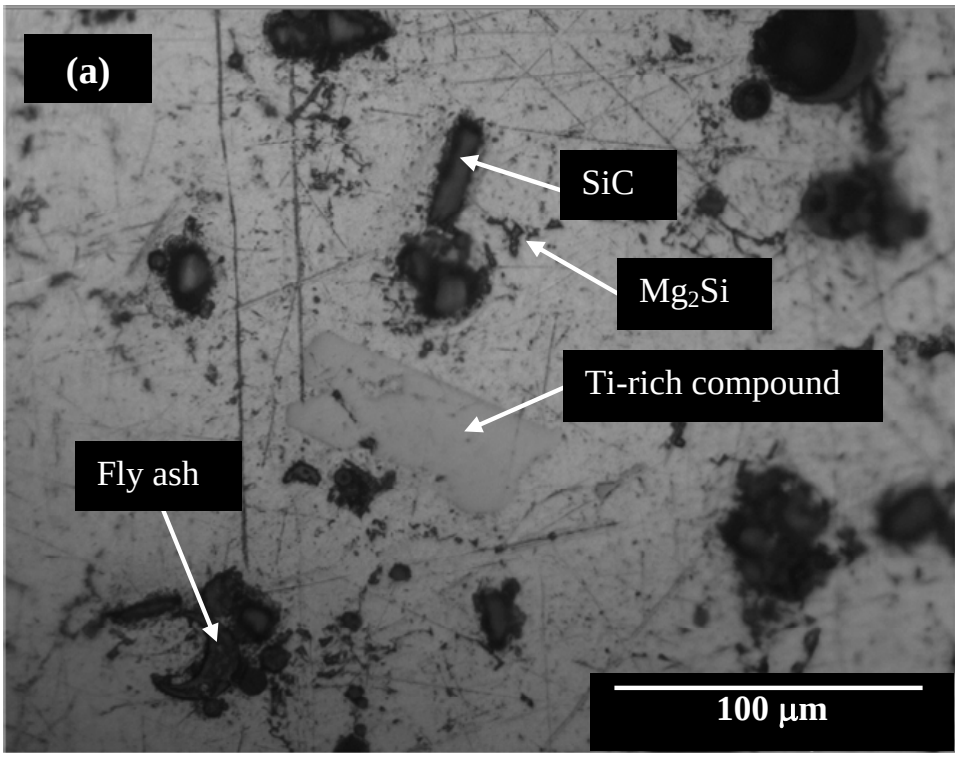

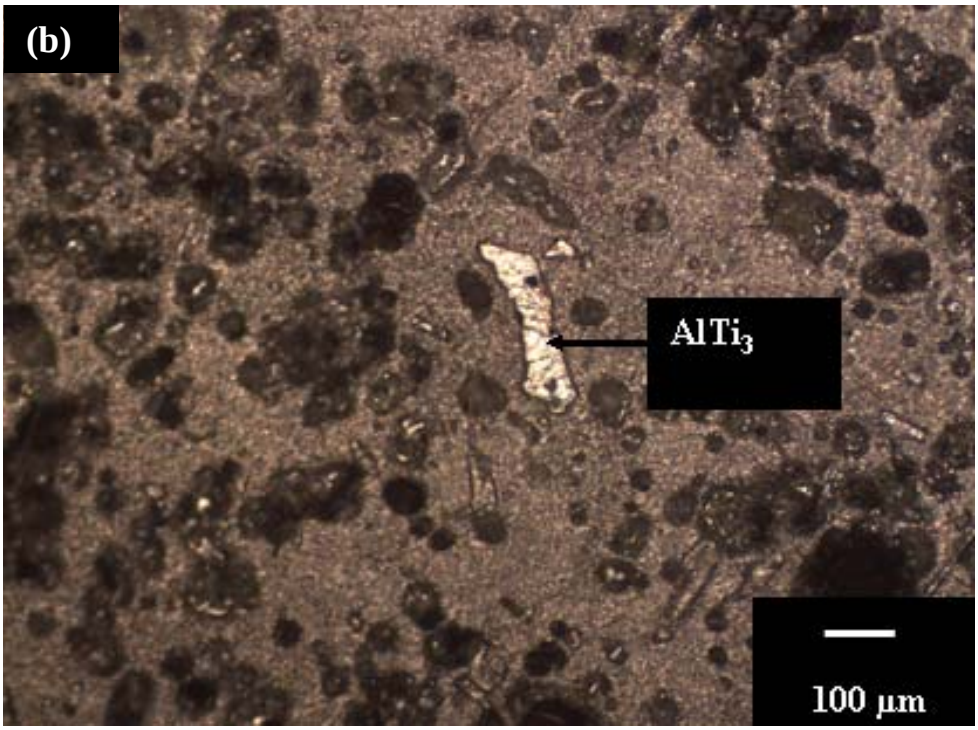

Figure 4.30. Optical micrographs of A535/hybrid/10_p (a) before and (b) after immersion in neutral 3.5 wt.% NaCl solution for 14 days.

intermetallics [36]. The same intermetallic compounds were found in A535/fly ash/10_p and A535/fly ash/15_p composites. After immersion in neutral 3.5 wt.% NaCl solution for 4 days, the composites exhibited similar corrosion behaviour to the matrix alloy in that the Mg_2Si and Al-Mg-rich phases corroded in preference to the matrix [76, 77] leaving pits behind.

4.3 Effects of pH on the Corrosion Behaviour of A535 and Its Composites

4.3.1. Corrosion in 3.5 Wt.% NaCl Solution Maintained at pH 4

Figure 4.31 shows the variation of weight loss with exposure time for specimens immersed in 3.5 wt.% NaCl solution maintained at pH 4 at room temperature. It can be seen that the weight loss for all the specimens increased as exposure time increased. Figure 4.32 shows the variation of the corrosion rate of the test materials with immersion time, from where it can be seen that it increased with fly ash content. The corrosion behaviour of the test materials in this solution is similar to that obtained for the materials immersed in the neutral salt water solution (See Figure. 4.25). However, the individual corrosion rates were less than those recorded for the samples immersed in neutral salt solution. The difference in corrosion rates in both media is attributable to the stability of the protective oxide films in both media. Pourbaix diagram (See Figure 2.1) shows that aluminum exposed in de-ionized water of pH 4 to 7 would form protective barrier film of Al_2O_3, which reduces corrosion activity. Though aluminum alloys would passivate under both media, Pourbaix [58] reported that the quality of the oxide films varies notably in its degree of hydration and porosity even within the passive zone. Kolics *et al.* [83] reported that the thickness of the oxide film formed on high purity aluminum immersed in NaCl solutions is strongly dependent upon the solution pH. Over a range $3 \leq pH \leq 11$, they observed maximum film thickness of 6.8 and 9.8 nm at pH = 3.8 and 10.7, respectively, while the thickness over the range of $4<pH<10$ varied between 4 and 4.5 nm. Furthermore, it was observed that the thickness

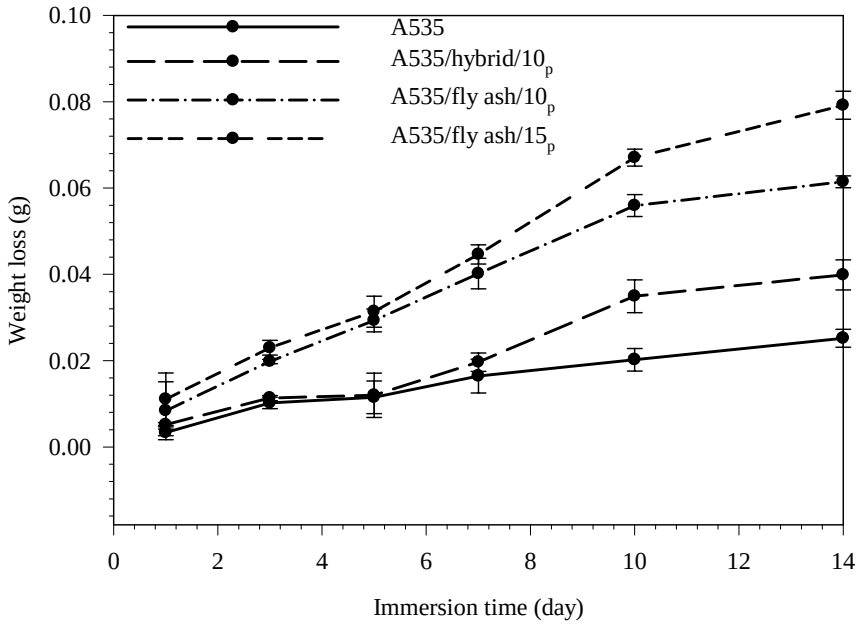

Figure 4.31. Variation of weight loss with time for A535 and its composites immersed in 3.5 wt.% NaCl solution (pH = 4) for 14 days. Error bars are based on standard deviation.

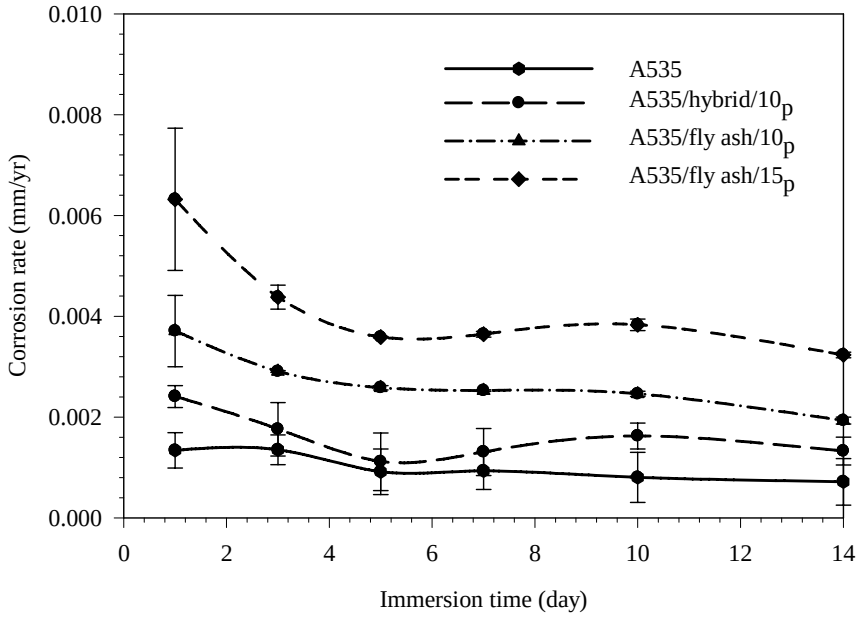

Figure 4.32. Variation of corrosion rate with time for A535 and composites immersed in 3.5 wt.% NaCl solution (pH = 4). Error bars are based on standard deviation.

of the oxide film in the active dissolution range of pH< 3 and pH>11 was thinner than the oxide film formed after polishing Al [83]. It may be inferred from Reference [83] that the test materials developed superior protective oxide films in 3.5 wt.% NaCl solution maintained at pH 4 than in neutral salt solution.

The potentiodynamic polarization curves for A535 and the composites reinforced in mildly acidic NaCl solution (pH = 4) are shown in Figure 4.33. The polarization curves follow a similar trend to that exhibited by samples tested in neutral salt solution (Figure 4.26). The corrosion potential of the samples became more active as their fly ash content increased. A535 had the most noble corrosion potential, while A535/hybrid/15_p had the most active potential. Table 4.4 summarizes the corrosion potentials, current densities, and Tafel contants obtained for the test materials. It can be seen that the corrosion potentials of the samples immersed in this solution are more noble than those obtained for samples immersed in the neutral salt solution. It has been reported that the oxide film formed on aluminum exposed to NaCl at solution pH 4 is thicker than film formed at neutral pH [83]. The thickness of the oxide film formed at the different solution pH in salt solution suggests that the film formed on the test samples exposed at pH 4 was more protective than that formed on samples immersed in neutral salt solution.

Figure 4.34 shows the cyclic polarization curves for A535 and the composites in salt solution maintained at pH 4. The trend of the curves is similar to those obtained in the neutral salt solution (see Figure. 4.27). Figures 4.35 and 4.36 show the effects of fly ash content on the pitting and repassivation potentials of A535 and its composites. The

Table 4.4. Corrosion potentials and current densities of A535 and its MMCs immersed in 3.5 wt.% salt solution maintained at pH 4.

Material	Corrosion potential (mV)	Corrosion current density i_{corr} (μ Acm^{-2})	Tafel constants (mV)
A535 alloy	-460 ± 1.6	0.60 ± 0.03	$\beta_a = 25 \pm 0.33$
			$\beta_c = 29 \pm 0.38$
A535/hybrid/10$_p$	-512 ± 1.3	0.865 ± 0.01	$\beta_a = 32 \pm 0.35$
			$\beta_c = 36 \pm 0.32$
A535/fly ash/10$_p$	-660 ± 3.8	2.65 ± 0.04	$\beta_a = 38 \pm 0.23$
			$\beta_c = 42 \pm 0.30$
A535/fly ash/15$_p$	-730 ± 8.8	2.72 ± 0.01	$\beta_a = 45 \pm 0.43$
			$\beta_c = 56 \pm 0.38$

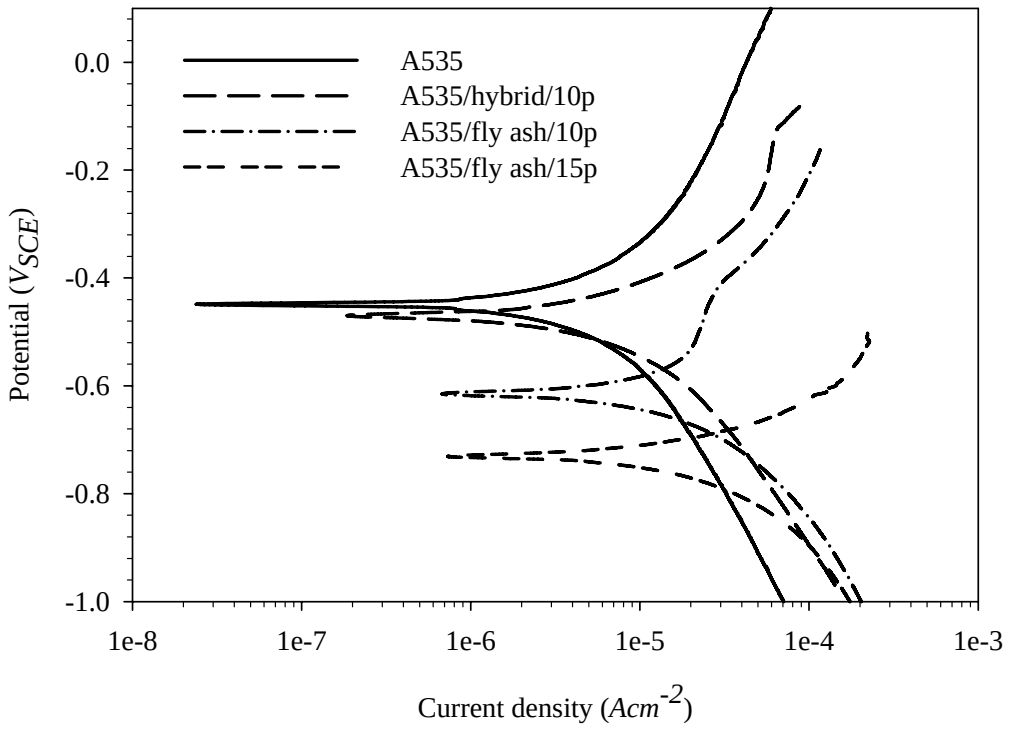

Figure 4.33. Potentiodynamic polarization curves for A535 alloy and its composites immersed in 3.5 wt.% NaCl solution (pH =4).

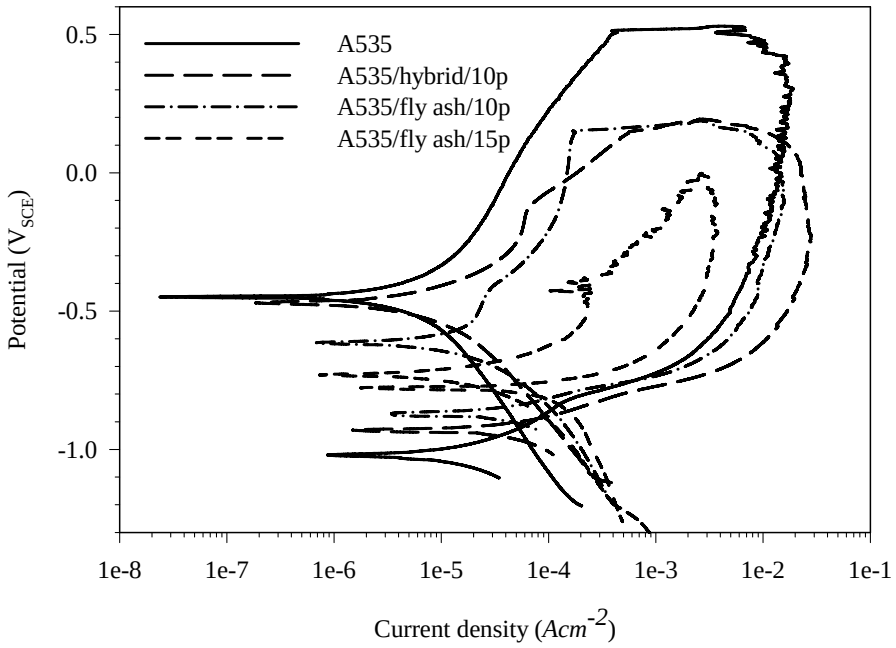

Figure 4.34. Cyclic potentiodynamic polarization curves for A535 and its composites immersed in 3.5 wt.% NaCl solution (pH = 4).

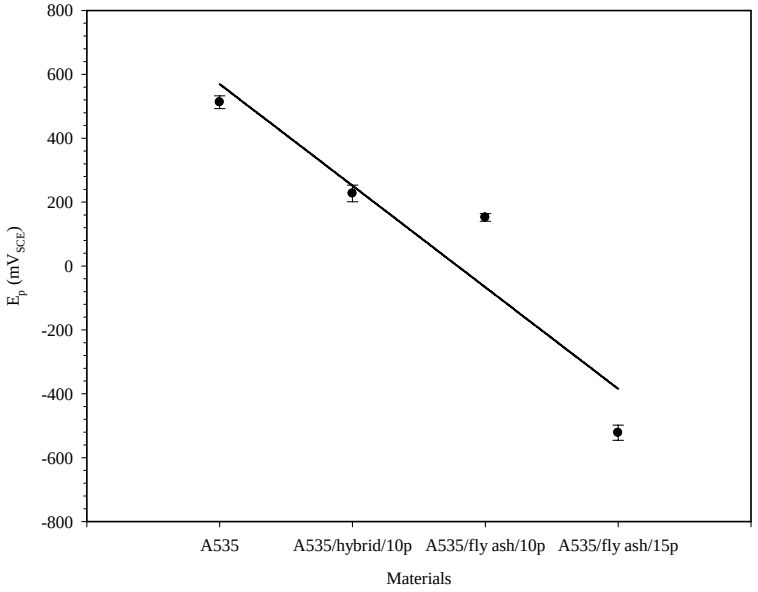

Figure 4.35. Effect of fly ash content on the pitting potential of A535 and its composites immersed in 3.5 wt.% NaCl solution (pH = 4). Error bars are based on standard deviation.

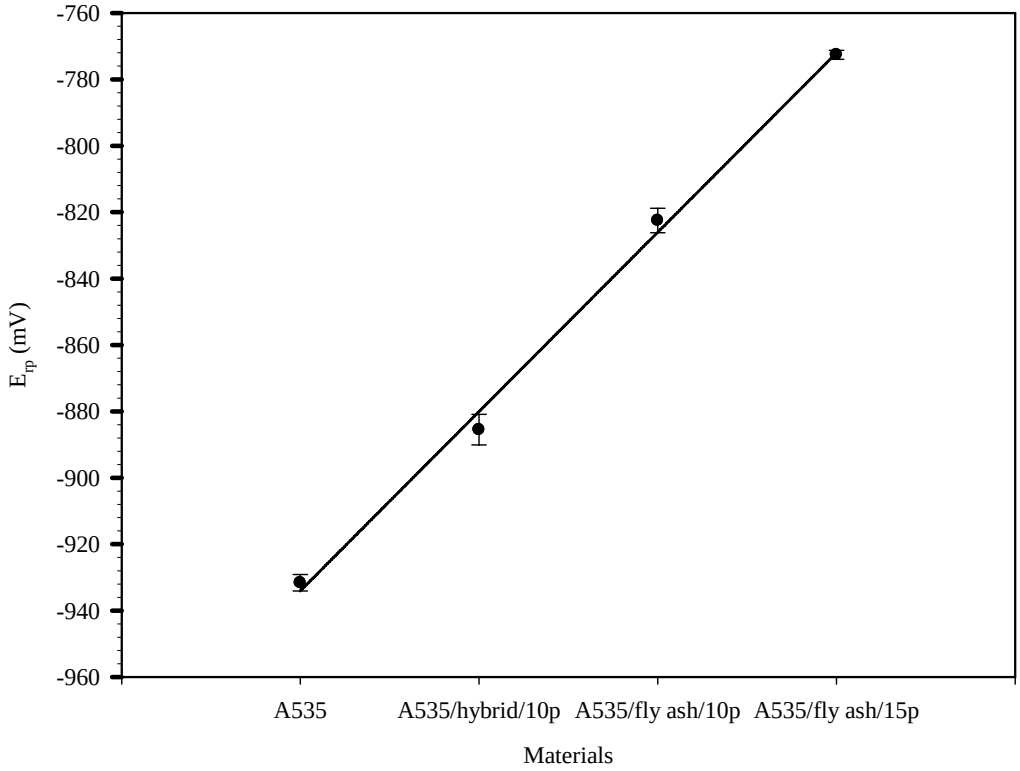

Figure 4.36. Effect of fly ash content on the repassivation potentials of A535 and its composites immersed in 3.5 wt.% NaCl (pH = 4). Error bars are based on standard deviation.

pitting potential became more negative, while the repassivation potential became more positive with increasing fly ash content of the composites. It has been reported [35] that Mg_2Si and Al-Mg-rich compound, which are anodic to the matrix [76, 77], increased with fly ash content thereby increasing the composites susceptibility to pitting corrosion. The superior repassivation potential exhibited by the MMCs containing fly ash is attributable to the reduction in the pit dissolution kinetics by the oxides of metals generated by introduction of fly ash particles into the matrix [60, 61]. Table 4.5 summarizes the pitting and repassivation potentials for A535 and its composites.

Table 4.5. Pitting and repassivation potentials of A535 and the MMCs immersed in 3.5 wt.% salt solution maintained at pH 4.

Material	Pitting potential (mV)	Repassivatin potential (mV)
A535 alloy	512.8 ± 20	-931 ± 2.5
A535/hybrid/10_p	277.3 ± 26	-885 ± 4.5
A535/fly ash/10_p	152 ± 12	-821 ± 3.7
A535/fly ash/15_p	-522 ± 24	-771 ± 1.3

Figure 4.37 shows the microstructure of A535 alloy and A535/hydrid/10_p composites after 14 days immersion in 3.5 wt.% NaCl solution maintained at pH 4. It can be seen that the corrosion damage on the test materials in this electrolyte is less severe than that observed for the materials immersed in the neutral salt solution (See Figure 4.14).

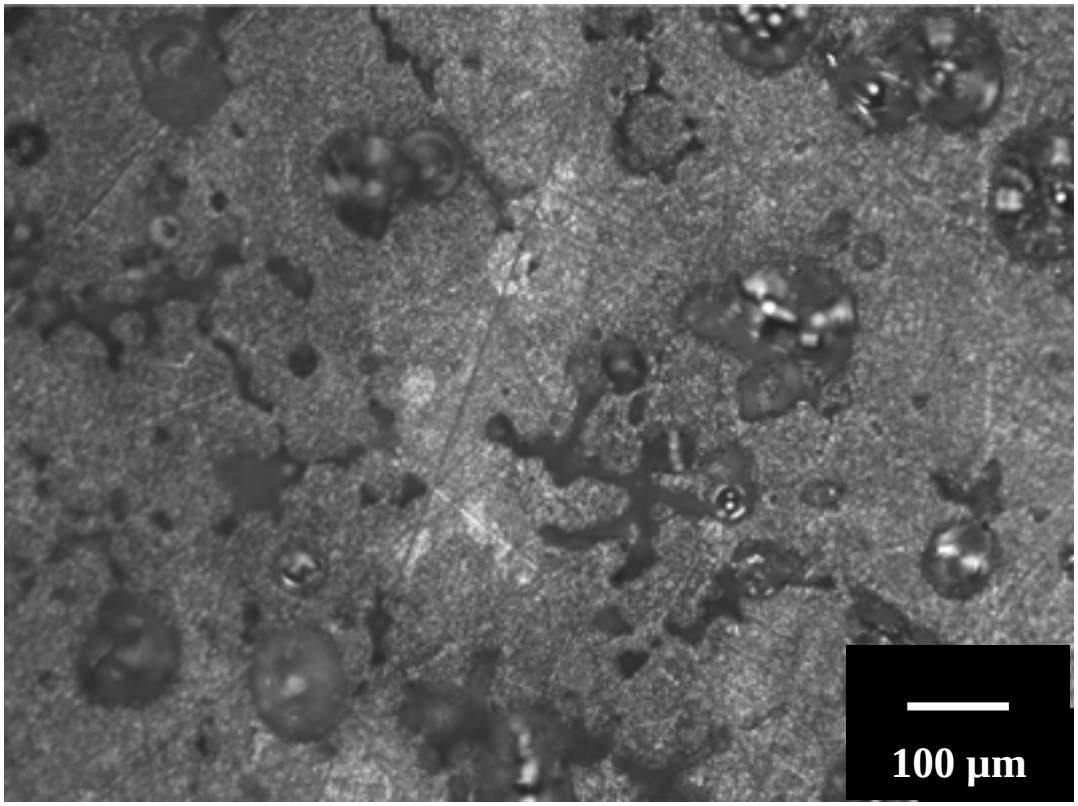

Figure 4.37. Optical micrograph of A535 alloy immersed in 3.5 wt.% NaCl solution (pH = 4) for 14 days.

4.3.2. Corrosion in 3.5 Wt.% NaCl Solution Maintained at pH 9

Figure 4.38 shows the variation of weight loss with immersion time for the specimens immersed in 3.5 wt.% NaCl solution maintained at pH 9 at room temperature. It can be seen that all the specimens lost more weight as exposure time increased. A535 and A535/fly ash/15_p lost the least and greatest weight, respectively. Figure 4.39 shows the variation of corrosion rate with exposure time for the test specimens. Their corrosion rate increased with increasing fly ash content. As in the previous salt solutions, it decreased rapidly during rapidly during the first three days of exposure and with further increase in exposure time, it became generally monotonous. A comparison of Figures 4.25, 4.32, and 4.39 shows that corrosion rates of the materials immersed in the alkaline salt solution is higher than that the corrosion rates obtained in the acidic and neutral solutions.

Kolics *et al.* [83] reported that over the range of 4<pH<10 the thickness of the oxide film formed on pure Al exposed in NaCl solution varied between 4 and 4.5 nm. Furthermore, Saraswathi *et al*. [75] studied the influence of pH on Al-Cu alloy AA2014 and Al-Si alloy composites reinforced with SiC, and exposed to 3.5 wt.% NaCl solution maintained at pH 7.5, synthetic mine water (1000 ml H_2O 0.5 ml HCl + 0.4 cm^3 H_2SO_4) maintained at pH 2.5, and 3.5 wt.% NaCl solution maintained at pH 11.5. He reported that the corrosion damage was more severe in the basic solution than in the acidic and neutral solutions. He attributed the inferior corrosion resistance in the basic solution to the formation of AlO_2^- ions which caused the dissolution of Al.

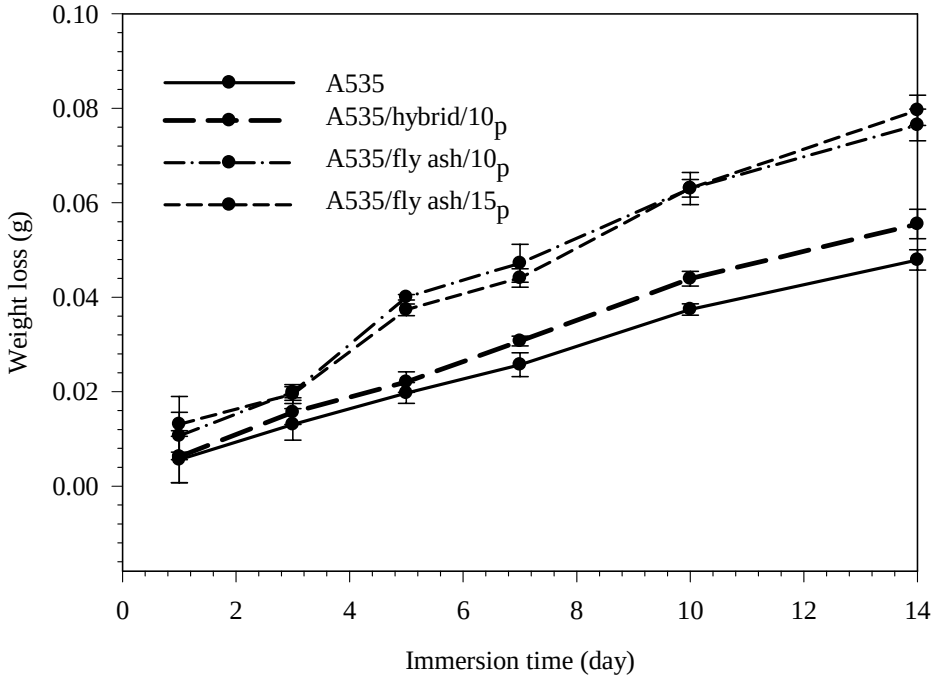

Figure 4.38. Variation of weight loss with time for A535 and its composites immersed in 3.5 wt.% NaCl solution (pH = 9). Error bars are based on standard deviation.

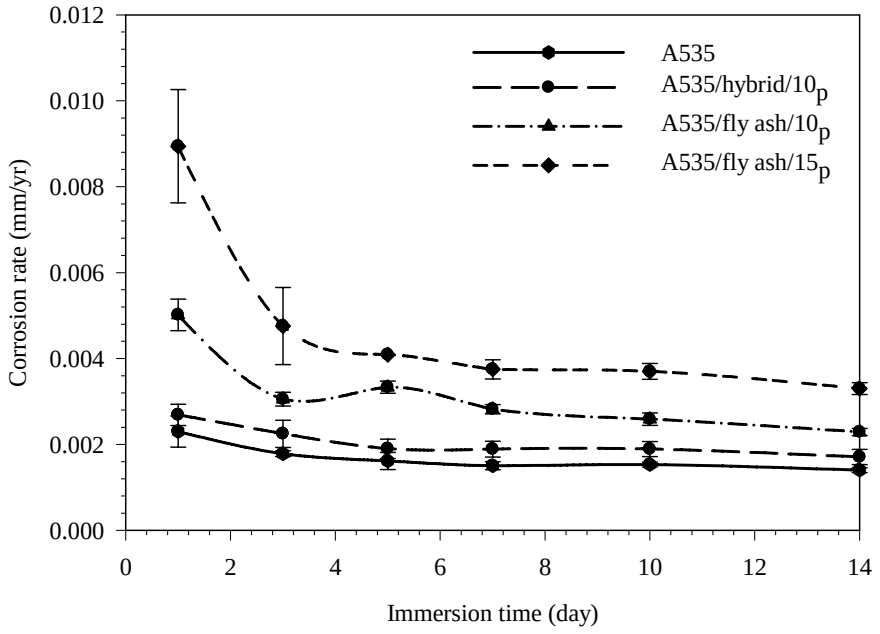

Figure 4.39. Variation of corrosion rate with time for A535 and its composites immersed in 3.5 wt.% NaCl solution (pH = 9). Error bars are based on standard deviation.

Figure 4.40 presents the potentiodynamic polarization curves for samples immersed in 3.5 wt.% NaCl solution maintained at pH 9. It can be seen that the corrosion potential of the test samples became more active with increasing fly ash content. The trend is similar to that obtained for samples exposed in the neutral salt solution. Table 4.6 summarizes the corrosion potentials, current densities, and Tafel constants obtained for A535 and its composites.

Figure 4.41 shows the cyclic polarization curves for test specimens in the present electrolyte. As in the neutral salt solution, the cyclic polarization behaviour of the test materials is similar. The pitting potentials of the alloy and composites are shown in Figure 4.42. Unlike the results obtained in the neutral and acidic salt solutions, the pitting potential of A535/fly ash/10_p in the alkaline solution is superior to that of A535/hybrid/10_p. Bienias *et al*.[37] noted that Al-SiC interface is a preferential site for corrosion attack in Al-SiC composites. Furthermore, Saraswathi *et al*. [75] observed more severe corrosion attack on AA2014 and Al-Si composites reinforced with SiC exposed to 3.5 % NaOH solution maintained at pH 11.5 than when the materials were exposed to neutral salt solution (pH 7.5) and synthetic acidic mine water (pH 2.5). He reported that the corrosion attack on the Al-SiC interface created voids around the SiC particles. Although Al-SiC interface is susceptible to attack in alkaline solution [75], it is also possible that experimental errors in reading the pitting potential from Figure 4.41 could have led to the observed discrepancies in the E_{pit} data presented in Figure 4.42.

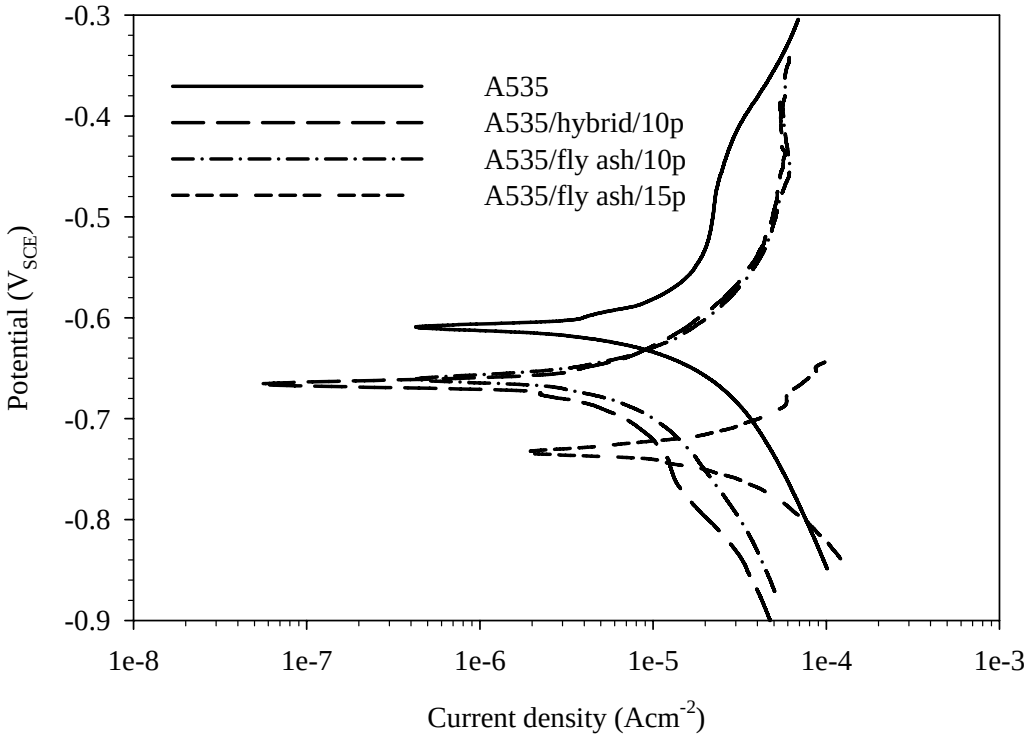

Figure 4.40. Potentiodynamic polarization curves for A535 alloy and its composites immersed in 3.5 wt.% NaCl solution (pH =9).

Table 4.6. Corrosion potentials, current densities, and Tafel constants of A535 and its composites immersed in 3.5 wt.% salt solution maintained at pH 9.

Material	Corrosion potential (mV)	Corrosion current density i_{corr} (μ Acm^{-2})	Tafel constants (mV)
A535 alloy	-613 ± 5.4	2.60 ± 0.01	$\beta_a = 42 \pm 0.43$
			$\beta_c = 48 \pm 0.41$
A535/hybrid/10_p	-674 ± 11.2	3.02 ± 0.01	$\beta_a = 55 \pm 0.48$
			$\beta_c = 67 \pm 0.51$
A535/fly ash/10_p	-685 ± 4.3	3.56 ± 0.03	$\beta_a = 63 \pm 0.55$
			$\beta_c = 72 \pm 0.53$
A535/fly ash/15_p	-716 ± 2.5	4.53 ± 0.01	$\beta_a = 75 \pm 0.59$
			$\beta_c = 83 \pm 0.49$

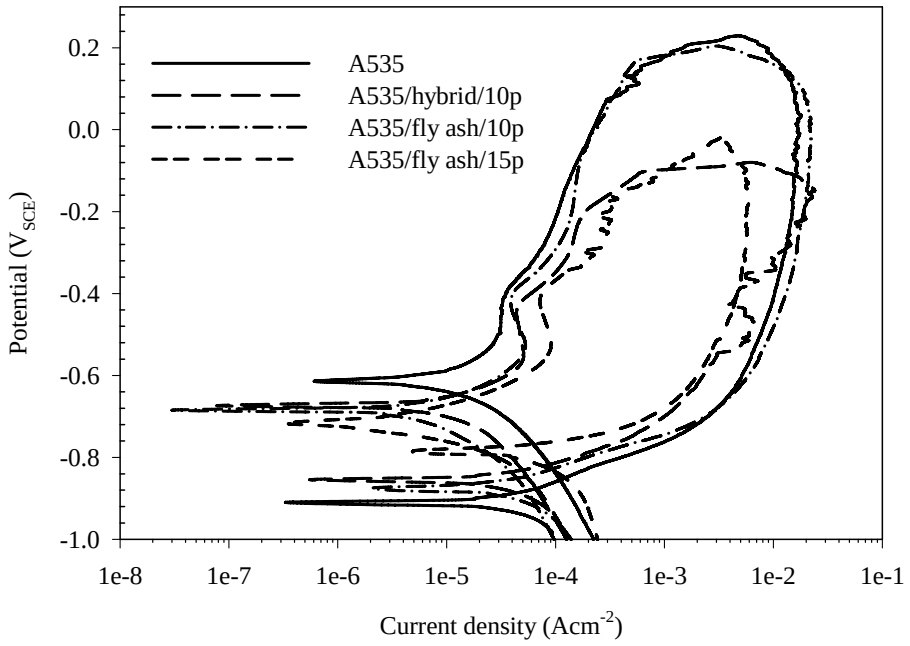

Figure 4.41. Cyclic potentiodynamic polarization curves for A535 and its composites immersed in 3.5 wt.% NaCl solution (pH = 9).

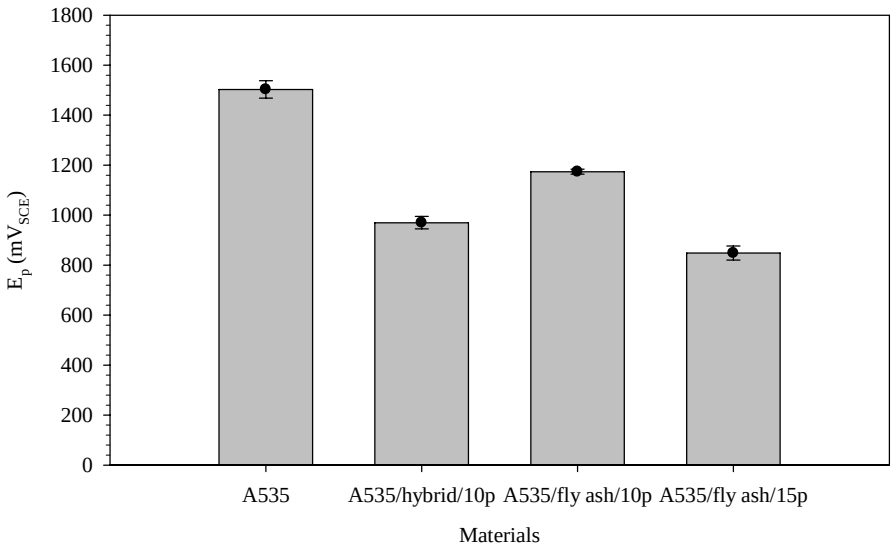

Figure 4.42. Effect of fly ash content on the pitting potential of A535 and its composites immersed in 3.5 wt.% NaCl solution (pH = 9). Error bars are based on standard deviation.

Figure 4.43 shows the plot of the repassivation potentials. The repassivation potential of the test materials became more positive as their fly ash content increased. The superior repassivation potential of the composites over the unreinforced alloy is attributable to the reduction of pit dissolution kinetics by metallic oxides introduced by the addition of fly ash to the matrix [60, 61]. Table 4.7 shows the pitting and repassivation potentials of the test materials.

Figure 4.44 shows the microstructures of A535 alloy and A535/hydrid/10_p after 14 days immersion in 3.5 wt.% NaCl solution maintained at pH 9. It can be seen that the alloy was more severely attacked in this medium than in both the neutral salt solution and acidified salt solution maintained at pH 4 (see Figures 4.14 and 4.37) .

Table 4.7. Pitting and repassivation potentials of A535 and the MMCs immersed in 3.5 wt.% salt solution maintained at pH 9.

Material	Pitting potential (mV)	Repassivatin potential (mV)
A535 alloy	109.5 ± 35	-874.6 ± 16
A535/hybrid/10_p	-104 ± 25	-833.2 ± 5
A535/fly ash/10_p	4 ± 10	-853 ± 38
A535/fly ash/15_p	-303.9 ± 28	-778.8 ± 42

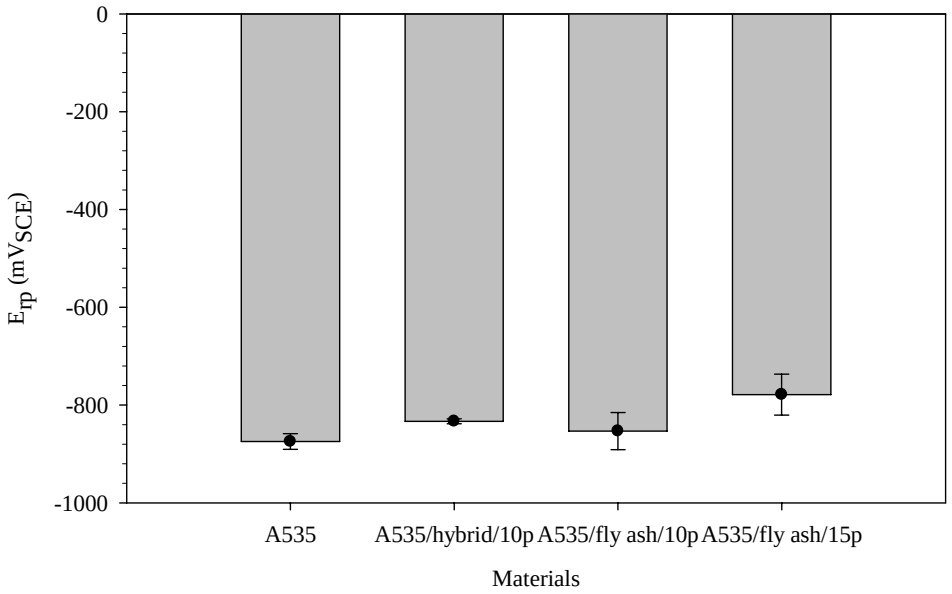

Figure 4.43. Effect of fly ash content on the repassivation potentials of A535 and its composites immersed in 3.5 wt.% NaCl solution (pH = 9). Error bars are based on standard deviation.

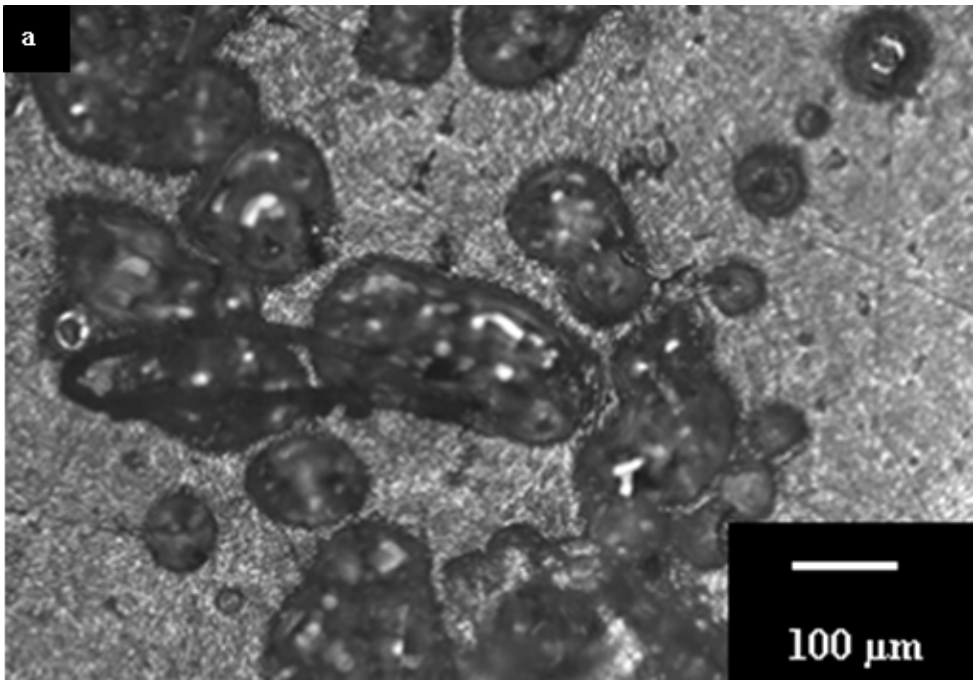

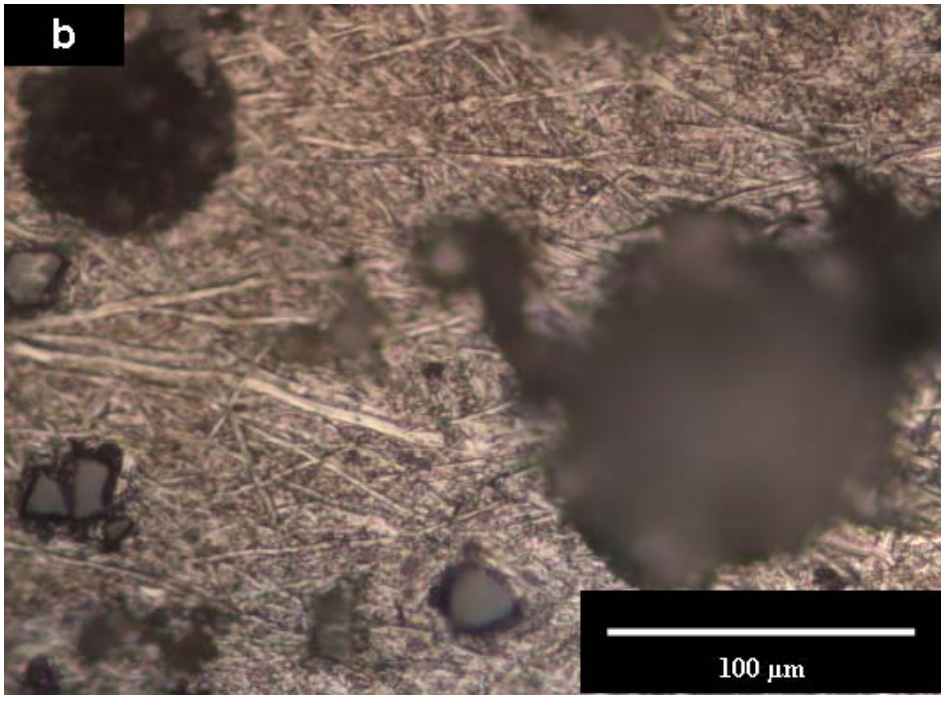

Figure 4.44. Optical micrographs of (a) A535 and (b) A535/hybrid/10_p immersed in 3.5 wt.% NaCl solution (pH = 9) for 14 days.

4.3.3 Corrosion in 3.5 Wt.% NaCl Solution Maintained at pH 3

The potentiodynamic curves obtained for the materials tested in 3.5 wt.% NaCl solution maintained at pH 3 are shown in Figure 4.45. As in the previous *E* vs *i* plots, it can be seen that A535 has the most noble corrosion potential in this solution. The corrosion potentials of the composites also became more active with increasing fly ash content. Table 4.8 summarizes the corrosion potentials, current densities, and Tafel constants determined for the test materials. Babic *et al.* [84] reported corrosion potentials (E_{corr}) of -751, -759, and -817 mV for Al, Al-Mg-Si, Al-Zn-Mg alloys, respectively, exposed to 0.5 M NaCl solution maintained at pH 1.3. The corrosion potential of Al exposed to 0.1 M HCl, which was reported to be -690 mV [85], is in agreement with the E_{corr} for A535 immersed in 3.5 wt.% NaCl solution maintained at pH 3.

Figure 4.46 shows the cyclic polarization curves for the test materials immersed in acidic NaCl solution maintained at pH 3. The curves are similar to those shown in Figures 4.27, 4.34, and 4.41 which show that the composites exhibited similar corrosion behaviour to the parent alloy. Fig. 4.47 shows the effect of fly ash content on the pitting potential of A535 and its composites. The pitting potential of the composites became more negative as the fly ash content of the MMC increased. The effect of fly ash content on the repassivation potentials of A535 and its MMCs is presented in Figure 4.48. The trend of the curves is similar to that obtained for the test materials in the neutral salt solution, where the repassivation potential became more positive as fly ash content of the composites increased. The superior repassivation potential exhibited by

Table 4.8. Corrosion potentials, current densities, and Tafel constants of A535 and the MMCs immersed in 3.5 wt.% salt solution maintained at pH 3.

Material	Corrosion potential (mV)	Corrosion current density i_{corr} (μ Acm^{-2})	Tafel constants (mV)
A535 alloy	-609 ± 11.2	3.86 ± 0.04	$\beta_a = 48 \pm 0.57$ $\beta_c = 58 \pm 0.53$
A535/hybrid/10$_p$	-666 ± 5.3	5.20 ± 0.06	$\beta_a = 57 \pm 0.62$ $\beta_c = 69 \pm 0.67$
A535/fly ash/10$_p$	-660 ± 4.6	6.30 ± 0.05	$\beta_a = 69 \pm 0.43$ $\beta_c = 78 \pm 0.63$
A535/fly ash/15$_p$	-732 ± 7.9	12.00 ± 0.03	$\beta_a = 78 \pm 0.88$ $\beta_c = 92 \pm 0.76$

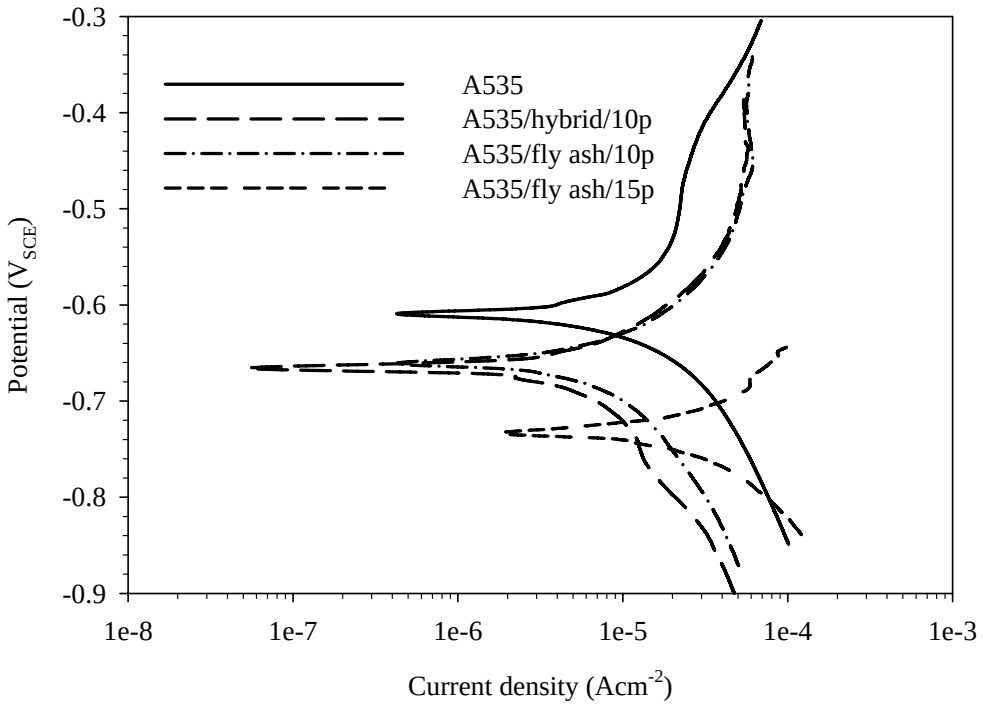

Figure 4.45. Potentiodynamic polarization curves for A535 alloy and its composites immersed in 3.5 wt.% NaCl solution (pH =3).

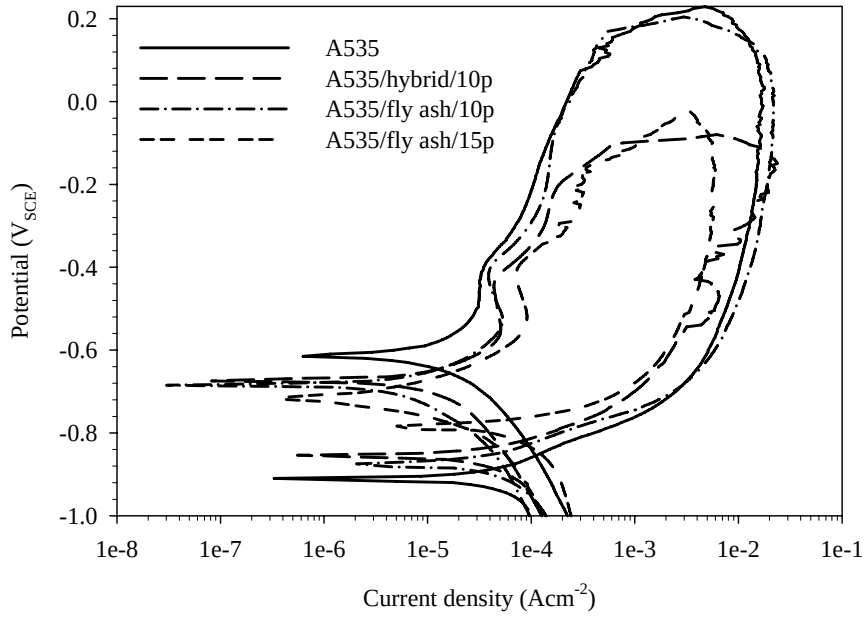

Figure 4.46. Cyclic potentiodynamic polarization curves for A535 and composites immersed in 3.5 wt.% NaCl solution (pH = 3).

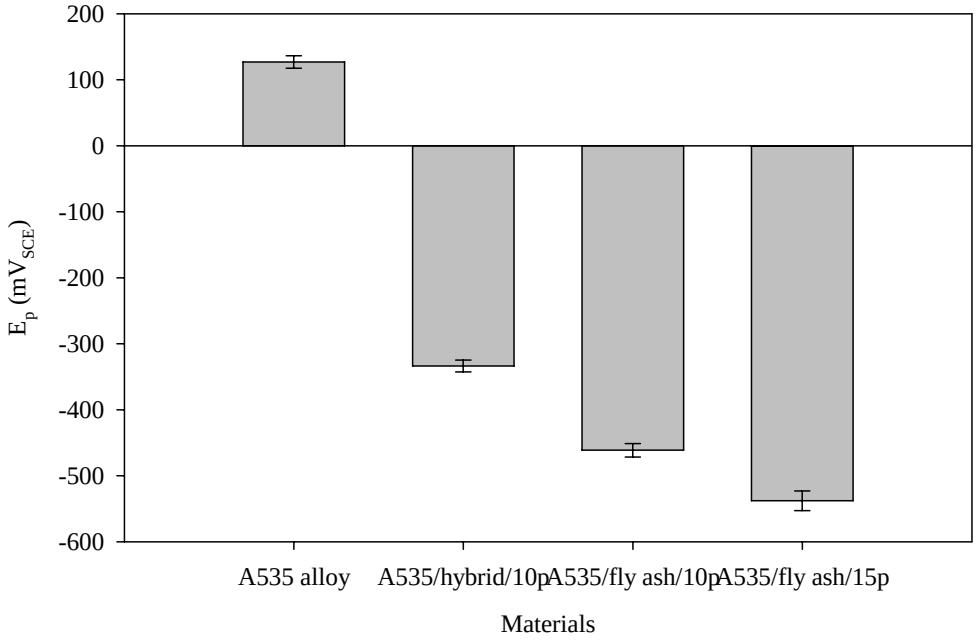

Figure 4.47. Effect of fly ash content on the pitting potential of A535 and its composites immersed in 3.5 wt.% NaCl solution (pH = 3). Error bars are based on standard deviation.

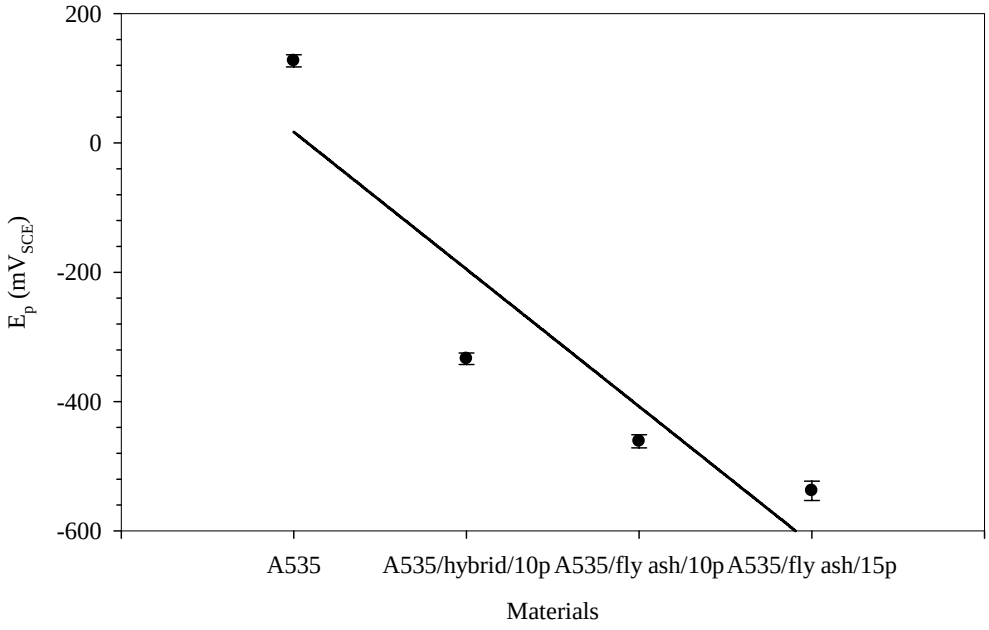

Figure 4.48. Effect of fly ash content on the repassivation potentials of A535 and its composites immersed in 3.5 wt.% NaCl solution (pH = 3). Error bars are based on standard deviation.

the composites containing fly ash is attributable to the reduction in the pit dissolution kinetics by the oxides of metals generated by introduction of fly ash particles into the matrix [60, 61]. Table 4.9 shows the pitting and repassivation potentials of the test materials, while Tables 4.10 and 4.11 summarize the effect of pH on the pitting and repassivation potentials of the test materials, respectively.

Table 4.9. Pitting and repassivation potentials of A535 and the MMCs immersed in 3.5 wt.% salt solution maintained at pH 3.

Material	Pitting potential (mV)	Repassivatin potential (mV)
A535 alloy	126.9 ± 35	-896 ± 3.8
A535/hybrid/10_p	-333.3 ± 25	-847.6 ± 10.0
A535/fly ash/10_p	-491.4 ± 10	-818.9 ± 5.0
A535/fly ash/15_p	-786.5 ± 28	--786.5 ± 6.7

Table 4.10. Effect of pH on pitting potential, $E_{p,}$ of A535 and the MMCs immersed in 3.5 wt.% salt solution

	Pitting potential, E_p (mV)				
Material	pH 3	pH 4	pH 7	pH 9	pH 8.2 (South Saskatchewan River water)
A535 alloy	126.9 ± 35	512.8 ± 20	116 ± 6.6	109.5 ± 35	1503 ± 35
A535/hybrid/10_p	-333.3 ± 25	277.3 ± 26	-66.3 ± 13.7	-104 ± 25	969.8 ± 27
A535/fly ash/10_p	-491.4 ± 10	152 ± 12	-117.2 ± 4.3	4 ± 10	1174 ± 15
A535/fly ash/15_p	-786.5 ± 28	-522 ± 24	-237.8 ± 8.9	-304 ± 28	848.5 ± 15

Table 4.11. Effect of pH on Repassivation potential, E_{rp} of A535 and the MMCs immersed in 3.5 wt.% salt solution

	Repassivation potential, E_{rp} (mV)				
Material	pH 3	pH 4	pH 7	pH 9	pH 8.2 (South Saskatchewan River water)
A535 alloy	-896 ± 3.8	-931 ± 2.5	-822 ± 1.8	-874 ± 16	-735.5 ± 18
A535/hybrid/10_p	-847 ± 10.0	-885 ± 4.5	-808 ± 5.4	-833 ± 5	-712.3 ± 11
A535/fly ash/10_p	-818 ± 5.0	-821 ± 3.7	-803 ± 15.6	-853 ± 38	-645 ± 14.67
A535/fly ash/15_p	-786 ± 6.7	-771 ± 1.3	-799 ± 6.5	-778 ± 42	-506 ± 4.3

4.5 Effects of Fly Ash Addition on the Corrosion Behaviour of A535 in South Saskatchewan River Water

Table 4.12 shows the main anion constituents of water from the South Saskatchewan River. It can be seen that it contains chloride ions and fluoride ions. The 0.000141 mol/l of chloride ions present is negligible when compared with 0.6 mol/l of chloride ions present in 3.5 wt.% NaCl solution. The low quantity of chloride ions in the South Saskatchewan River water was responsible for the superior corrosion resistance exhibited by the test specimens in it.

Figure 4.49 shows the variation of weight loss with exposure time for the specimens immersed in room temperature water collected from the South Saskatchewan River. It can be seen that the weight loss for all the specimens increased as the exposure time increased. However, a comparison of Figures 4.24 and 4.49 shows that the weigh loss for specimens immersed in the fresh water was smaller than those obtained for specimens immersed in the salt solutions. The variation of corrosion rate with immersion time for A535 and the composites in the river water is shown in Figure 4.50. It can be seen that the trend is similar to that shown in Figure 4.25 for specimens immersed in neutral salt solution. As expected, the corrosion rates for each test material in the fresh water is lower than the rates obtained for specimens immersed in the neutral salt solution. It is believed that the high chloride content of the salt solution was responsible for the inferior corrosion rates recorded for the samples. The observation that pitting corrosion increases with increase in the concentration of chloride ions is

Table 4.12. Anion composition of the South Saskatchewan River water.

Anions	***mg/L***	**Molarity (mol/L)**
Cl^-	5	0.000141
NO_3^-	0	0
F^-	0.14	$7.3684 x 10^{-6}$
SO_4^{2-}	80	0.0025

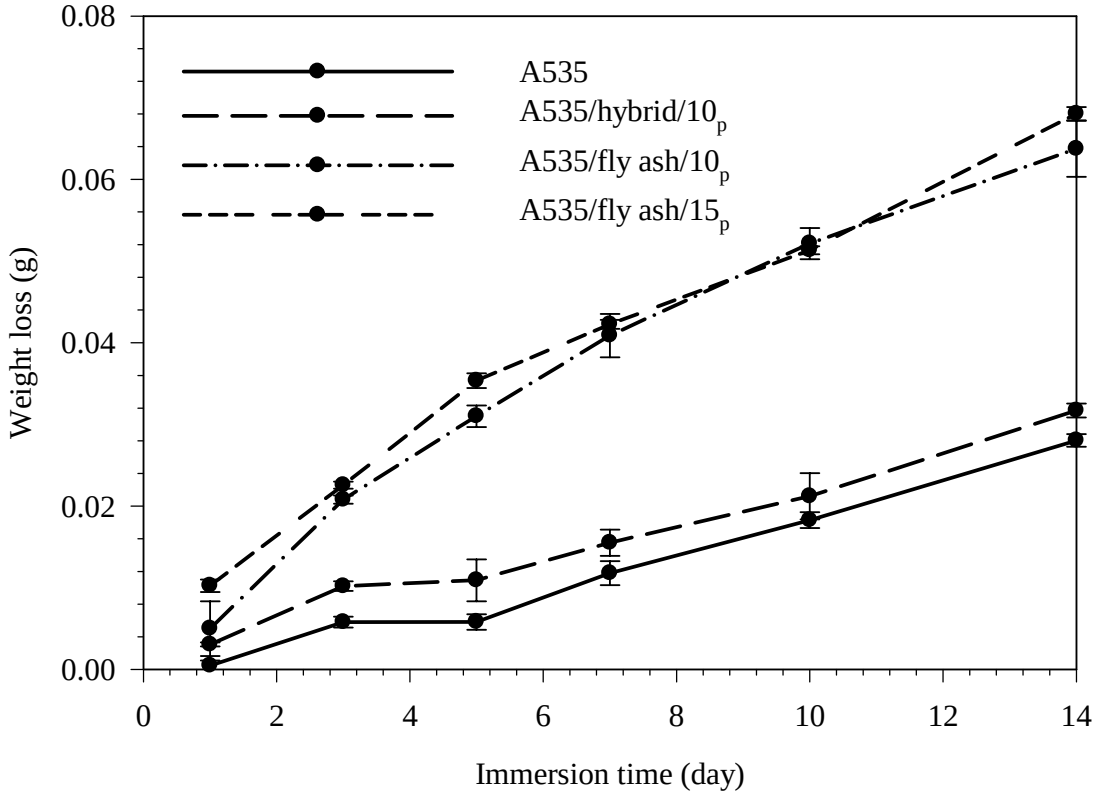

Figure 4.49. Variation of weight loss with time for A535 and its composites immersed in water from the South Saskatchewan River. Error bars are based on standard deviation.

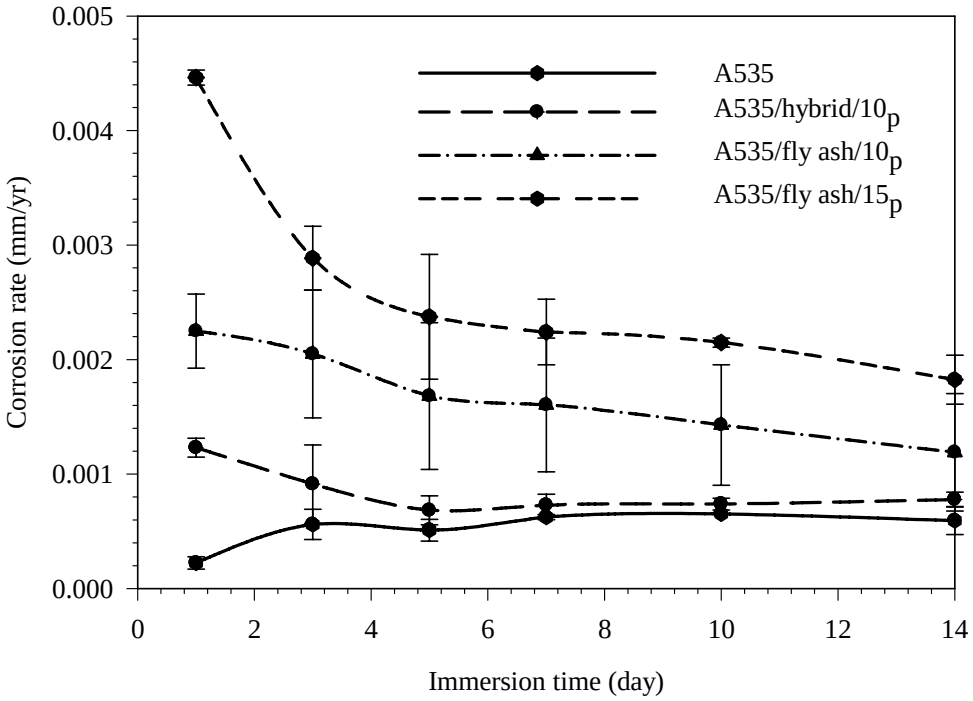

Figure 4.50. Variation of corrosion rate of A535 and its composites immersed in river water. Error bars are based on standard deviation.

supported by considerable experimental studies [51, 60, 86-89]. Jones [51] observed that the presence of chloride ions causes an increase in the anodic current at all potentials, while Szklarska-Smialowska [60] reported that chloride ions decrease the pitting potential of Al. Reboul [86] noted that chloride ions disrupt the formation of the passive film thereby creating initiation sites for pit formation, while Cao [89] reported that chloride ions increased the corrosion rate of an Al-Cu alloy. The potentiodynamic curves obtained for the test materials immersed in river water are shown in Figure 4.51. Table 4.13 summarizes the corrosion potentials, current densities, and Tafel constants obtained for the test materials immersed in the river water. The data trend is similar to that obtained for specimens immersed in neutral salt solution. The corrosion

Table 4.13. Corrosion potentials, current densities, and Tafel constants of A535 and the MMCs immersed in river water.

Material	Corrosion potential (mV)	Corrosion current density i_{corr} (μ Acm^{-2})	Tafel constants (mV)
A535 alloy	-243 ± 1.7	0.25 ± 0.01	$\beta_a = 12 \pm 0.12$ $\beta_c = 18 \pm 0.17$
A535/hybrid/10$_p$	-275 ± 1.3	0.41 ± 0.01	$\beta_a = 19 \pm 0.18$ $\beta_c = 23 \pm 0.23$
A535/fly ash/10$_p$	-305 ± 1.5	0.59 ± 0.02	$\beta_a = 23 \pm 0.35$ $\beta_c = 29 \pm 0.29$
A535/fly ash/15$_p$	-357 ± 4.8	0.88 ± 0.01	$\beta_a = 30 \pm 0.21$ $\beta_c = 37 \pm 0.16$

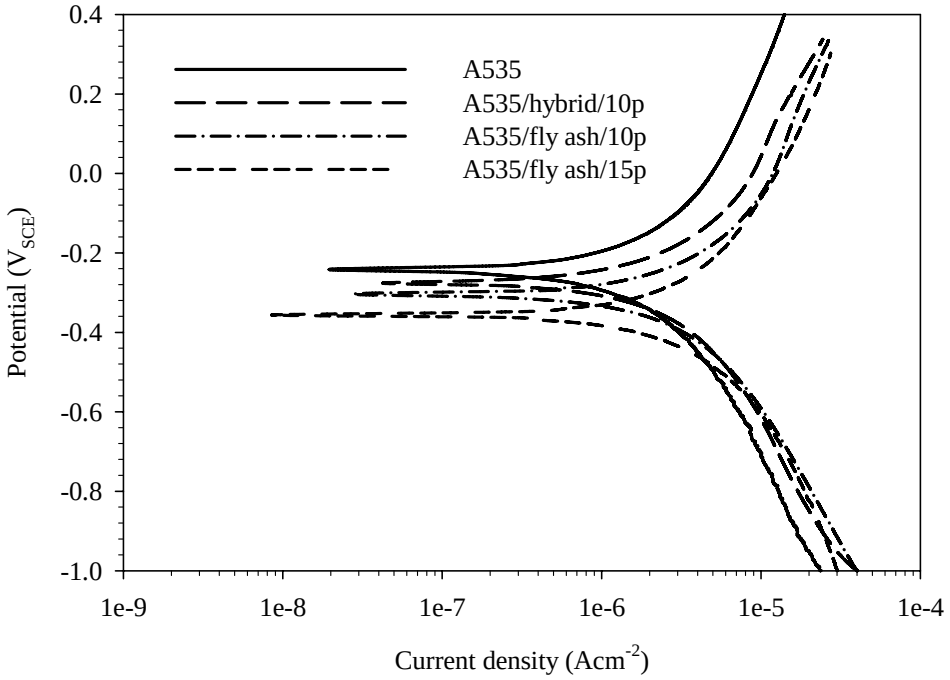

Figure 4.51. Potentiodynamic polarization curves for A535 alloy and its MMCs immersed in river water.

potential of the test materials became more negative with increasing fly ash content. A comparison of Tables 4.2 and 4.13 shows that the corrosion potentials of the specimens immersed in the river water are more noble than those obtained in the neutral salt solution.

Figure 4.52 shows the cyclic polarization curves for A535 and its MMCs immersed in the Saskatchewan River water. The trend of the curves is similar to that obtained for specimens immersed in neutral salt solution. The corrosion potentials are however more noble in the neutral salt solution than in the river water. Figures 4.53 and 4.54 show the effect of fly ash content on the pitting and repassivation potentials of the alloy and the composites in immersed in water collected from the South Saskatchewan River. Table 4.14 summarizes the pitting and repassivation poatentials of the test materials. The pitting potential became more negative with increase in the fly ash content of the composites. Mg_2Si and Al-Mg-rich compound, which are anodic to the matrix [76, 77], increased with fly ash content making the composites more susceptible to pitting corrosion. Unlike the results obtained in neutral and acidic salt solutions, the pitting potential of A535/fly ash/10_p in Saskatchewan water (pH = 8.2) is superior to that of A535/hybrid/10_p. Kolics *et al*. [83] reported that the thickness of oxide film on pure Al varied between 4 and 4.5 nm over the range 4<pH<10. Saraswathi *et al.* [73] observed that corrosion attack on an Al-Si alloy reinforced with SiC was more severe in an alkaline medium than in acidic and neutral media. However, it is possible that the observed discrepancy in pitting corrosion presented in Table 4.14 may be as a result of experimental errors in reading the E_{pit} data from Figure 4.52.

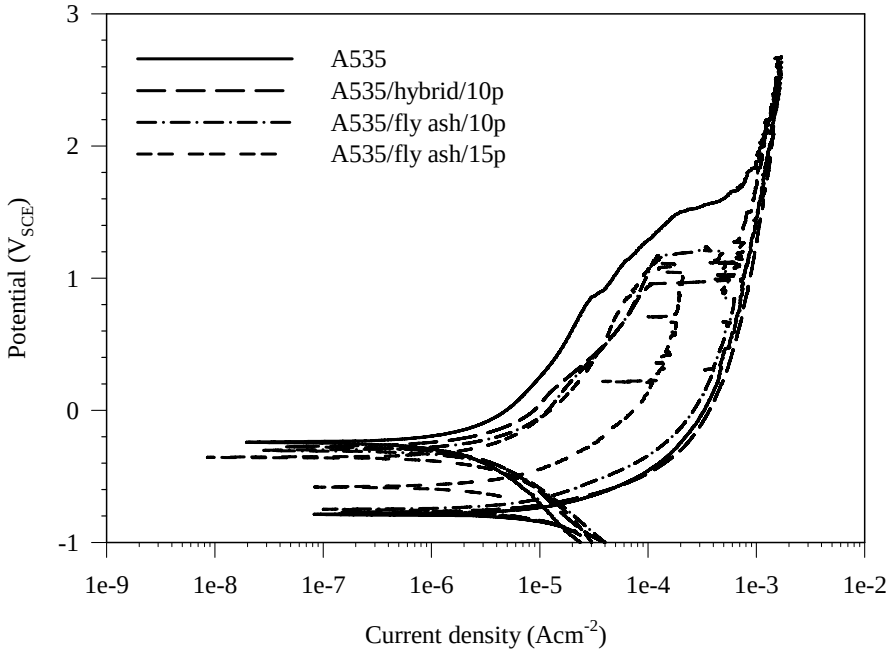

Figure 4.52. Cyclic polarization curves for A535 and the composites immersed in river water.

Table 4.14. Pitting and repassivation potentials of A535 and the MMCs immersed in river water.

Material	Pitting potential (mV)	Repassivatin potential (mV)
A535 alloy	1503 ± 35	-735.5 ± 18
A535/hybrid/10_p	969.8 ± 27	-712.3 ± 11
A535/fly ash/10_p	1174 ± 15	-645 ± 14.67
A535/fly ash/15_p	848.5 ± 15	-506 ± 4.3

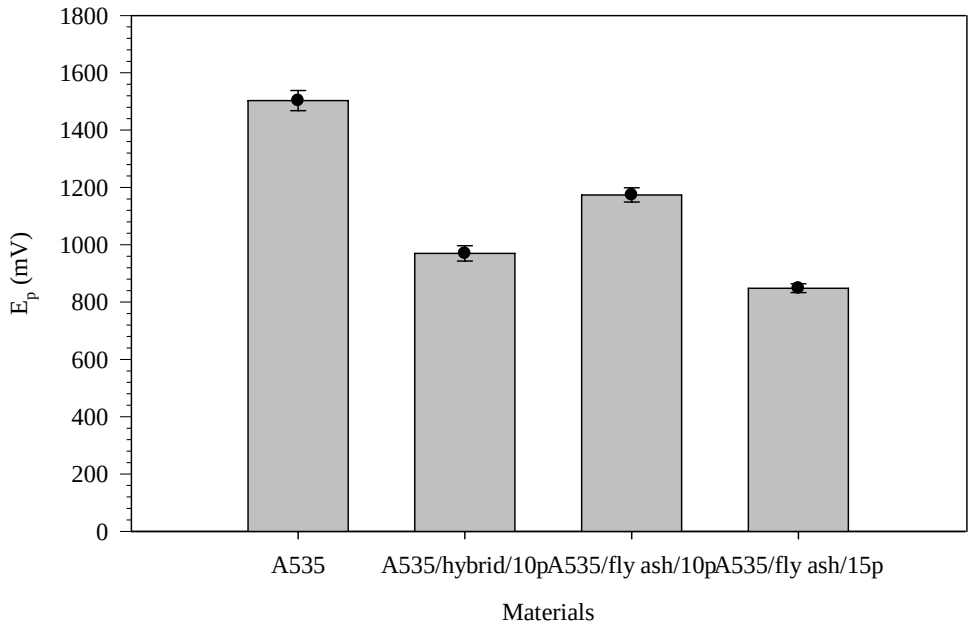

Figure 4.53. Effect of fly ash content on the pitting potentials of A535 and the composites immersed in river water. Error bars are based on standard deviation.

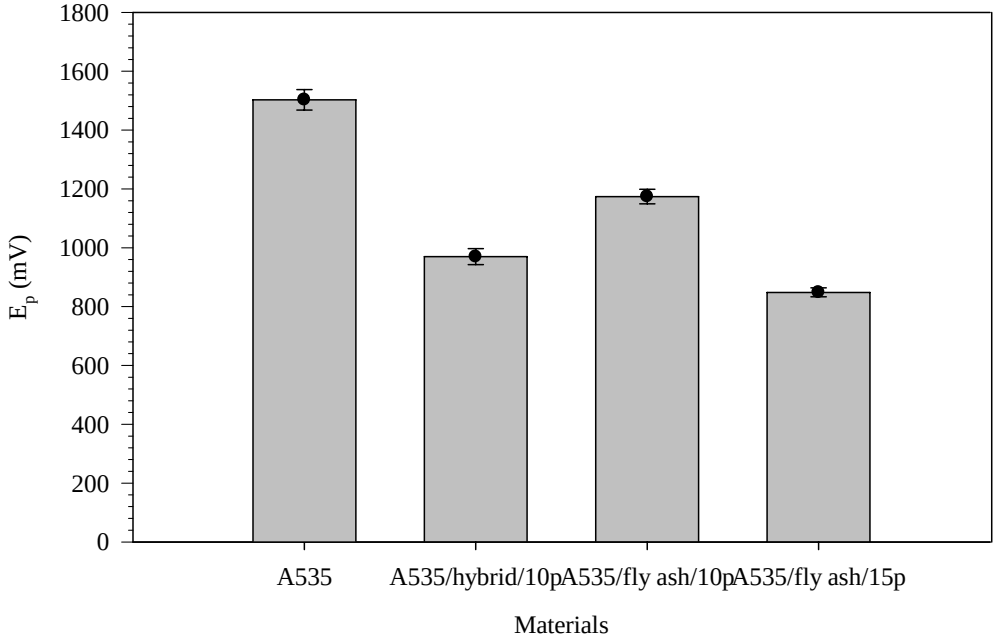

Figure 4.54. Effect of fly ash content on the repassivation potentials of A535 and the composites immersed in river water. Error bars are based on standard deviation.

The repassivation potentials of the composites became more positive with increase in fly ash content of the composites. The superior repassivation potential exhibited by the composites over the over the unreinforced alloy is attributable to the reduction in the pit dissolution kinetics in the matrix by metallic oxides introduced by the addition of fly ash [60, 61].

Figures 4.55 and 4.56 show the microstructures of A535 alloy and A535/fly ash/10_p after 14 days exposure in the South Saskatchewan River water. Comparing the figures with Figure 4.45, it can be seen that the corrosion attack in the fresh water was less severe than that in the neutral salt solution.

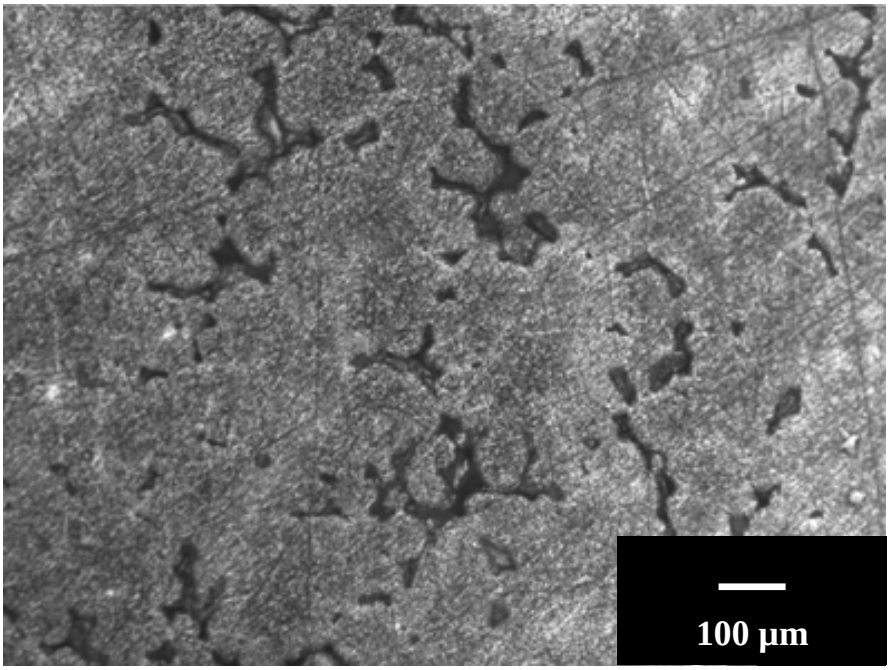

Figure 4.55. Optical micrograph of A535 alloy immersed in river water for 14 days.

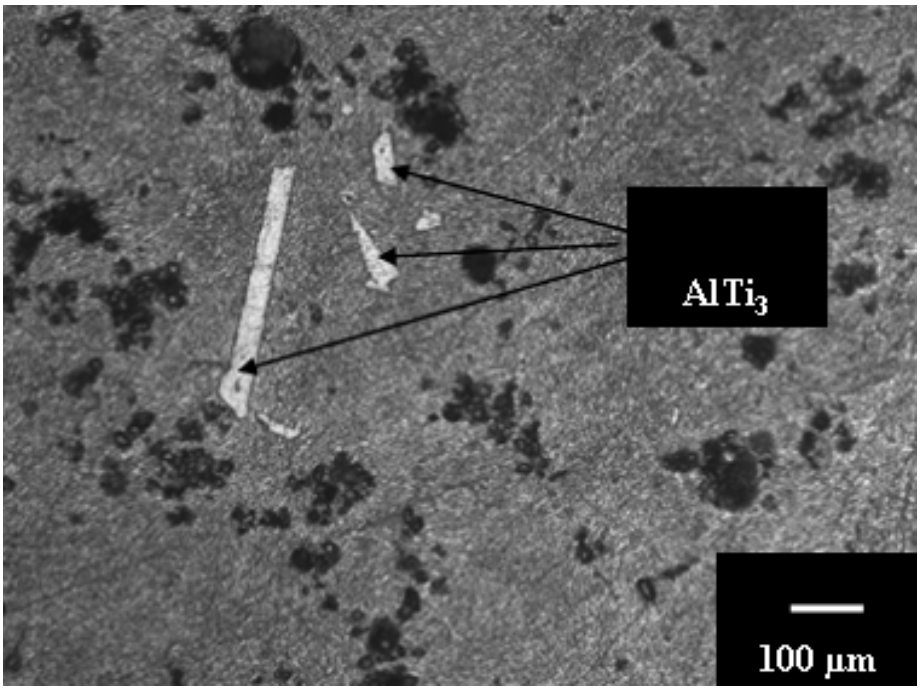

Figure 4.56. Optical micrographs of A535/hybrid/10_p, immersed in river water for 14 days.

5.0 CONCLUSIONS AND RECOMMENDATIONS

In this work, the corrosion behaviour of cast Al-Mg alloy A535 and its MMCs containing 10 wt.% and 15 wt.% fly ash, and 10 wt.% hybrid reinforcement (5 wt.% fly + 5 wt.% SiC) was investigated using weigh-loss and electrochemical corrosion tests, optical microscopy, scanning electron microscopy (SEM), and energy dispersive X-ray spectroscopy (EDS). The tests were conducted in fresh water collected from the South Saskatchewan River and 3.5 wt. % NaCl maintained at room temperature. The pH of the salt solution varied from 3 to 9. For comparison, two other aluminum alloys, AA2618 and AA5083-H116, were tested in the same electrolytes. The conclusions derived from the results presented in the chapter 4 are summarized here. Also, suggestions for future work are presented.

5.1 Conclusions

1. The immersion test results in neutral salt water solution showed that the corrosion rate of cast Al-Mg alloy A535 was superior to those of AA5083-H116 and AA2618. The electrochemical polarization results showed that the corrosion and pitting potentials of A535 were superior (more noble) to those of A5083-H116 and AA2618. However, the three alloys possessed similar repassivation potentials.

2. In neutral salt solution, the weight loss and, hence, the corrosion rate of the MMCs increased with increasing fly ash content. A535 and A535/fly ash/15_p had the lowest and highest weight loss and corrosion rate, respectively. The corrosion and pitting potentials of the MMCs became more negative as their fly ash content increased. The repassivation potential of the MMCs became more positive (more noble) with increase in fly ash content. The addition of the fly ash to A535 increased the amount of Mg_2Si formed in the matrix. Preferential dissolution of this anodic phase in the matrix is responsible for the decrease in the corrosion and pitting potentials of the MMCs. Furthermore, the addition of fly ash to the matrix introduced insoluble or partially soluble oxides. These oxides caused metastable pits to passivate and drove the repassivation potentials of the MMCs to more noble potentials.

3. The corrosion behaviour of the test materials exposed in water collected from the Saskatchewan River showed a similar trend to that obtained in neutral, acidic, and alkaline salt solutions. However, the weight loss and corrosion rate were lower that those measured in the neutral salt solution. The pitting and repassivation potentials for the test materials were equally more noble than the values obtained in salt solution. The chloride content of the fresh water is negligible when compared to that of the salt solution. This difference in chloride content of the two solutions is responsible for superior corrosion performance in water collected from South Saskatchewan River.

4. In acidified salt water solution maintained at pH 4, the corrosion and pitting potentials of the test materials were superior to those measured in the neutral, alkaline, and acidic (pH =3) salt solutions.

5.2 Recommendations for Future Work

The following investigations are suggested for future work to enable a better understanding of the corrosion behaviour of A535 and its MMCs.

1. A detailed microstructural study of the corrosion products formed on the corroded A535 and its MMCs specimen in different media and pH. Knowledge of the microstructure and chemical composition of the corrosion products would provide more information on the nature and stability of the protective oxide film formed on the test materials.

2. An investigation into the effect of heat treatment on the corrosion behaviour of A535 and its MMCs in salt and fresh water solutions of different pH is recommended. Heat treatment relieves residual stresses generated during the solidification of the materials. The presence of residual stresses may have influenced the results obtained in this study.

3. The effect of temperature of the corrosive medium on the corrosion behaviour of A535 and the MMCs in salt and fresh water solutions of different pH should be

evaluated. This study will determine the influence of temperature variation on the corrosion performance of the test materials.

4. An investigation into the effect of heat treatment on the morphology of the Mg_2Si and Al-Mg-rich compounds which are responsible for the pitting corrosion of A535 alloy and its composites reinforced with fly ash. This study will determine the influence of the morphology of the intermetallic phases on the corrosion behaviour of the materials.

REFERENCES

1 J. R. Davis (Ed.), *Corrosion: Understanding the Basics*, ASM International, Ohio, 2000.

2. S. A. Shipilov, *Sessions of Corrosion Education and Training*: 16th International Corrosion Congress (16ICC2005), Beijing, 2005, http://www.16icc2005.com/EN/Education.PDF accessed on 8th September, 2008.

3. G. Koch, *Cost of Corrosion*, http://www.corrosioncost.com/news/2002/corrosioncosts.htm accesssed on 8th September, 2008.

4. N. Chawla and Y. Shen, "Mechanical Behaviour of Particle Reinforced Metal Matrix Composites", *Advanced Engineering Materials*, 2001, Vol. 3, No. 6, pp. 357-370.

5. D. J. Lloyd, "Particle-Reinforced Aluminum and Magnesium Matrix Composites", *International Materials Reviews*, 1994, Vol. 39, No. 1, pp. 1-23.

6. L. H. Hihara, R. Bregman, P. K. Takahashi, "Marine Applications for Advanced Composites Materials", *Proceedings of the International Conference on Advanced Composite Materials*, Publ by Minerals, Metals and Materials Society (TMS), Warrendale, PA, USA, 1993, pp. 95-100.

7. M. K. Surappa, "Aluminum Matrix Composites: Challenges and Opportunities", *Sadhana – Academy Proceedings in Engineering Sciences*, 2003, Vol. 28, No. 1-2, pp. 319 -334.

8. D. L. Erich, “Metal Matrix Composites: Problems, Applications, and Potential in the PM Industry”, *Metal Powder Report*, 1988, Vol. 43, No. 6, pp. 418-423.

9. P. Rohatgi, “Cast Aluminum-Matrix Composites for Automative Applications”, *Journal of Materials Science*, 1991, Vol. 43, No. 4, pp. 10-15.

10. A. I. Nussbaum, “New Applications for Aluminum-Based Metal Matrix Composites”, *Light Metal Age*, 1997, Vol. 55, No. 1-2, pp. 3-7.

11. R. W. Mohn and D. Vukobratovich, “Recent Applications of Metal Matrix Composites in Precision Instruments and Optical Systems”, *Optical Engineering*, 1988, Vol. 27, No. 2, pp. 90-98.

12. R. W. Mohn and G. A. Gegel, “Dimensionally Stable Metal Matrix Composites for Guidance Systems and Optics Applications”, *Advanced Composites: The Latest Developments, Proceedings of the Second Conference*, ASM International, Metals Park, Ohio, USA, 1986, pp. 69-73.

13. P. C. R Nunes and L. V. Ramanathan, “Corrosion Behaviour of Alumina-Aluminum and Silicon Carbide-Aluminum Metal Matrix Composites”, *Corrosion Science*, Vol. 51, No. 8, 1995, pp. 610-617.

14. P. P. Trzaskoma, “Pit Morphology of Aluminum Alloy and Silicon Carbide/Aluminum Alloy Metal Matrix Composites” *Corrosion Science*, Vol. 46, No. 5, 1990, pp. 402-409.

15. M. M. Buarzaiga and S.J. Thorpe, “Corrosion Behaviour of As-Cast, Silicon Carbide Particulate-Aluminum Alloy Metal-Matrix Composites”, *Corrosion Science*, Vol. 50, No. 3, 1994, pp. 176-185.

16. Z. Ahmad and B. J. A. Aleem, “Effect of Temper on Seawater Corrosion of an Aluminum-Silicon Carbide Composite Alloy”, *Corrosion Science,* Vol. 52, No. 11, 1996, pp. 857-864.

17. W. Neil and C. Garrard, “The Corrosion Behaviour of Aluminum-Silicon Carbide Composites in Aerated 3.5% Sodium Chloride”, *Corrosion Science,* Vol. 36, No. 5, 1994, pp. 837-851.

18. S. Golledge and J. Kruger, “Effect of Anodic Film Properties on the Corrosion Behaviour of SiC/Al Metal Matrix Composites”,*Electrochemical Society*, Vol. 85, 1985, pp. 227-228.

19. I. N. A. Oguocha and S. Yannacopoulous, “Precipitation and Dissolution Kinetics in Al-Cu-Mg-Fe-Ni Alloy 2618 and Al-Alumina Particle Metal Matrix Composites”, *Materials Science and Engineering A: Structural Materials: Properties, Microstructure and Processing*, 1997, Vol. A231, No. 1-2, pp. 25-33.

20. I. N. A. Oguocha and S. Yannacopoulous, “Behaviour of Alumina Particle-Reinforced 2618 Aluminum”, *Proceedings of the International Symposium on Developments and Applications of Ceramics and New Metal Alloys,* Publication by Canadian Institute of Mining, Metallurgy and Petroleum, Montreal, Quebec, Canada, 1993, pp. 245- 258.

21. I. N. A. Oguocha and M. Radjabi, S. Yannacopoulous, “Thermal Shock Behaviour of Particle Reinforced 2618 Al/Al_2O_3 MMC”, *Canadian Metallurgical Quarterly*, 2001, Vol. 40, No. 2, pp. 245-254.

22. I. N. A. Oguocha and M. Radjabi, S. Yannacopoulous, “Effect of Cooling Rate on The Quench Sensitivity of 2618 Al/Al_2O_3 MMC”, *Journal of Materials Science*, 2000, Vol. 35, No. 22, pp. 5629-2634.

23. K. H. W. Seah, M. Krishna, V. T. Vijayalakshmi, and J. Uchil, “Corrosion Behaviour of Garnet Particulate Reinforced LM13 Al alloy MMCs”, *Corrosion Science*, 2002, Vol. 44, pp. 917-925.

24. J. Uchil, V. T. Vijayalakshmi, and M. Krishna, “A Case Study on Corrosion Properties of Garnet Particles Reinforced Aluminum Composites”, *Proceedings of the Second International Conference on Processing Materials for Properties*, 2000, pp. 145-148.

25. M. Saxena, O. P. Modi, A. H. Yegneswaran, and P. K. Rohatgi, “Corrosion Characteristics of Cast Aluminum Alloy-3 wt.% Graphite Particulate Composites in Different Environments”, *Corrosion Science*, 1987, Vol. 27, No. 3, pp. 249-256.

26. I. Saxena, A. K. Jha, and S. Upadhyaya “Corrosion Behaviour of Sinstered 6061 Aluminum Alloy-graphite Particle Composites”, *Corrosion Science*, 1993, Vol. 28, pp. 4053-4058.

27. D. Nath and T. K. G. Namboodhiri, “Some Corrosion Characteristics of Aluminum-Mica Particulate Composites”, *Corrosion Science*, 1989, Vol. 29, No. 10, pp. 1215-1229.

28. P. K. Rohatgi, “Low-Cost, Fly-Ash-Containing Aluminum-Matrix Composites”, *Journal of Materials*, 1994, Vol. 46, No. 11, pp. 55-59.

29. E. Gatima, M. Mwinyihija, and K. Killham, “Assesment of Pulverised Fly Ash (PFA) as an Ameliorant of Lead Contaminated Soils”, *American Journal of Environmental Science*, 2005, Vol. 1, No. 3, pp. 230-238.

30. S. Macakova, F. Siska, N. Pliesovska, and M. T. Hepworth, “Solidification of Fly Ash From Municipal Solid Waste Incinerator By The Use of Sorel Cement”, *Acta Montanistica Slovaca*, 1996, Vol. 1, pp. 35-42.

31. V. Saraswathy, S. Muralidharan, K. Thangavel, and S. Srinivasan, “Influence of Activated Fly Ash on Corrosion-Resistance and Strength of Concrete”, *Cement and Concrete Composites*, 2003, Vol. 25, pp. 673-680.

32. S. Ghosal and S. A. Self, “Particle Size-Density Relation and Cenosphere Content of Coal Fly Ash”, *Fuel*, 1995, Vol. 74, No. 4, pp. 522-529.

33. E. Gikunoo, O. Omotoso, I. N. A. Oguocha, “Effects of Fly Ash Particles on the Mechanical Properties of Aluminum Casting Alloy 535”, *Materials Science and Technology*, 2005, Vol. 21, No. 2, pp. 143-152.

34. E. Gikunoo, O. Omotoso, I. N. A. Oguocha, “Effect of Fly Ash Addition on the Mg Content of Casting Aluminum Alloy A535”, *Journal of Materials Science*, 2005, Vol. 40, No. 2, pp. 487-490.

35. E. Gikunoo and I.N.A. Oguocha, “Investigation of Fly ash-Aluminum Alloy Reaction Using XRD and XFS”, *Proceedings of the Sixth Joint Canada-Japan Workshop on Composites*, Ed. by J. Lo, T. Nishino, S.V. Hoa, H. Hamada, A. Nakai, and C. Poon, DEStech Publications, Inc.,Toronto, Canada, 2006, pp. 387-395.

36. E. Gikunoo, “Effect of Fly Ash Particles on the Mechanical Properties and Microstructure of Aluminum Casting Alloy A535”, M.Sc Thesis, University of Saskatchewan, Saskatoon, 2004.

37. J. Bienias, M. Walczak, B. Surowska and J. Sobczak, “Microstructure and Corrosion Behaviour of Aluninum Fly Ash Composites”, *Journal of Optoelectronics and Advanced Materials*, Vol. 5 No. 2, 2003, pp. 493-502.

38. M. Ramachandra and K. Radhakrishna,, “Microstructure, Mechanical Properties, Wear and Corrosion Behaviour of Al-Si/Fly Ash Composite”, *Materials Science and Technology*, 2005, Vol. 21, No. 11, pp. 1337-43.

39. N. Sobczak, J. Sobczak, J. Morgiel and L. Stobierski, “TEM Characterization of the Reaction Products in Aluminum-Fly Ash Couples”, *Materials Chemistry and Physics*, 2003, No. 81, pp. 296-300.

40. R. C. Joshi and R. P. Lohtia, *Fly Ash in Concrete Production, Properties and Uses*, Gordon and Breach Science Publishers, Australia, 1997, pp. 1-47.

41. P. P. Trzaskoma, E. Mccafferty and C. R. Crowe, “Corrosion Behaviour of SiC/Al Metal Matrix Composites”, *Journal of The Electrochemical Society*, 1983, Vol. 130, No. 9, pp. 1804-1809.

42. D. M Aylor and P. J. Moran, “Effect of Reinforcement on the Pitting Behaviour of Aluminum-Base Metal Matrix Composites”, *Journal of the Electrochemical Society*, 1985, Vol. 321, No. 6, pp. 1277-1281.

43. A. Pardo, M. C. Merino, F. Viejo, S. Feliu, M. Carboneras, and R. Arrabal, “Corrosion Behaviour of Cast Aluminum Matrix Composites (A3xx.x/SiC_p) in

Chloride Media," *Journal of the Electrochemical Society*, 2005, Vol. 152, Issue 6, pp. B198-B204.

44. A. J. Trowsdale, B. Nobles, S. J. Harris, I. S. R. Gibbins, G. E. Thompson, and G. C. Wood, "Influence of Silicon Carbide Reinforcement on the Pitting Behaviour of Aluminum", *Corrosion Science*, 1996, Vol. 38, No. 2, pp. 177 – 191.

45. A. J. Griffiths and A. Turnbull, "An Investigation of the Electrochemical Polarisation Behaviour of 6061 Aluminum Metal Matrix Composites", *Corrosion Science*, 1994, Vol. 36, No. 1, pp. 23-35.

46. Z. Ahmad, B. J. A. Aleem, and U. Ul-Hamid, "Effect of Al/SiC Interface and Intermetallic Particles on Elevated Temperature Corrosion of Hypoeutectic Al-Si-Mg Composites", *Corrosion Science*, 2004, Vol. 60, No. 10, pp. 954 – 964.

47. A. Pardo, M. C. Merino, F. Viejo, S. Feliu, M. Carboneras, and R. Arrabal, "Corrosion Behaviour of Cast Aluminum Matrix Composites (A3xx.x/SiC_p) in Chloride Media", *Journal of the Electrochemical Society*, 2005, Vol. 152, No. 6, pp. 198-204.

48. H. Sun, E. Y. Koo, and H. G. Wheat, "Corrosion Behaviour of SiC_p/6061 Al Metal Matrix Composites, *Corrosion Science*, 1991, Vol. 47, No. 10, pp. 741-753.

49. G. W. Roper and P. A. Attwood, "Corrosion Behaviour of Aluminum Matrix Composites", *Journal of Materials Science*, 1995, Vol. 30, No. 4, pp. 898 – 903.

50. Z. Feng, C. Lin, J. Lin, and J. Luo, "Pitting Behaviour of SiC_p/2024 Al Metal Matrix Composites," *Journal of Materials Science*, 1998, Vol. 33, pp. 5637-5642.

51. J. R. Davis (Ed.), *Corrosion of Aluminum and Aluminum Alloys*, ASM International, Ohio, USA, 1999.

52. D. A. Jones, *Principles and Prevention of Corrosion*, 2nd Ed., Prentice Hall International, Inc., Singapore, 1996.

53. R. W. Revie (Ed.), *Uhlig's Corrosion Handbook*, 2nd Edition, John Willey and Sons, Inc., New York, USA, 2000, pp. 1227-1238.

54. Y. L. Cheng, Z. Zhang, F. H. Cao, J. F. Li, J. Q. Zhang, J. M. Wang and C. N. Cao, "Study of the Potential Electrochemical Noise During Corrosion Process of Aluminum Alloys 2024, 7075 and Pure Aluminum", *Materials and Corrosion*, 2003, Vol. 54, pp. 601-608.

55. R. M. Souto and G. T. Burstein, "Study of Corrosion Processes with Electrochemical Noise Measurements", *Materials Science Forum*, Vol. 289, Issue 2, 1998, pp. 799-806.

56. F. A. Fasoyinu, J. Thomson, D. Cousineau, T. Castles, and M. Sahoo, "Gravity Permanent Mold Casting of Al-Mg Alloy 535", *AFS Transations*, Vol. 02, Issue 145, 2002, pp. 1-19.

57. F. A. Fasoyinu, J. P. Thomson, D. Cousineau, J. Barry, and M. Sahoo, "Mechanical Properties and Metallography of Al-Mg Alloy 535.0", *AFS Transations*, Vol. 03, Issue 115, 2003, pp. 1-13.

58. M. Pourbaix, *Atlas of Electrochemical Equilibria in Aqueous Solutions*, translated by J. A. Franklin, Pergamon Press, Oxford, Londond, Paris, 1966, pp. 168-176.

59. G. C. Wood, "Porous Anodic Films on Aluminum", *Oxide and Oxide Films*, Vol. 2, Ed. by J.W. Diggle, Marcel Dekker, Inc., New York, 1973, pp. 167-268.

60. Z. Szklarska-Smialowska, “Pitting Corrosion of Aluminum”, *Corrosion Science*, Vol. 41, No. 9, 1999, pp. 1743-1767.

61. Z. Szklarska-Smialowska, “Insight into the Pitting Corrosion Behaviour of Aluminum Alloys” *Corrosion Science*, Vol. 33, No. 8, 1992, pp. 1193-1202.

62. G. Kiourtsidis and S. M. Skolianos, “Corrosion Behaviour of Squeeze-cast Silicon Carbide-2024 Composites in Aerated 3.5 wt.% Sodium Chloride”, *Materials Science and Engineering*, Vol. A 248, 1998, pp. 165-172.

63. A. Pardo, M. C. Merino, F. Viejo, S. Feliu, M. Carboneras, and R. Arrabal, “Influence of Reinforcement Proportion and Matrix Composition on Pitting Corrosion Behaviour of Cast Aluminum Matrix Composites (A3xxx.x/SiCp), *Corrosion Science*, Vol. 47, Issue 7, 2005, pp. 1750-1764.

64. S. Candan and E. Bilgic, “Corrosion Behaviour of Al-60 Vol.% SiC_p Composites in NaCl Solution”, *Materials Letters*, Vol. 58, 2004, pp. 2787-2790.

65. A. K. Bhattamishra and K. Lal, “Influence of Ageing on Corrosion Behaviour of Al-Mg-Si Aloys in Chloride and Acid Media”, *Materials Research and Advanced Techniques*, 1998, Vol. 89, No. 11, pp. 793-796.

66. D. R. Baer, C. F. Windisch, Jr., M. H. Engelhard, M. J. Danielson, R. H. Jones, and J. S. Vetrano, “Influence of Mg on the Corrosion of Al”, *Journal of Vacuum Science and Technology*, 2000, Vol. A18, No. 1, pp. 131-136.

67. F. Bovard, “Sensitization and Environmenal Cracking of 5xxx Aluminum Marine Sheet and Plate Alloys”,*Electrochemical Society*, 2005, pp. 232-243.

68. J. R. Flores, H. Terryn, O. Steenhaut, and J. H. W. de Wit, “Influence of Mg Enrichment in the Corrosion Behaviour of Al-Mg Alloys”, *Electrochemical Society Proceedings*, 2003, Vol. 23, pp. 131-140.

69. E. Lunarska, E. Trela, and Z. Szklarska-smialowska, “Pitting Corrosion of Powder Metallurgy AlZnMg Alloys”, *Corrosion*, 1987, Vol. 43 , No. 4 , pp. 219-228.

70. G. Svenningsen, J. E, Lein, A. Bjorgum, J. H. Nordlien, Y. Yu, and K. Nisancioglu, “Effect of Low Copper Content and Heat Treatment on Intergranular Corrosion of Model AlMgSi Alloys”, *Corrosion Science*, 2006, Vol. 48, pp. 258-272.

71. A. V. Sameljuk, O. D. Neiko, A. V. Krajnikov, Y. V. Milman, and G. E. Thompson, “Corrosion Behaviour of Powder Metallurgical and Cast Al-Zn-Mg Base Alloys”, *Corrosion Science*, 2004, Vol. 46, pp. 147-158.

72. L. Leyun, Z. Qihai, and Y. Zhimin, “Influence of Precipitates and Their Distribution on Seawater Corrosion Resistance of Al-Mg Alloy”, *Transactions of Nonferrous Metals Society of China*, 1997, Vol. 7, No. 1, pp. 116-119.

73. P. P. Niskanen, “Influence of Microstructure on the Corrosion of Al-Li, Al-Li-Mn, Al-Li-Mg and Al-Li-Cu Alloys in 3.5 wt.% NaCl Solution”, *Aluminum-Lithium Alloys: Proceedings of the First International Aluminum-Lithium Conference*, Atlanta, USA, 1981, pp. 347-376.

74. C. A. Turnbull, “Review of Corrosion Studies on Aluminum Metal Matrix Composites, *British Corrosion Journal*, 1991, Vol. 27, Issue 1, pp. 27-35.

75. Y. L. Saraswathi, S. Das, and D. P. Mondal, “Influence of Microstructure and Experimental Parameters on the Erosion-Corrosion Behaviour of Al Alloy Composites”, *Materials Science and Engineering*, Vol. A 425, 2006, pp. 244-254.

76. N. N. Birbilis and R. G. Buchheit, “Electrochemical Characteristics of Intermetallic Phases in Aluminum Alloys: An Experiemtal Survey and Discussion”. *Journal of the Electrochemical Society*, Vol. 152, No. 4, 2005, pp. B140-B151.

77. R. G. Buchheit, “Compliation of Corrosion Potentials Reported for Intermetallic Phases in Aluminum Alloys”, *Journal of the Electrochemical Society*, Vol. 142, 1995, pp. 3994-3996.

78. R. Ambat and E. S. Dwarakadasa, “Studies on the Influence of Chloride Ion and pH on the Electrochemical Behaviour of Aluminum alloys 8090 and 2014”, *Journal of Applied Electrochemistry*, 1994, Vol. 24, pp. 911-916.

79. R. G. Bucheeit, L. P. Montes, M. A. Martinez, J. Michael, and P. F. Hlava, “Electrochemical Characteristics of Bulk-Synthesized Al_2CuMg”, *Journal of Electrochemical Society*, Vol. 146, No. 12, 1999, pp. 4424-4428.

80. A. M. Lafront, W. Zhang, S. Jin, R. Tremblay, D. Dube, E. Ghali, “Pitting Corrosion of AZ91D and AJ62x Magnesium Alloys in Alkaline Chloride Medium Using Electrochemical Techniques”, *Electrochimica Acta*, 2005, Vol. 51, pp. 489-501.

81. R. G. Kelly, M. E. Inman, and J. L. Hudson, “Analysis of Electrochemical Noise for Type 410 Stainless Steel in Chloride Solutions”, *Electrochemical Noise Measurement For Corrosion Applications*, Ed. by J. R. Kearns, J. R. Scully, P. R.

Roberge, D. L. Reichert, and J. L. Dawson, American Society For Testing and Materials, West Conshohocken, USA, 1996, pp. 101-113.

82. F. Mansfeld and H. Xiao, "Electrochemical Noise and Impedance Analysis of Iron in Chloride Media", *Electrochemical Noise Measurement For Corrosion Applications*, Ed. by J. R. Kearns, J. R. Scully, P. R. Roberge, D. L. Reichert, and J. L. Dawson, American Society For Testing and Materials, West Conshohocken, USA, 1996, pp. 59-78.

83. A. Kolics, A. S. Besing, P. Baradlai, R. Haasch, and A. Wieckowski, "Effect of pH on Thickness and Ion Content of the Oxide Film on Aluminum in NaCl Media", *Journal of the Electrochemical Society*, 2001, Vol. 148, No. 7, pp. 251-259.

84. R. Babic, M. Metikos-Hukovic, S. Omanovic, Z. Grubac, S. Brinic, "Electrochemical Behaviour of Aluminum Based Alloys in Presence of Chloride Ions", *British Corrosion Journal*, Vol. 30, No. 4, 1995, pp. 288-291.

85. B. Bereket and A. Pinarbasi, "Electrochemical Thermodynamic and Kinetic Studies of the Behaviour of Aluminum in Hydrochloric Acid Containing Various Benzotriazole Derivaties", *Corrosion Engineering, Science and Technology*, Vol. 39, No. 4, 2004, pp. 308-312.

86. M. C. Reboul, "A Ten-Step Mechanism for the Pitting Corrosion of Aluminum", *Materials Science Forum*, Vol. 217, Issue 3, 1996, pp. 1553-1558.

87. S. H. Sanad, "Corrosion of Al-Mg Alloys in Sodium Chloride Solutions", *Corrosion Prevention and Control*, Vol. 29, Issue 3, 1982, pp. 21-23.

88. V. Guillaumin and G. Mankowski, “Localized Corrosion of 6056 T6 Aluminum Alloy in Chloride Media”, *Corrosion Science*, Vol. 42, 2000, pp. 105-125.

89. F. Cao, “Electrochemical Features During Pitting Corrosion of LY12 Aluminum Alloy in Different Neutral Solutions”, *Acta Metallurgica Sinica*, Vol. 16, Issue 4, 2003, pp. 319-326.

APPENDICES

The appendix is divided into 5 sections. Section A presents the average weigh loss when samples were immersed in the test solutions. Section B shows the sample dimensions and surface areas computations used for the determination of the current densities and corrosion rates. In section C, a typical calculation used to determine the corrosion rate is shown. Section D presents the average values for the corrosion rates in the test solutions. Section E shows two cyclic polarization curves for A535 and the composites immersed in neutral 3.5 wt.% NaCl solution.

A. Average values for weight loss in test solutions

The following tables present the average weight loss (mg) for the specimens exposed during immersion corrosion test in different solutions.

Table A.1. Average values for weight loss for A535 and composites immersed in 3.5 wt.% NaCl solution maintained at pH 4.

	Weight loss (g)			
Time (day)	A535	A535/hybrid/10_p	A535/fly ash/10_p	A535/fly ash/15_p
1	0.003 ± 3.7E-06	0.005 ± 2.4E-06	0.008 ± 3.3E-05	0.01 ± 3.0E-05
3	0.01 ± 6.6E-06	0.01 ± 5.8E-06	0.02 ± 3.3E-05	0.02 ± 1.7E-05
5	0.01 ± 1.8E-05	0.01 ± 5.1E-05	0.03 ± 2.6E-05	0.03 ± 3.59E-05
7	0.02 ± 1.9E-05	0.02 ± 2.1E-05	0.04 ± 3.5E-05	0.04 ± 2.22E-05
10	0.02 ± 1.3E-05	0.03 ± 3.7E-05	0.05 ± 2.5E-05	0.07.95E-05
14	0.02 ± 3.1E-05	0.04 ± 3.4E-05	0.06 ± 1.3E-4	0.08 ± 3.2E-05

Table A.2. Average values for weight loss for A535 and composites immersed in 3.5 wt.% NaCl solution maintained at pH 7.

	Weight loss (g)			
Time (day)	A535	A535/hybrid/10_p	A535/fly ash/10_p	A535/fly ash/15_p
1	0.005 ± 2.5E-05	0.006 ± 3.0E-05	0.009 ± 7.5E-06	0.04 ± 3.E-05
3	0.005 ± 5.1E-06	0.007 ± 7.3E-06	0.02 ± 1.4E-05	0.04 ± 1.7E-05
5	0.007 ± 2.7E-05	0.02 ± 1.4E-05	0.03 ± 8.9E-06	0.06 ± 3.6E-05
7	0.01 ± 1.0E-05	0.03 ± 1.7E-03	0.04 ± 2.3E-05	0.08 ± 2.2E-05
10	0.02 ± 4.6E-05	0.03 ± 3.2E-05	0.05 ± 1.6E-05	0.08 ± 1.9E-05
14	0.02 ± 4.4E-05	0.04 ± 3.9E-05	0.06 ± 2.1E-05	0.09 ± 3.2E-05

Table A.3. Average values for weight loss for A535 and composites immersed in 3.5 wt.% NaCl solution maintained at pH 9.

	Weight loss (g)			
Time (day)	A535	A535/hybrid/10_p	A535/fly ash/10_p	A535/fly ash/15_p
1	0.005 ± 4.9E-05	0.006 ± 2.7E-05	0.01 ± 2.5E-05	0.01 ± 3.0E-05
3	0.01 ± 3.3E-05	0.02 ± 2.5E-05	0.02 ± 1.1E-05	0.02 ± 4.0E-05
5	0.02 ± 2.2E-05	0.02 ± 2.1E-05	0.04 ± 5.8E-06	0.04 ± 2.5E-05
7	0.03 ± 2.5E-05	0.03 ± 1.3E-05	0.05 ± 4.0E-05	0.04 ± 3.8E-05
10	0.04 ± 1.2E-05	0.04 ± 1.5E-05	0.06 ± 3.4E-05	0.06 ± 3.7E-05
14	0.05 ± 2.1E-05	0.06 ± 3.1E-05	0.08 ± 3.3E-05	0.08 ± 6.4E-05

Table A.4. Average values for weight loss for A535 and composites immersed in water from South Saskatchewan River.

	Weight loss (g)			
Time (day)	A535	A535/hybrid/10_p	A535/fly ash/10_p	A535/fly ash/15_p
1	0.0004 ± 2.0E-05	0.003 ± 2.6E-05	0.005 ± 2.3E-05	0.01 ± 0.4
3	0.006 ± 1.5E-05	0.01 ± 1.1E-05	0.02 ± 9.7E-06	0.02 ± 0.4
5	0.006 ± 2.5E-05	0.01 ± 9.7E-06	0.03 ± 1.4E-05	0.03 ± 0.4
7	0.01 ± 1.8E-05	0.02 ± 2.7E-05	0.05 ± 3.7E-05	0.04 ± 0.4
10	0.02 ± 1.7E-05	0.02 ± 1.8E-05	0.05 ± 2.1E-05	0.05 ± 0.4
14	0.03 ± 1.8E-05	0.03 ± 2.7E-05	0.06 ± 4.2E-05	0.07 ± 0.3

B. Surface Area Calculations

The surface areas of the specimens were calculated using the expression:

External surface area = 2 [(length)(width)+(width)(depth)+(length)(depth)]

The porosities were mapped on a scaled (graph) paper. The average diameters of the mapped porosities were measured and subtracted from the corresponding plane dimensions. The expression for the external surface area was then applied to evaluate the surface area of each specimen. Tables B.1-B.4 present the modified dimensions and external surface area of the specimens exposed in different solutions.

Sample Calculation:

Length of specimen = 1 cm

Width of specimen = 1 cm

Depth of specimen = 0.5 cm

Average diameter of a pore along the length axis = 0.1 cm

Average diameter of a pore along the width axis = 0.15 cm

Average diameter of another pore along the depth axis = 0.2

External surface area

$= 2[(1-0.1)(1-0.15)+(1-0.15)(0.5-0.2)+(1-0.1)(0.5-0.2)]$

$= 2.58\ cm^2$

Table B.1. Dimensions of samples immersed in 3.5 wt.% NaCl solution maintained at pH 4.

Specimen	Length (cm)	Width (cm)	Depth (cm)	External surface area (cm^2)
A535	0.95	0.93	0.49	3.61
A535/hybrid/10_p	0.93	0.91	0.48	3.5
A535/fly ash/10_p	0.90	0.90	0.47	3.31
A535/fly ash/15_p	0.87	0.88	0.37	2.80

Table B.2. Dimensions of samples immersed in 3.5 wt.% NaCl solution maintained at pH 7.

Specimen	Length (cm)	Width (cm)	Depth (cm)	External surface area (cm^2)
A535	0.97	0.98	0.5	3.8
A535/hybrid/10_p	0.96	0.95	0.47	3.62
A535/fly ash/10_p	0.95	0.95	0.46	3.55
A535/fly ash/15_p	0.87	0.88	0.37	3.10

Table B.3. Dimensions of samples immersed in 3.5 wt.% NaCl solution maintained at pH 9.

Specimen	Length (cm)	Width (cm)	Depth (cm)	External surface area (cm^2)
A535	0.92	0.91	0.5	3.50
A535/hybrid/10_p	0.9	0.9	0.47	3.30
A535/fly ash/10_p	0.89	0.86	0.47	3.12
A535/fly ash/15_p	0.88	0.89	0.3	2.60

Table B.4. Dimensions of samples immersed in South Saskatchewan River.

Specimen	Length (cm)	Width (cm)	Depth (cm)	External surface area (cm^2)
A535	0.98	0.98	0.5	3.61
A535/hybrid/10_p	0.97	0.98	0.46	3.5
A535/fly ash/10_p	0.97	0.93	0.45	3.31
A535/fly ash/15_p	0.87	0.9	0.37	2.88

C. Corrosion rate calculations

The corrosion rates of the specimens were calculated using the expression specified by ASTM G1-90:

$$mm/yr = \frac{87.6W}{DAt}$$

where W is weight loss in mg, D is density in g/cm^3, A is surface area in cm^2, and t is time in hours.

Table C.1. Densities of A535 alloy and its composites [36].

Specimen	Density (gcm^{-3})
A535	2.6
A535/hybrid/10$_p$	2.56
A535/fly ash/10$_p$	2.48
A535/fly ash/15$_p$	2.38

C.1. Sample Corrosion Rate Calculation:

The corrosion rate in mm/yr for A535 alloy exposed in neutral 3.5 wt.% NaCl solution for one day is determine by the using the expression:

$$mm/yr = \frac{87.6W}{DAt}$$

where

W = 0.00516 mg (See Appendix A)

A = 3.61 cm^2 (See Appendix B)

D = 2.6 gcm^{-3} (See Appendix C)

t = 24 hours

$$\text{Corrosion rate (mm/yr)} = \frac{(87.6)(0.00516mg)}{(2.6gcm^{-3})(3.61cm^2)(24hours)}$$

$$= 0.002 \text{ mm/yr.}$$

D. Average values for corrosion rate in test solutions

Table D.1. Average values for corrosion rates for A535 and composites immersed in 3.5 wt. % NaCl solution maintained at pH 4.

	Corrosion rate (mm/yr)			
Time (day)	A535	A535/hybrid/10_p	A535/fly ash/10_p	A535/fly ash/15_p
1	0.001 ± 3.5E-04	0.002 ± 2.2E-04	0.004 ± 7.1E-04	0.006 ± 1.4E-03
3	0.001 ± 2.9E-04	0.002 ± 5.3E-04	0.003 ± 1.7E-05	0.004 ± 2.4E-04
5	0.0009 ± 4.5E-04	0.001 ± 5.7E-04	0.003 ± 4.4E-05	0.004 ± 1.4E-05
7	0.0009 ± 3.7E-04	0.001 ± 4.7E-04	0.003 ± 1.5E-05	0.004 ± 5.8E-05
10	0.0008 ± 5.0E-04	0.002 ± 2.6E-04	0.003 ± 5.2E-05	0.004 ± 1.1E-04
14	0.0007 ± 4.6E-04	0.001 ± 2.8E-04	0.002 ± 6.8E-05	0.003 ± 5.7E-05

Table D.2. Average values for corrosion rates for A535 and composites immersed in 3.5 wt.% NaCl solution maintained at pH 7.

	Corrosion rate (mm/yr)			
Time (day)	A535	A535/hybrid/10_p	A535/fly ash/10_p	A535/fly ash/15_p
1	0.002 ± 3.2E-04	0.002 ± 1.5E-03	0.003 ± 1.5E-03	0.02 ± 4.6E-04
3	0.0006 ± 9.0E-05	0.0008 ± 9.0E-04	0.001 ± 1.2E-03	0.007 ± 5.4E-04
5	0.0005 ± 3.9E-04	0.0013 ± 6.3E-04	0.002 ± 5.6E-04	0.006 ± 9.4E-05
7	0.00005 ± 8.1E-04	0.001 ± 4.0E-04	0.002 ± 4.1E-04	0.005 ± 7.8E-06
10	0.0007 ± 2.7E-04	0.001 ± 2.7E-04	0.002 ± 2.9E-04	0.004 ± 1.1E-04
14	0.0007 ± 1.1E-04	0.001 ± 1.3E-04	0.002 ± 8.3E-05	0.003 ± 1.2E-04

Table D.3. Average values for corrosion rates for A535 and composites immersed in 3.5 wt.% NaCl solution maintained at pH 9.

	Corrosion rate (mm/yr)			
Time (day)	A535	A535/hybrid/10_p	A535/fly ash/10_p	A535/fly ash/15_p
1	0.002 ± 3.6E-04	0.0027 ± 2.5E-04	0.0048 ± 3.7E-04	0.008 ± 1.3E-03
3	0.002 ± 6.6E-05	0.002 ± 3.2E-04	0.003 ± 1.6E-04	0.004 ± 9.0E-04
5	0.002 ± 2.0E-04	0.002 ± 2.3E-04	0.004 ± 1.4E-04	0.004 ± 2.0E-06
7	0.002 ± 9.2E-05	0.002 ± 1.9E-04	0.003 ± 1.1E-04	0.004 ± 2.2E-04
10	0.002 ± 5.3E-05	0.002 ± 1.8E-04	0.003 ± 1.5E-04	0.004 ± 1.8E-04
14	0.001 ± 5.6E-05	0.002 ± 1.8E-04	0.0023 ± 8.4E-05	0.003 ± 1.4E-04

Table D.4. Average values for corrosion rates for A535 and composites immersed in water from the South Saskatchewan River.

	Corrosion rate (mm/yr)			
Time (day)	A535	A535/hybrid/10_p	A535/fly ash/10_p	A535/fly ash/15_p
1	0.0002 ± 5.5E-05	0.001 ± 8.2E-05	0.002 ± 3.2E-04	0.004 ± 6.6E-05
3	0.0007 ± 1.3E-04	0.001 ± 3.4E-04	0.003 ± 5.6E-04	0.0034 ± 2.8E-04
5	0.0004 ± 9.5E-05	0.0008 ± 1.3E-04	0.003 ± 6.4E-04	0.003 ± 5.5E-04
7	0.0006 ± 2.2E-05	0.0008 ± 9.6E-05	0.001 ± 5.8E-04	0.003 ± 2.9E-04
10	0.0006 ± 2.0E-06	0.0008 ± 5.2E-05	0.002 ± 5.3E-04	0002 ± 4.0E-05
14	0.0007 ± 1.2E-04	0.0008 ± 6.5E-05	0.002 ± 5.1E-04	0.002 ± 2.1E-04

E. Samples of cyclic Polarization Plot

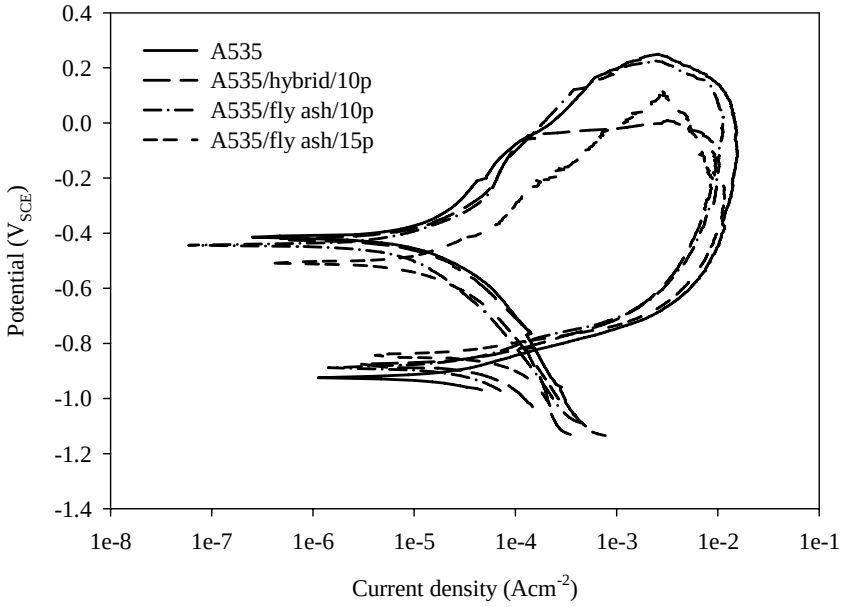

(a)

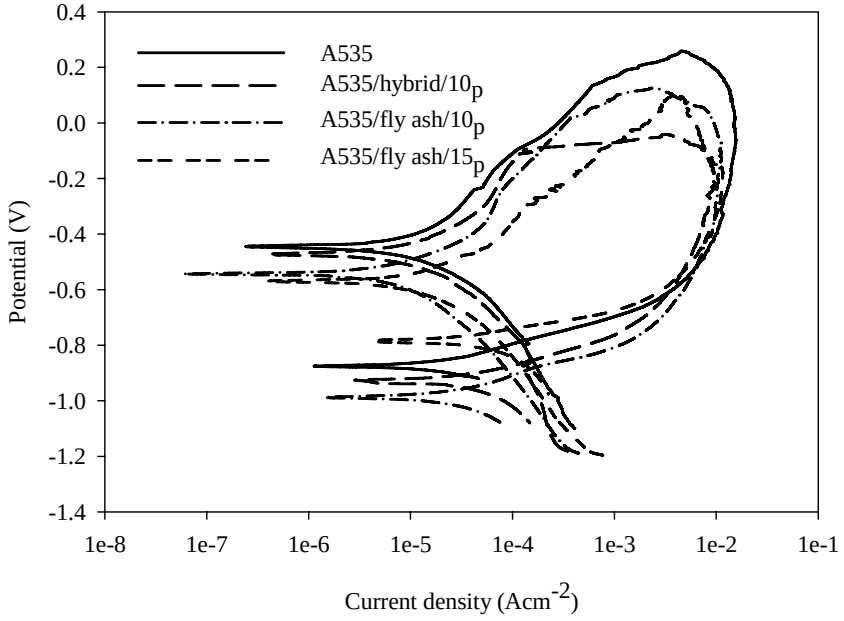

(b)

Figure E.1. Cyclic polarization curves for A535 and the MMCs exposed in neutral 3.5 wt.% NaCl solution.